UNIVERSITÀ
DEGLI STUDI
DI FERRARA
- EX LABORE FRUCTUS -

DOTTORATO DI RICERCA IN
SCIENZE DELLINGEGNERIA

CICLO XXXVI

Coodinatore Prof. Stefano Trillo

INTELLIGENT CONTROL METHODS FOR MAXIMUM POWER POINT TRACKING CONTROL APPLIED TO WIND ENERGY CONVERSION SYSTEMS

Degree work to qualify for a Doctor of Engineering degree
Control Engineering Area

Settore Scientifico Disciplinare ING-INF/04

Dottorando
Dott. Edy Ayala

Tutore
Dott. Silvio Simani

Anni 2018/2021

ACCEPTANCE NOTE

_____

_____

_____

_____

_____

President of the Jury

_____

Jury

_____

Jury

_____

Jury

Declaration of originality

February 6, 2021, Cuenca - Ecuador,

I, Edy Leonardo Ayala Cruz MSc:

"I declare that this thesis has not been submitted to qualify for a degree, either in the same way or with variations, in this or any other university".

Signature

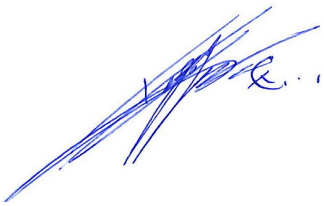

Abstract

Wind energy has demonstrated numerous advantages regarding energy production worldwide. It is environmentally friendly, can be implemented in most geographic locations around the world, and because of its electrical and mechanical characteristics, it is able to produce high amounts of power when grouped in wind farms. Consequently, wind energy demand has been increasing exponentially every year as governments become more interested in clean energies including wind energy for onshore and offshore configurations. Despite it's advantages, wind turbine design can be challenging because it is necessary to understand the entire system to implement control strategies for optimal performance. All the dynamics that depend on the mechanical and electrical components must be carefully modelled in order to obtain a precise control for maximum power extraction.

In this thesis, the Maximum Power Point Tracking (MPPT) control of wind turbines is investigated/analysed in order to propose innovative solutions for power maximization during partial load operation between the minimum and maximum rotor speeds. The control strategy for this region must consider all the electrical and mechanical element characteristics depending on the type of configuration. Moreover, the strategy must consider different aspects such as the wind turbine inertia, electrical and mechanical limitations, and grid requirements. Finally, because the wind speed is a fictitious variable and most subsystems depend on its variations, the dynamic system becomes a complex model. Consequently, the control strategy must consider different aspects such as the wind turbine inertia, electrical and mechanical limitations, and grid requirements.

The MPPT controller must be designed to allow the wind turbine to reach the maximum Power Coefficient (C_p). The C_p depends on the pitch angle and the Tip Speed Ratio (TSR) which implies a family of possible curves for tracking. There are some MPPT strategies that have been proposed and that is the case of techniques based on maximum power, optimum tip speed, and optimization algorithms resulting in the improvement of power generation performance.

In this work, a Fatigue, Aerodynamics, Structures, and Turbulence (FAST),

Matlab-Simulink software and available data from some manufacturers have been used for the model representation. These technical data are important because even though it is possible to use a generic C_p equation based on approximations, there are other losses to be considered as they may alter the expected results. The presented simulations include multiple schemes: for instance, the MPPT strategy has been firstly performed by using the Indirect Speed Control (ISC) method to test the system dynamics. Then, two proposed methods have been tested using more complex Direct Speed Controllers (DSC) based on two observers: Luenberger state observer and fuzzy Proportional Integral (PI) control strategy. Finally, the aforementioned tests have been compared to a classic PI - MPPT controller response in order to investigate the functionality of the proposed schemes.

Multiple simulations have been carried out for testing the MPPT performance; thus, verifying that the active power remains near the nominal value while assuring some reactive power absorption from the grid. Different wind speed curves have been defined for testing the C_p response in terms of stability and maximum operating point performance. Moreover, the High Shaft Speed (HSS) has been carefully observed to be maintained within the specifications range. The current reference used for the power electronic back-to-back converter has been controlled to avoid saturation conditions.

Acknowledgments

I would like to first show my appreciation to my supervisor, Professor Silvio Simani, for his important support and guidance. He has inspired me as a person, and his academic support has been of great value to accomplish this research. Thanks to my co supervisor, Professor John Morales, for his directions throughout the process. I also express my gratitude to the University of Ferrara and Universidad Politécnica Salesiana for making this international cooperation program possible. Lastly, I would like to express my gratitude to my wife, family, and friends for their support.

This work is in memory of Eliza Estefanía Guerra Ambrosi.

Contents

Index of Figures

Index of Tables

Chapter 1

Introduction

Nowadays, wind energy is a renewable source that has grown worldwide because of it's multiple advantages. According to the American Wind Energy Association (AWEA), wind turbines help in preventing 198 million metric tons of CO_2 production annually which is equivalent to 43 million cars' emissions and wind technology has been improved in order to obtain as much energy as possible from the source [AWEA, 2015]. Wind energy production has increased exponentially during last decades, and this rising demand has also required more complex controllers in order to optimize the output power generation. Moreover, it is important to note that according to the World Wind Energy Association (WWEA) [WWEA, 2010] the wind energy worldwide is projected to be increased near 20% of total power produced in the near future.

The principal components in a wind turbine can be observed in Figure 1.2 divided in modules. For wind turbine operations, the transition from no load to full load is crucial for managing energy production. Wind turbine design is also important and it involves not only the aerodynamic characteristics but also the proper control strategy which leads to an optimal active power production as well as reactive power absorption from the electric grid. Wind turbine efficiency is mainly reduced because of the mechanic of fluid (air mass flow).

The Betz´s law establishes that 59.3% of total wind power can be used for power generation. Moreover, the efficiency of the wind turbine depends on multiple non-linear variables along the system. This efficiency can be quantified by the C_p which is a reference parameter that indicates the rate of produced active power and the available power in the wind. The $C_p$can be improved if the variables that allow the power extraction maximization are properly determined and controlled which is important for a wind turbine control design. The non-linearity and complex velocity vector fields of wind

demands different control strategies, *i.e.*, yaw control which allows the nacelle to follow the direction of the wind, rotor speed control which is achieved by adjusting the angle of wind incidence determined by the pitch controller, also by the brake system and the power electronic converters. The AC/DC/AC device allows to match the voltage, frequency, phase of the generated and the grid or load electric requirements. It also allows matching of the output active power which can be optimized by using a MPPT controller during partial load operations and breakers can be activated when the turbine is required to stop completely [Abad et al., 2011].

Wind Turbine variations are very fast, hence the speed of command signal controllers must allow the system to act as fast as these variations occur. It implies that the semiconductor characteristics play a key role for an optimal MPPT. Nowadays it is very common to use high frequency switching devices such as Insulated Gate Bipolar Transistor (IGBT) which also drive high power demand of currents and voltages. The back to back converter controller configuration allows for command of the machine side and consequently the grid side power flows. Filters and protections are also included in order to improve the quality of the voltage signals. This setting is very common for individual wind turbines and they can be grouped into wind farms which allows for increases in the total power. A wind farm can be modelled as a single nonlinear wind turbine, however, in practice each one requires its own control setting. The MPPT control works individually and the total performance relies on this precision and speed for tracking the input variations. The MPPT controller must command the power electronic converter for adjusting the variables in order to attain the maximum $C_p$operation point.

Also, grid characteristics are important for finding the balance between active and reactive power quantities. These control strategies usually consider variables such as: wind speed, electromagnetic torque, HSS, pitch angle, output active power and TSR. Commercial wind turbines usually include MPPT controllers based on the torque and angular speed measurements. These variables are the control system inputs and the output must be a command reference signal for the power electronic converter. Other control strategies conceived for tracking $C_p$curves can be achieved by implementation of controllers based on TSR, Power Signal Feedback (PSF), Optimal Torque Control (OPT), and Hill Climb Search (HCS) optimizer which is comparable with the Perturb and Observe (P&O) method used for solar panels. The HCS technique can be combined with other controllers improving power generation performance [Thongam and Ouhrouche, 2011].

The aforementioned controllers have in common the ability to generate a reference signal that is introduced into the power electronic converters connected to the machine and the grid side. It is important to consider

that wind turbines could have different generator types, however, the most popular are: Permanent Magnet Synchronous Generators (PMSG), Squirrel Cage Induction Generators (SCIG) and Doubly Fed Induction Generator (DFIG). Consequently, each electric machine type would require a specific control method based on its electric model and characteristics. One of the most popular machines found in wind turbines is the DFIG. This is because this particular configuration includes a wounded rotor, meaning higher slip controllability. The advantage of this generator is the capability to produce high amounts of power using low power electronics requirements. This is because the rotor is able to control the generated power at the stator windings reducing the size of the electronic components. As a result, the output can be controlled by varying the voltage on the rotor while the stator side is connected directly to the grid usually bypassed by a transformer. The DFIG also has a wide slip angle which allows more controllability specially for variable speed wind turbines where it is important to continue generating active power during the wind variations.

Indeed, there can be many contributions found in the MPPT control strategies that are overcome by different generator types. Most of them highlight the necessity of advance controllers observing the variables and predicting their impact on the $C_p$tracking, *e.g.* those dealing with wind speed, electromagnetic torque, rotor speed, pitch angle and output power observations, see *i.e.* [Bakouri et al., 2014],[Fu et al., 2018] and [Meharrar et al., 2011]. They highlight the development of algorithms for ensuring the tracking of the $C_p$peak independent on the variations of the wind speed during partial load. These algorithms generate the required reference for the controllers allowing the wind turbine to reach the MPPT optimum operation point. This combination results in an advance control strategy that allows the system to operate within its range while maximizing the active power production and reaching the ideal operation point. This permits the wind turbine to operate with the best conditions that increase the machine lifetime.

This research presents the ISC and DSC strategies applied to a DFIG as well as HCS for a small PMSG wind turbine. This thesis is motivated by the MPPT control design challenges which include knowledge of the entire system from the mechanical to the electrical components. This thesis covers some of the basics of wind turbines but it is mostly focused on the technical considerations for the controller model and the simulation results.

The following sections will present a brief review of the nomenclature recognized in the literature review, also general aspects for MPPT operations as well as the overall wind turbine implications for power maximization. The comprehensive view of the present work is presented in the section 1.4. The variable speed wind turbine modelling, the DFIG electrical characteristics,

the ISC and DSC control strategy as well as the MPPT simulation results integrating Fatigue, Aerodynamic, and Structure and Turbulence (FAST) and Matlab-Simulink simulations are covered in the following sections. The results presented in these simulations are compared to a classic PI controller to highlight the improvements of C_p. The HCS for low inertial PMSG applications become the reference for future investigations. The DSC based on Luenberger observer has demonstrated the best results for dynamic response, the fuzzy PI controller produces a more stable $C_p$and the ISC also displays slight improvements of power extraction.

1.1 Nomenclature

The American Wind Energy Association (AWEA) established in 1974 consists of organizations involved in renewable energies around the word based on wind power [AWEA, 2015]. This association has defined the following terms:

- Wind Energy: Process of generating electricity by capturing the energy from the wind.
- Wind: Air flowing from natural process in earth atmosphere due to changes in temperature and pressure.
- Wind turbine: Device used to capture kinetic energy from the wind in order to transform it into electric power for electric grids or stand-alone loads.
- Onshore Wind Turbine: Refers to the wind turbines implemented on land or any geological formation inside continents.
- Offshore Wind Turbine: Refers to the wind turbines implemented on the continental shelf in large water areas.

1.2 Wind Turbine Control Structures

According to National Renewable Energy Laboratory (NREL), the principal control structures can be classified into four principal controllers: blade pitch angle control, variable-speed torque control, HSS brake control and nacelle yaw control [NREL, 2005]. It is important to note that even though all these controllers are responsible of different variables of the wind turbine, all of them have an impact on the MPPT strategy. The MPPT controller usually works the power electronic converter since they are the fastest components for

maximizing the power output, however, the other controllers may influence directly or indirectly. For instance, the pitch blade controller can decrease or increase the HSS and the torque drastically as well as the HSS brake control which limits the maximum speed of the generator usually activated only when a fault or an over wind speed flow occurs.

Pitch blade control is the most common strategy for the turbine speed control. The controller works independently from other controllers in order to provide more degrees of freedom to the system. For the blade modelling in this work, the different torque requirements, friction of the bearings and the structural dynamics are calculated using FAST [Abad et al., 2011].

According to Abad, the speed of the pitch variation is limited to about 10 degrees per second for normal conditions and can be doubled in the event of faults [Abad et al., 2011]. The control loop of the pitch angle controller can be observed in Figure 1.1.

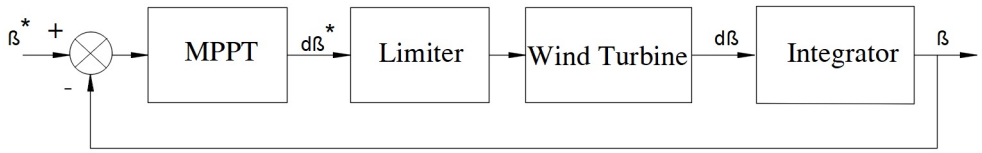

Figure 1.1: Pitch system and control model.

The variable-speed torque control is also used in order to control the turbine speed and torque. This controller design requires a complicated analysis of the aerodynamic and mechanical model which is usually conducted by the manufacturers. Even tough this controller can be modelled using a first-order dynamic system, the interactions with the pitch controller is important for the power extraction. The variable-speed torque control strategy combined with the pitch controller can be observed in Figure 1.2 [Abad et al., 2011].

The MPPT control works independently from the other regulators, however, the control strategy for the whole wind turbine also considers other aspects defined as levels such as: rotor and grid side control, MPPT control and the grid integration control. In Figure 1.3, the general control scheme for DFIG controller is presented divided in three hierarchical levels. In control-level I, the energy transferred from generator to the grid is controlled using the rotor controller also known as the machine side controller. In control-level II, there are two main objectives, the first one is to guarantee the maximum power extraction available in the wind also named MPPT, and the second one is to make possible an appropriate response of the reactive and active power frame which is useful in some conditions, *e.g.*, when the grid

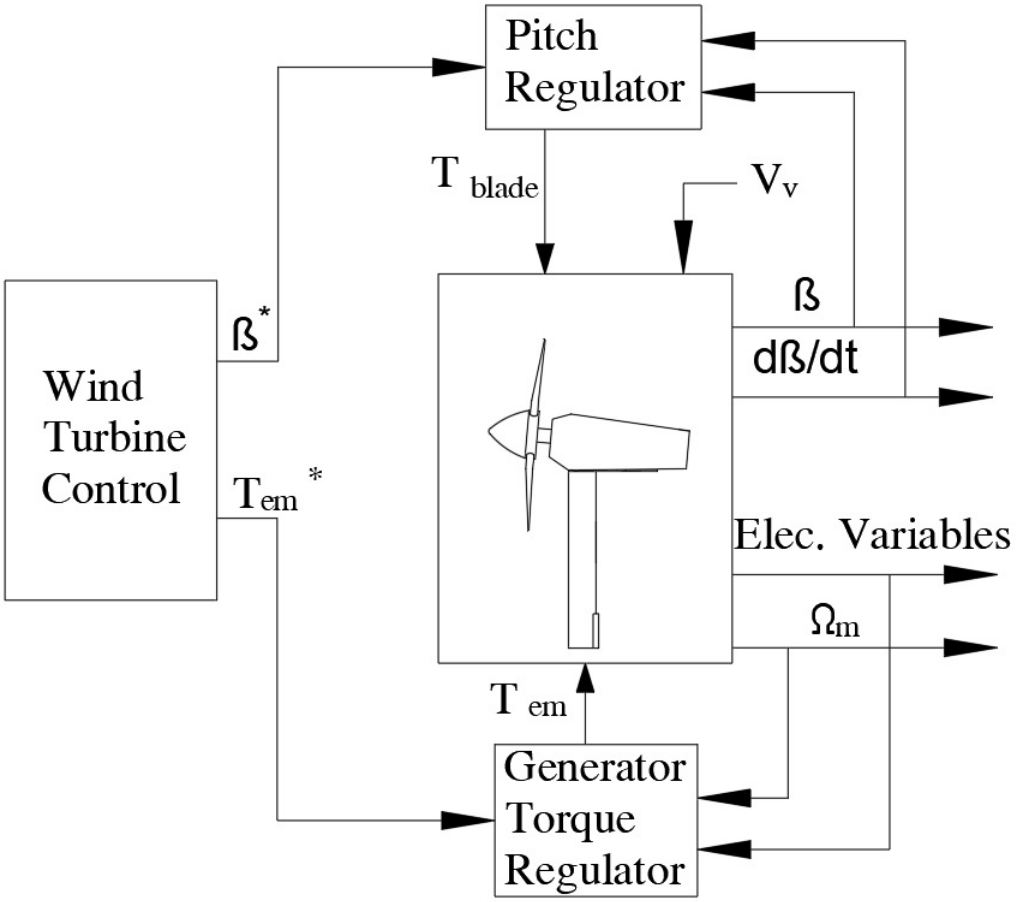

Figure 1.2: Pitch regulated variable speed wind turbine control.

relays deeply on the wind energy generation. Finally, in control-level III it is assured the electrical grid integration with the whole wind turbine system [Abad et al., 2011].

The nacelle yaw control also works independently from other controllers. Its main objective is to control the position of the nacelle in order to follow the wind direction. The yaw mechanism is usually activated by the controller using electric motors that rotate the turbine slowly in order to alienate the rotor with the wind direction sensed by the wind vane.

Finally, the HSS brake control is responsible for stopping the wind turbine automatically once the wind speed exceeds a typical value of 25 meters per second. This is one of the most critical controllers in terms of safety and the area protection since the over-speed of wind turbines is one of the most dangerous faults for the system itself and the environment. The manufacturers

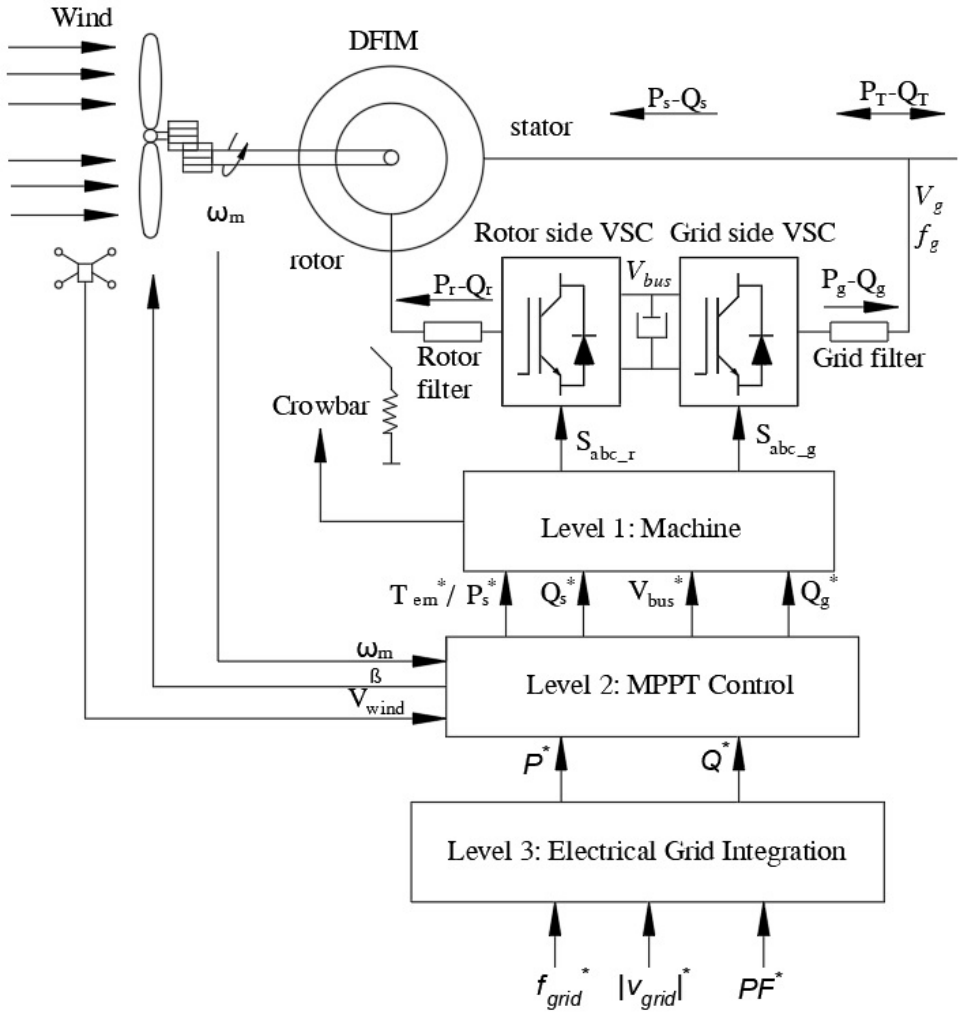

Figure 1.3: General wind turbine control strategy based on DFIM.

usually provide the brake speed boundaries as well as other parameters. For this work simulations, the information provided in [Abad et al., 2011] is considered in order to configure the wind turbine.

1.3 Maximum Power Point Tracking Control

The MPPT depends mainly on the type of machine to be used as a generator. There are generally two common types of machines used, synchronous or asynchronous generators. Their difference relies basically on their electromagnetic field synchronisation of the rotor and the stator. There are multiple factors

to be considered for a proper electric machine selection for a wind turbine. For instance, maintenance, cost, grid requirements, size of the wind turbine, control complexity in terms of robustness, wind speed and its variations.

The asynchronous generator or induction generator is a machine type that is able to produce electricity depending basically on its input torque. The induction generator does not depend on the load, instead it only requires an input torque between non load and full load operation. This is helpful for wind turbines since the wind produces a variant torque and the pitch, yaw and MPPT controller are able to adjust the required torque in order to allow the generator to produce active power. Basically for energy production, the rotor must rotate faster than the synchronous speed otherwise it may behave as a motor. However, it can not control on its own the grid frequency.The DFIG is one of the most common type of induction machine used for wind turbines. Squirrel Cafe Induction Generators (SCIG) are also common for wind turbine applications.

The synchronous generator or alternator is a machine type able to produce electricity by rotating the rotor. The stator produces voltage at a synchronous speed rate referred to the rotor speed. The magnetic field of the rotor can be generated by magnets or can be produced by external excitation using a field coiled electromagnet. Depending on those configurations the rotor could be brush-less or not.The PMSG is one of the most common electric machines used for wind turbines.

Wind energy conversion systems can be used for extracting the maximum available power, which is also dependant on multiple factors that are covered along the following sections. The MPPT control strategies play a key role in the wind turbine efficiency. For this reason, it is important to select the proper strategy. The control methods depend basically on the variables to be observed and controlled. There are multiple researches in this topic, but the most traditionally employed are TSR, PSF and HCS [Thongam and Ouhrouche, 2011].

1.4 Outline of the Thesis

A brief description of the contents of this thesis is presented in this section in order to provide a general approach to the proposed research topic.

Chapter 2 presents the general system of a wind turbine, the components, strategies and control areas depending on the wind speed among other mechanical and electrical characteristics, but with special emphasis on the aerodynamic model. The description of the existing models of the proposed system is presented, as well as the variables involved in the electrical and

mechanical systems which provide information on the behaviour of the wind turbine. In addition, the wind turbine control principle is presented in detail, as well as the work areas where the strategy are implemented. Finally, MPPT control strategies for a wind turbine are detailed.

Chapter 3 presents a detailed analysis of the model selected for the development of the proposal. It can also be found the electrical model specified to the type of electrical machine taking into consideration the timing of the electromagnetic field. In addition, a description is given regarding control of the power electronic devices that control the power produced by the wind turbines. The DFIG, including the lateral control of the machine grid, as well as a description of the operation of the IGBTs normally used for the control of electric generators, is detailed in more depth.

Chapter 4 describes the selected techniques (ISC and DSC) based on the literature review and technical sheets of commercial wind turbines proposed to carry out the modelling and simulation tests. The first part describes the integration of the simulation software with the help of FAST and Matlab-Simulink. Subsequently, the control strategy implemented to the wind turbine with a DFIG machine is detailed according to the ISC criterion. Finally, several methods of DSC proposed using different strategies are presented.

Chapter 5 presents the results of the simulations carried out in this investigation. For example, the performance, speed response, and power extraction of the wind turbine through different wind signals, as well as an analysis of the behaviour of the control strategies implemented using noise signals to verify the robustness of control proposed in the system.

Chapter 6 presents a brief summary of the results obtained and proposes some important future contributions that can be developed taking as a reference the results achieved in this work with an emphasis on the implementation of models in real applications.

Chapter 2

Variable Speed Wind Turbine Modelling

The wind turbine model consists in all mechanical and electrical components that can be simulated. The principal components are the blades where wind forces are captured, the nacelle where generator is allocated including the gear box, the tower which supports the wind turbine, and the connection to the grid or load.

2.1 System Description

The MPPT control allows the system to provide most of the available active power by controlling the power electronic converter. For instance, the most popular converter is the back to back (AC/DC/AC) configuration. Since power electronic devices can reach high speed frequency response, it results easier to command the voltage signal which leads a MPPT control. First of all, a fully controlled rectifier sets the optimum voltage for maximizing the extractable power from the generator. Then, this maximum power associated with the maximum torque point is constantly tracked to guarantee ideal operation. Finally, a fully controlled inverter produces the output voltage signal which has to be synchronized with the load or grid requirements. It allows the system to work continually while the yaw and pitch controllers work simultaneously for finding the best direction and pitch angle [Heier, 1988].

MPPT control is performed by different proposed methods [Muhamamad, 2014]: maximum power control, optimum torque control, and optimum tip speed control. Maximum generated power control requires wind speed sensors to generate a torque reference signal which is used for controlling the digital controller block. The general control block diagram can be observed in Figure 2.1.

It is important to note that those sensors cannot be implemented in the wind turbine since the wind changes when the blades are rotating because of the shadow effects. Optimum generated torque control uses torque measurements at the generator which are transformed into a torque reference. Similarly, as in the maximum generated power control system, grid voltage and current are measured and used by the digital controller in order to command the power converter. Moreover, the generated electromagnetic torque measured T_{em}, grid voltage and current v_g, i_g as well as the electromagnetic torque measured reference estimated based on the actual wind speed $T_{em}{}^*$ are used as auxiliary control signals as shown in Figure 2.2. A variation of this method results in a PSF which uses records of output power from the grid where the maximum power curves are stored and computed for creating a reference. This signal and the output measured power command are sent to the digital controller.

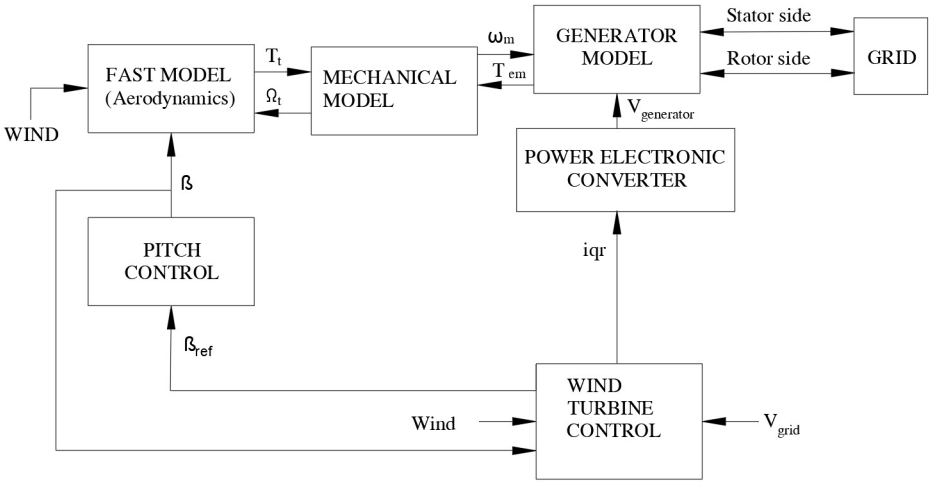

Figure 2.1: Maximum power control diagram.

Multiple algorithms can be applied for maximum power control to produce a stable and constant C_p at the output of the generator shown in Figure 2.2. The model input considers all the variables related to the rotor speed and pitch angle, the output is the pitch angle command [Castellani et al., 2014].

Section 2.2 explains the wind turbine model, the mathematical equations for the simulation as well as the controller characteristics.

2.1.1 Wind Energy Basics

Wind energy is produced by wind forces that usually are transformed into electricity due to the movement of turbine blades. This energy is captured and transmitted to an electric generator. The whole system is called a wind

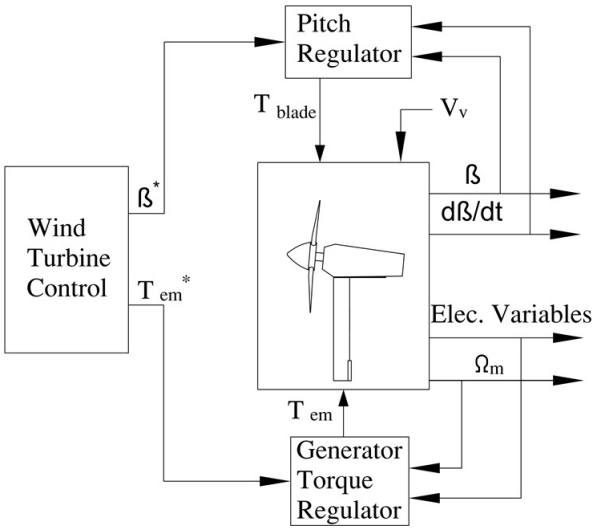

Figure 2.2: PI control system for the C_p extraction.

turbine which can vary in size depending on the location wind conditions. This renewable source of energy allows the generation of electric power as long as wind is present. There are two types of electric generators preferred: synchronous and asynchronous. The first requires external DC power supply for the rotor or permanent magnets. The second relies on induction principle where rotational magnetic field from the rotor induces voltage in the stator winding. Nowadays, multiple wind turbine options can be found depending on generator type. Another wind turbine common configuration is the PMSG because of the operation simplicity and low cost. Induction machines are selected such as wounded rotor DFIG, and Squirrel Cage Induction Generator (SCIG) including single or double cage.

One of the wind turbine's most important parameters is the Performance Coefficient C_p which indicates the efficiency of the system in terms of energy transformation. It considers all possible losses that affect the wind turbine performance including mechanical and electrical characteristics. This parameter is usually provided by the manufacturer based on laboratory tests and mathematical model simulations. The generator is able to produce a certain amount of power if the torque and speed can reach its electrical design characteristics. Consequently, blade-length is important for achieving the corresponding torque and rotational speed. Mechanically, C_p depends mainly on the relation between rotational speed, length of the blades and wind speed. This parameter is known as TSR (λ) described in Eq. 2.1. In order to understand how the C_p is attained, it is important to recap the basics of wind energy and power. These concepts are used in order to derive the Betz

Limit which represents the turbine efficiency in terms of mass conservation. This law states that it is possible to capture up to 59.5 % of C_p from total available wind [Castellani et al., 2014].

2.1.2 Wind Turbine Aerodynamics

The dynamics of the system are one of the most important characteristics because the control strategy is designed by using mechanical and electrical models. The mechanical load must be modelled depending on the number of masses, the gearbox ratio, and the friction losses along the system. Electrical characteristics, grid connection, power electronic converter, and the generator losses are also included. Although there are different types of electric generators, there are, on the market, two main popular wind turbines: The PMSG which is usually selected for minimizing the cost of maintenance and the DFIG commonly used for high power applications [Hofmann and Okafor, 2001], [Hallak et al., 2018], [Ayala and Simani, 2019]. The DFIG wind turbine configuration has the advantage of permitting high amounts of power extraction; thus, minimizing the cost of power electronic devices. Further, the control strategy can be widely adjusted since the slip angle is adaptable in a typical range of +/- 30 % from the operational speed around the synchronous speed [Abad et al., 2011]. The MPPT control is usually designed by considering the wind speed, rotor speed, output power, and pitch angle. One simple control strategy consists of tracking the electromagnetic torque vs Low Shaft Speed (LSS) curve; thus, it allows the system to reach the MPPT using the natural dynamic response by ISC [Abad et al., 2011], [Bedoud et al., 2015]. In this article, an ISC strategy for a DFIG wind turbine in order to attain the MPPT is presented. For this simulation, a 1.5 MW wind turbine using Matlab-Simulink and FAST software has been selected [(NREL), 2020], [MathWorks., 2018].

The amount of available energy that is finally extracted by the wind turbine directly depends on both the wind speed and other important factors related to its construction and characteristics. Inertia is very important to consider for modelling the corresponding dynamics of the system as well as all the parameters that allow estimating the output power as explained in [Bedoud et al., 2015]. As a result, the power extracted from the wind can be expressed as:

$$P = \frac{1}{2}\rho C_p(\lambda, \beta) A V_w^3 \tag{2.1}$$

$$\lambda = \frac{w_r R}{V_w} \tag{2.2}$$

Where P is the mechanical power of the rotor ($Watt$), V_w is the wind speed (m/s), ρ is the air density (kg/m^3), C_p is the rotor power coefficient, $A = \pi R^2$ is the swept area (m^2), R is the distance from the centre of the rotor to the end of the length of the blades (m), w_r is the angular velocity of the rotor (rad/s), β is the pitch angle of the blades ($degrees$) , λ is the TSR which is defined as the relationship between the speed of the tip of the blades and the speed of the wind over the rotor.

2.1.3 Mechanical System

The mechanical representation of a wind turbine to achieve a more precise response of its dynamic behaviour against wind fluctuations can be approximated as a two-mass power-train model [Uluyol et al., 2011] as detailed in Figure 2.3. From this representation, applying Newton's second law of motion to its free-body diagram, the dynamic equations of the mechanical system are extracted [Michalke, 2008]. The relationships between units are considered:

$$w = \frac{d\theta}{dt} = \dot{\theta} \; \dot{w} = \frac{d\dot{\theta}}{dt} = \ddot{\theta} \tag{2.3}$$

$$N = \frac{\dot{\theta_{hs}}}{\dot{\theta_{ls}}} = \frac{\theta_{hs}}{\theta_{ls}} = \frac{T_{ls}}{T_{hs}} \tag{2.4}$$

$$J_r\ddot{\theta_r} + D_{ls}(\dot{\theta_r} - \dot{\theta_{ls}}) + K_{ls}(\theta_r - \theta_{ls}) + D_r\dot{\theta_r} = T_r \tag{2.5}$$

$$J_g\ddot{\theta_g} + D_{hs}(\dot{\theta_g} - \dot{\theta_{hs}}) + K_{hs}(\theta_g - \theta_{hs}) + D_g\dot{\theta_g} = -T_g \tag{2.6}$$

$$J_r\ddot{\theta_{ls}} - D_{ls}(\dot{\theta_r} - \dot{\theta_{ls}}) - K_{ls}(\theta_r - \theta_{ls}) = -T_{ls} \tag{2.7}$$

$$J_g\ddot{\theta_{hs}} - D_{hs}(\dot{\theta_g} - \dot{\theta_{hs}}) - K_{hs}(\theta_g - \theta_{hs}) = T_{hs} \tag{2.8}$$

where, θ_r and θ_g are respectively the angular positions of the rotor and the generator $\dot{\theta_r}$ and $\dot{\theta_g}$ are respectively the angular speeds of the rotor and the generator (rad/s); $\ddot{\theta_r}$ and $\ddot{\theta_g}$ are the angular accelerations of the rotor and the generator correspondingly (rad/sec^2); J_r and J_g are the moments

of inertia of the rotor and the generator (kg/m^2); T_r and T_g are respectively the aerodynamic torque of the turbine and the electromagnetic torque of the generator (Nm); D_{ls} and D_{hs} are the equivalent damping coefficients defined on the low speed and high speed axis correspondingly (Nms/rad); K_{ls} and K_{hs} are the equivalent stiffness coefficients defined in the low speed and high speed shaft respectively (Nm/rad) and N is the gearbox ratio that joins the low and high speed shafts.

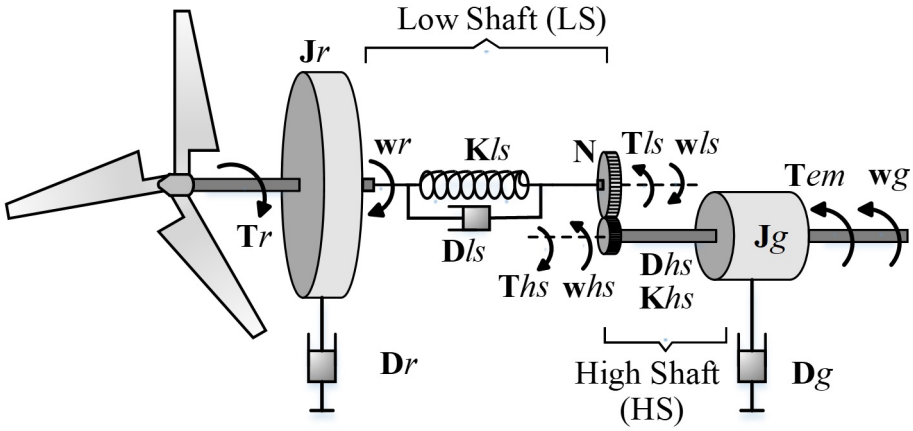

Figure 2.3: Two mass mechanical model of the wind turbine.

Assuming as negligible the gearbox inertia, as well as the global damping and rigidity coefficients of the rotor and the generator, the terms $\ddot{\theta_{hs}}$, $\ddot{\theta_{ls}}s$, D_r and D_g are removed from the movement expressions. With this consideration, and rearranging the Eqs. 2.5, 2.6, 2.7, 2.8; the following expressions are defined:

$$J_r\ddot{\theta}_r = T_r - T_{ls} \tag{2.9}$$

$$J_g\ddot{\theta}_g = -T_g + T_{hs} \tag{2.10}$$

Relating Eqs. 2.9 and 2.10 with the gearbox factor N, Eq. 2.4 and dividing the angular acceleration of the generator $\ddot{\theta}_g$, we obtain the simplification:

$$J_r + N^2 J_g = \frac{T_r - NT_g}{\dot{w}_r} \tag{2.11}$$

where, the total moment of inertia of the mechanical system is given by:

$$J_{total} = J_r + N^2 J_g \tag{2.12}$$

2.1.4 Electrical System

The electrical operation of the DFIG can be expressed and analysed in more detail by means of the Park transform to simplify the analysis, making use of a two-component orthogonal rotating reference frame d-q, separating the rotor and stator parts as shown in Figure 2.4. The corresponding mathematical representation is defined from the voltage equations, according to the literature in: [Ben Amar et al., 2017], [Bakouri et al., 2014], and [Bharti et al., 2015].

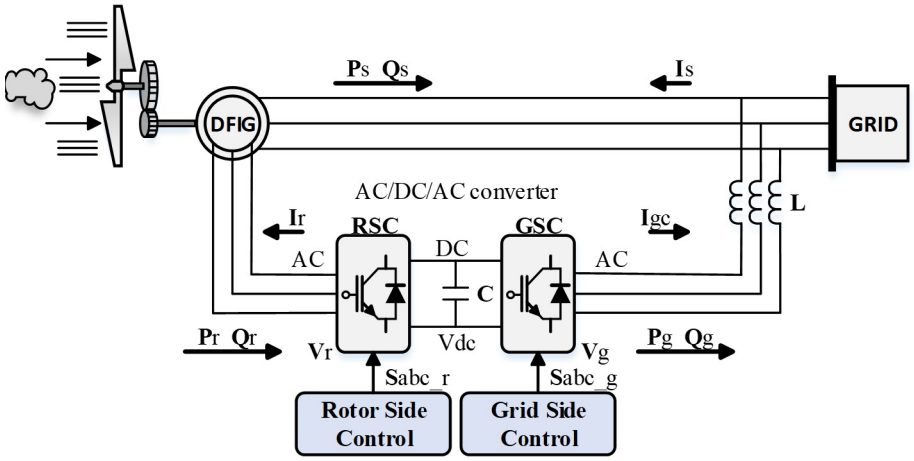

Figure 2.4: Electrical model of a DFIG based wind turbine.

$$V_{ds} = R_s i_{ds} + \frac{d\varphi_{ds}}{dt} - w_s \varphi_{qs} \tag{2.13}$$

$$V_{qs} = R_s i_{qs} + \frac{d\varphi_{qs}}{dt} + w_s \varphi_{ds} \tag{2.14}$$

$$V_{dr} = R_r i_{dr} + \frac{d\varphi_{dr}}{dt} - w_r \varphi_{qr} \tag{2.15}$$

$$V_{qr} = R_r i_{qr} + \frac{d\varphi_{qr}}{dt} + w_r \varphi_{dr} \tag{2.16}$$

and the flux is expressed due to the magnetic decoupling of the d and q axes as:

$$\varphi_{ds} = L_s i_{ds} + M i_{dr} \tag{2.17}$$

$$\varphi_{qs} = L_s i_{qs} + M i_{qr} \tag{2.18}$$

$$\varphi_{dr} = L_r i_{dr} + M i_{ds} \tag{2.19}$$

$$\varphi_{qr} = L_r i_{qr} + M i_{qs} \tag{2.20}$$

The impedances of the electrical model are presented in Eqs. 2.21 and 2.22:

$$L_s = L_{ls} + M \tag{2.21}$$
$$L_r = L_{lr} + M \tag{2.22}$$

where, V_{ds}, V_{qs},V_{dr} and V_{qr} are the voltages of the stator and of the rotor in the reference frame d-q; i_{ds}, i_{qs},i_{dr} and i_{qr} are the stator and rotor currents in the d-q frame; R_s and R_r are the stator and rotor resistances; M is the mutual inductance; L_s and L_r are the stator and rotor inductances and L_{lr} and L_{ls} are the rotor and stator leakage inductances respectively. Electromagnetic torque and reactive power of the stator are given by Eq. 2.23 and 2.24 in [Boukhezzar and Siguerdidjane, 2009], [Ouezgan et al., 2017]:

$$T_{em} = \frac{3}{2}\rho\frac{M}{L_s}(\varphi_{qs}i_{dr} - \varphi_{ds}i_{qr}) \tag{2.23}$$
$$Q_s = \frac{3}{2}(V_{qs}i_{ds} - V_{ds}i_{qs}) \tag{2.24}$$

where ρ is the pair of poles of the DFIG. It should also be noted that the electro-magnetic torque and reactive power are negative because the machine behaves as generator.

From Eq. 2.23, according to [Ouezgan et al., 2017], it can be noted that the components qd of the rotor current are fundamental in the control of the DFIG, since they are directly proportional, i_{qr} to the electromagnetic torque and i_{dr} to the reactive power. Therefore, using these variables, it is possible to control the torque of the machine and consequently its speed, as well as the reactive power. Also, as indicated in [Ohiero, 2015], there is the possibility to control the speed of the machine from the rotor or stator side. This operating principle is followed for the incorporation of the proposed controller, acting on the rotor side for speed control, with effects on torque, power, and current.

2.2 Control of Variable Speed Wind Turbines

Wind turbines usually use the PI controller since the dynamics of the system requires a rapid response rather than reduction of maximum values. In this context, the general expression for the PI controller is presented in Eq. 2.25.

$$u(t) = K_p e(t) + K_i \int_0^t e(t) + K_d \frac{de(t)}{dt} \tag{2.25}$$

There are three controllers mainly implemented on wind turbines: brake, yaw and pitch controller. Brake control is mainly used for emergency or maintenance operations. It can also stop the wind turbine when the wind is critically high and pitch control is not able to reduce the rotor speed. Yaw control allows to operate the wind turbine following the direction of the wind in order to maximize power extraction as well as reducing stress of the mechanical system. The pitch controller rotates wind turbine blades at different angles to increase or decrease the speed of the rotor. Currently the controllers can even manipulate the inclination of each blade independently. This advantage gives greater versatility since having more combinations of positions can reduce the stress on the blades.

The rotation of the angle is controlled as shown in Figure 1.1 by a proportional integrative controller PI that generates a reference rate of speed change. The angle of inclination itself is obtained by integrating the variation of the angle [Mahmoud and Oyedeji, 2019].

The pitch controller is very important for a wind turbine because a mechanical control of the torque is needed in order to regulate the generator HSS which leads the reference to maintain optimum operating speed. This response is slow, but it is necessary in order to guarantee the nominal speed operation of the system and regulate the wind turbine once it enters into a full operation zone. The idea is to reduce the speed before it is necessary to apply the brake system which produces high friction.

2.2.1 Control of Wind Turbines and Speed Zones

The C_p indicates a reliable measure of the efficiency in the extraction of power, highlighting the fraction or percentage of kinetic energy of the incident wind on the blades, which is then converted by the turbine into useful mechanical energy. The C_p has a maximum range established by the Betz's limit at $C_p = 59.3\% = 0.593$ [Thongam and Ouhrouche, 2011], [Baldo, 2012], and it depends on both the pitch angle and the TSR [Abdullah et al., 2012].

During MPPT, as a desired situation in a wind turbine, the TSR reaches its optimum value λ_{opt}. To meet this condition in the face of wind variations, the rotor speed must be controlled in some way to keep track of the maximum operating point given by the relationship C_p and TSR [Abdullah et al., 2012], [Boukhezzar and Siguerdidjane, 2011]. The wind turbine torque is calculated from the Eq. 2.26 which is the base for DSC technique since the rotor torque T_r is related to the angular speed w_r and the mechanical power P:

$$T_r = \frac{P}{w_r} \tag{2.26}$$

The wind turbine operates, in accordance with the value of incident wind speed, within three zones or regions of operation, as shown in Figure 2.5, they correspond to zone of non-operation, the MPPT control region, and the pitch control region [Thongam et al., 2009a]. In this context, the operational speed range is limited, on one hand the cut-in wind speed from which the wind generator generates power; on other hand, the cut-out wind speed establishes the limit of the maximum speed that can be reached to protect the whole system [Hallak et al., 2018].

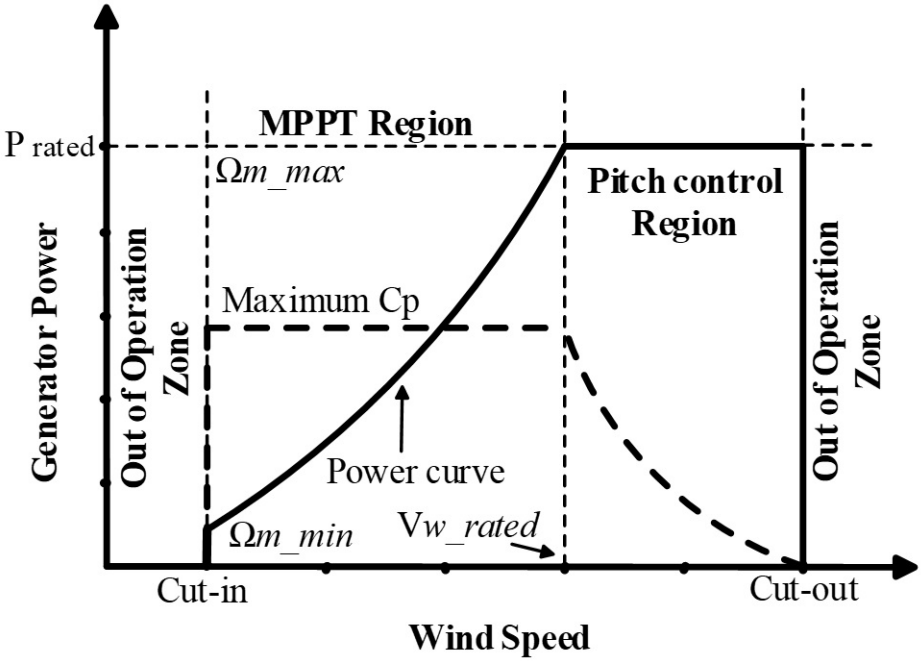

Figure 2.5: Operation zones of a wind turbine.

In this thesis, the simulations are considered to operate in Zone 2 which corresponds to the MPPT region since the objective is to maximize the power extracted from the wind at different speeds within the operating range. In this thesis, the rotor speed is controlled as a function of the rotor torque. The pitch angle is always kept at its minimum value to capture the maximum power of the wind. The control strategy is based basically on the variables of the wind turbine that can be accessed by sensors or estimated by any algorithm as shown in Figure 2.6.

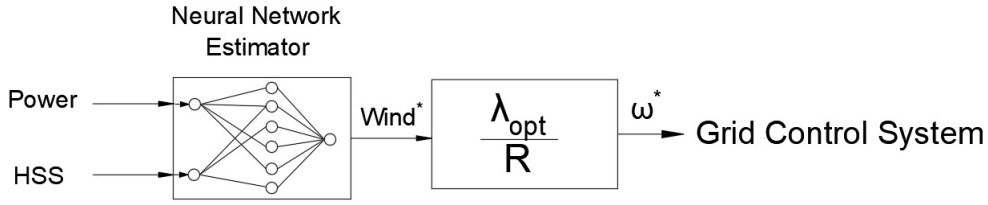

Figure 2.6: Artificial neural network estimator for MPPT.

2.2.2 Minimum and Maximum Speed Zones Control

First of all, it is necessary to define the type of generator. Once defined, the WECS can produce energy reducing mechanical fatigue and electrical faults. The MPPT represents the wind conditions where the highest amount of power can be extracted from wind. The C_p vs λ curve is used to represent this concept based on manufacturer information. The mathematical model can be achieved based on constants that are involved in the general C_p expression. In particular, Figure 2.7 shows the general C_p coefficient with respect to its relation with the λ parameter, using the simulation data provided in [Bedoud et al., 2015] with the following parameters: $c_1 = 0.5176$, $c_2 = 116$, $c_3 = 0.4$, $c_4 = 5$, $c_5 = 21$, and $c_6 = 0.0068$ resulting in a $C_{pmax} = 0.48$ and $\lambda_{opt} = 8.1$.

According to Quincy and Liuchen [Thongam and Ouhrouche, 2011] there are mainly three algorithms for finding this MPPT: PSF based on optimum torque control, HCS based on the maximum power control, and TSR based on the optimum tip speed control. PSF provides a power reference based on the load or grid side electric characteristics and then the inverter is configured to maximize the power extraction. HCS applies an intelligent memory method using techniques such as "search-remember-reuse" algorithm in order to find the maximum wind power extraction without the need to know the parameters of the wind turbine or the electrical load/grid connection. Finally, TSR method allows for production of the maximum power by measuring or estimating the wind speed and the generator rotational speed. Additionally, it is required knowledge of the optimum TSR operational point.

There are different characteristics to be considered to calculate C_p in Eq. 2.1 which has been taken from [Mohammadi et al., 2014]. Note that for specific turbine models there can be variations of this expression:

$$C_p = 0.5176\left(\frac{116}{\lambda_i} - 0.4\beta - 5\right)\exp\left(\frac{-21}{\lambda i}\right) + 0.0006795\lambda \tag{2.27}$$

where, λ_i is equal to Eq. 2.28 and β is the pitch angle:

$$\lambda_i = (\frac{1}{\lambda + 0.08\beta} - \frac{0.035}{(\beta^3 + 1)})^{-}1 \tag{2.28}$$

By knowing the C_p expression, it is possible to calculate every point of its curve in real time during power generation. Moreover, using Eq. 2.27 it is possible to establish the variable inputs and outputs for the controller design to stabilize the C_p at a desired point. Considering that pitch angle allows the wind turbine to speed up, it is important to control by establishing a relationship between the wind speed and the pitch angle. Therefore, a general pitch angle mathematical expression can be obtained using a trigonometrical expression taken from the general blade design procedure [Castellani et al., 2014] presented in Eq. 2.29.

$$\frac{\partial}{\partial_\beta}(sin^2\beta(cos\beta - \lambda sin\beta)(sin\beta + \lambda cos\beta) = 0) \tag{2.29}$$

After some simplifications the optimum relative wind angle also known as pitch angle for a local TSR is reduced to Eq. 2.30:

$$\beta = \frac{2}{3}tan^{-1}(\frac{v_m}{w_r R}) \tag{2.30}$$

Usually, the generator speed is intended to remain constant to produce constant voltage and power. However, when TSR is applied w_r may change as well. That means that the frequency may vary. However, stand-alone loads do not affect dc link but the total amount of delivered power must be set to constant. However, if this method is intended to be connected to a grid the output power signal must be connected thought a converter.

The consideration for inertial forces at the generator is explained in [Thongam and Ouhrouche, 2011]. The valid input for this algorithm is the measured power P_m which depends on the applied torque T_f, the wind turbine angular speed w, the overall electrical efficiency of the system from generator input to inverter output η, which represents the most important variable:

$$P_m = P_{load} + T_f w + wJ\frac{dw}{dt} = \frac{1}{\eta}P_{out} + T_f w + wJ\frac{dw}{dt} \tag{2.31}$$

Eq. 2.31 indicates the amount of power that is produced and in terms of angular speed and more importantly how the inertial forces $J\frac{dw}{dt}$ can add extra power to the system.

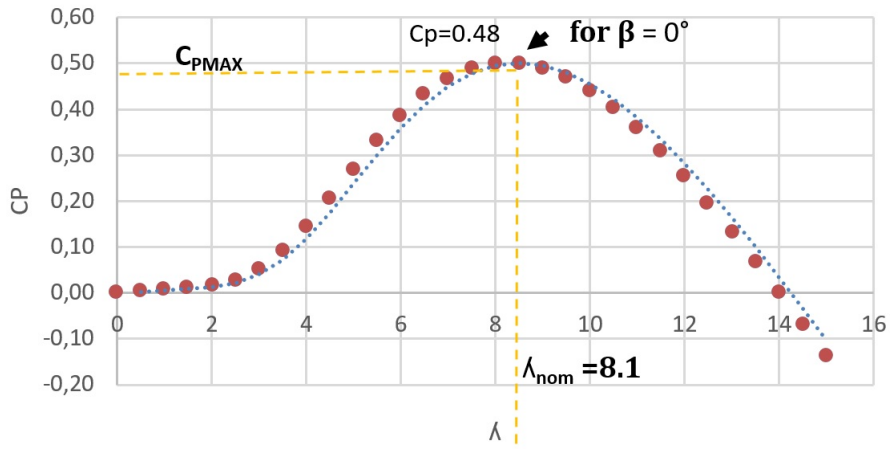

Figure 2.7: Performance coefficient C_p versus TSR λ at $\beta = 0$.

Once the power is determined, any MPPT strategy should be able to track rapidly the variations over the C_p. The points should be tracked and analysed in order to modify the electric characteristics of the generator in order to adjust the electric model and modify the resulting C_p. These effects are shown in Figure 2.8.

2.2.3 Maximum Power Tracking Control Basics

Some manufacturers must perform multiple experiments in order to obtain the appropriate power coefficient curves depending on the TSR and pitch angle. This is because the efficiency of the turbine depends on all possible losses in mechanical and electrical components. This process is very challenging because the wind is a fictitious model that usually is a representation of the real wind speed and direction. This is difficult to measure because the presence itself of the wind turbine tower, nacelle and blades produce shadow effects that alter the measurements of the sensors. Moreover, the implementation of sensors along the blades is difficult because it affects the aerodynamic efficiency. Consequently, the maximization of the power generation must be performed analysing the components that are involved in the electric model. For instance, the electric generator must rotate at a nominal speed also involving a certain level of torque. The power electronic converters are used to couple the voltages and frequencies of the grid with the one present at the generator. This operation also allows to control the reactive and active power direction flow and level.

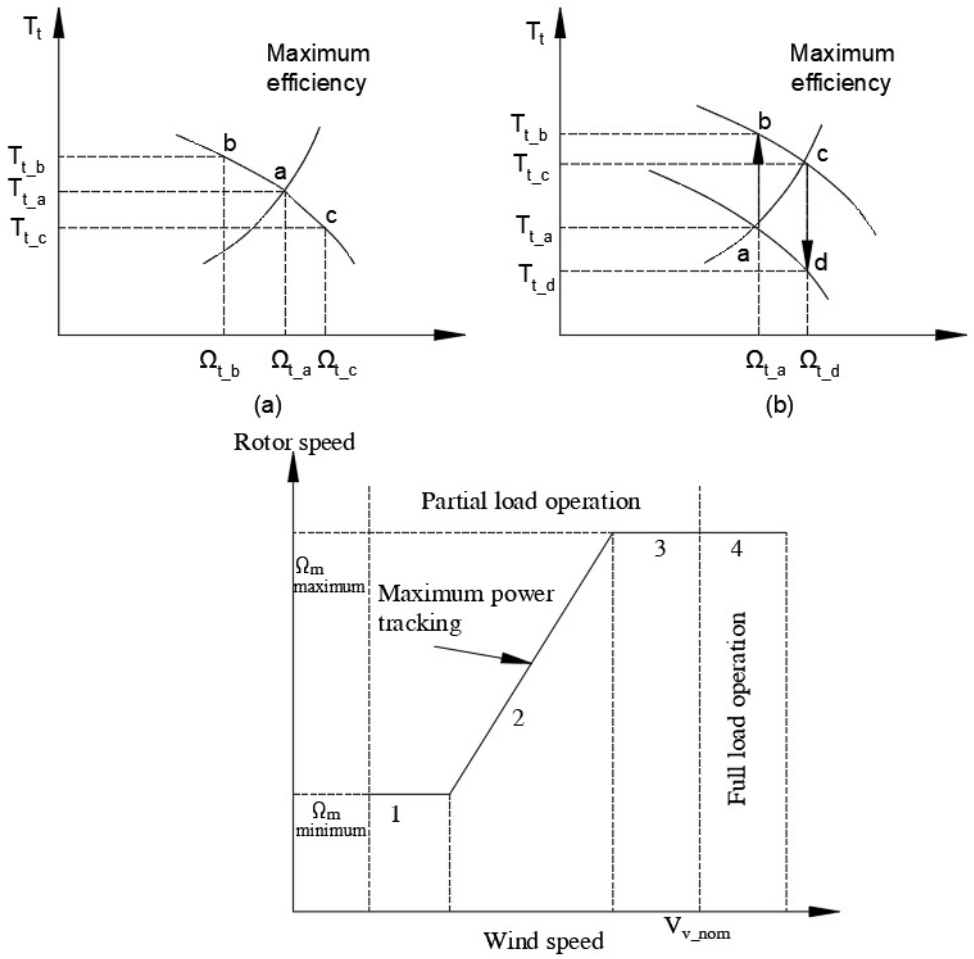

Figure 2.8: Minimum and maximum speed zones control varying from (a) to (b) because of a change in conditions such as pitch angle.

2.3 MPPT Control Strategies for Wind Turbines

This section presents the most common control strategies depending principally on the type of generator and variables to be measured and controlled in order to achieve the MPPT. For instance, rotor and wind speed among other mechanical and electrical characteristics are usually used for control. The aerodynamic model is also important as well as the size of the generator among other characteristics. For instance, the wind farm which is usually modelled as a single unit can be observed in Figure 2.10.

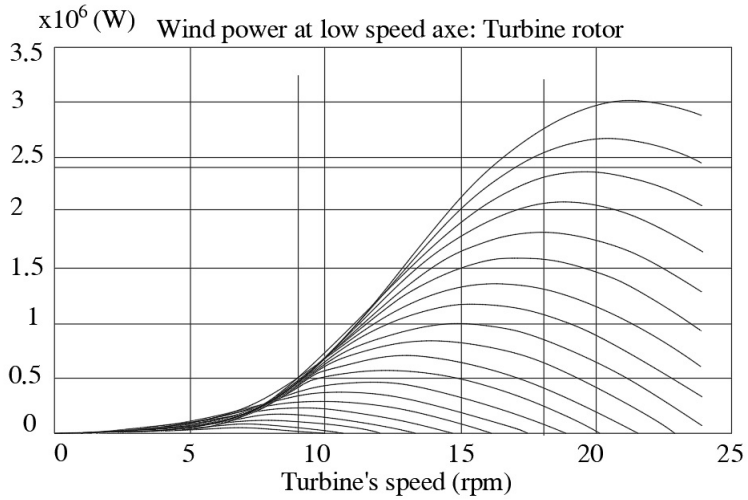

Figure 2.9: Characteristic curves C_p vs TSR.

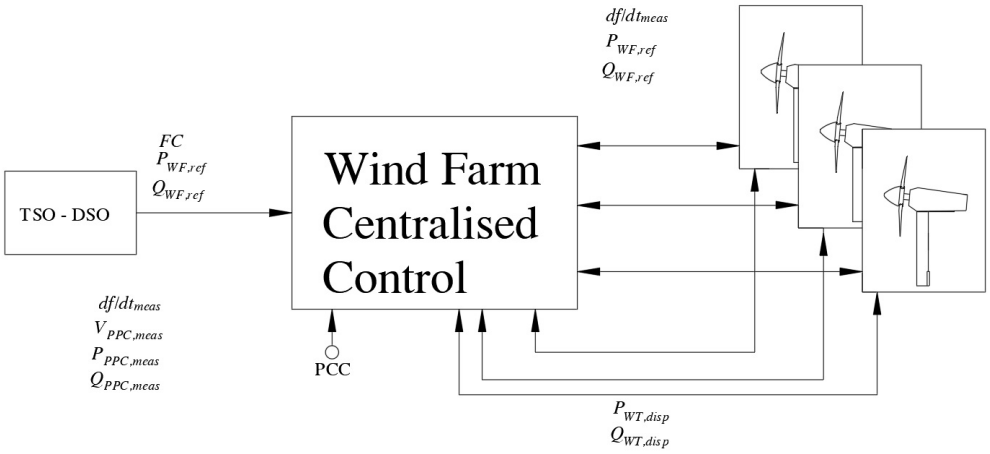

Figure 2.10: Wind farm centralised control model.

2.3.1 Tip Speed Ratio Control

TSR method is a control technique for MPPT which regulates the rotor angular speed in order to maintain the TSR into the optimum value. The speed variation rate is wind speed and angular speed dependent, so both of these variables need to be measured by sensors and fed into the controller. The general scheme for TSE is presented in Figure 2.11. For PMSG wind turbines, the TSR MPPT control is achieved using estimations of the wind speed in terms of the mechanical power and the rotor speed. The configurations of an Artificial Neural Network (ANN) is presented in Figure 2.6. The power

electronics converter configuration applied to a PMSG is presented in Figure 2.12. The mechanical power P_m can be modelled using Eq. 2.32 where w_r is the rotor speed, J is the inertia and P_e is the mechanical losses:

$$P_m = w_r(J\frac{dw_r}{dt}) + P_e \tag{2.32}$$

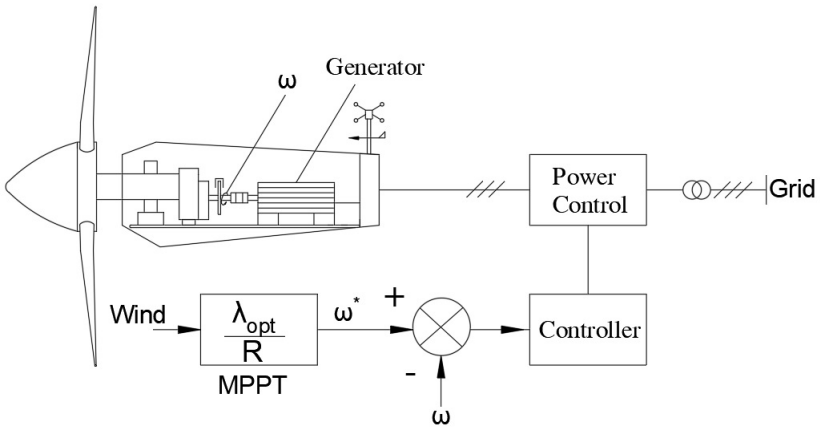

Figure 2.11: Tip speed ratio control strategy.

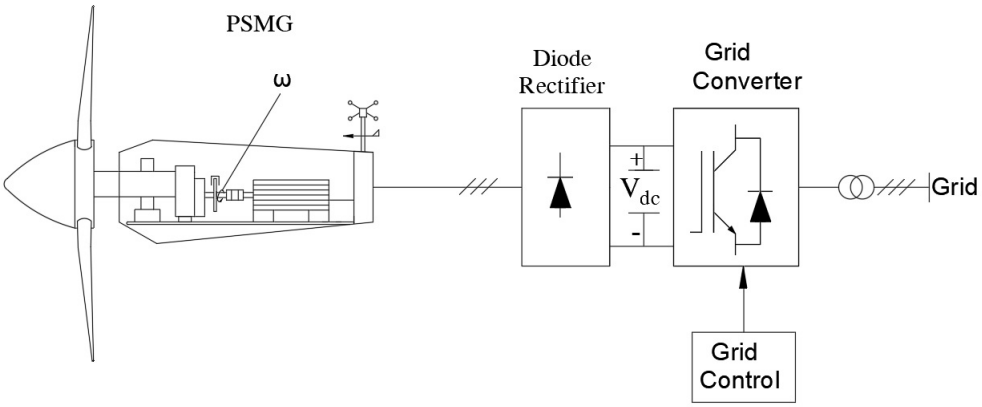

Figure 2.12: PMSG wind energy conversion system control.

For SCIG wind turbine, the TSR MPPT control requires a fully back to back converter using Pulse With Modulation (PWM) in order to allow the power extraction maximization similarly to the PMSG control. The general scheme is presented in Figure 2.13.

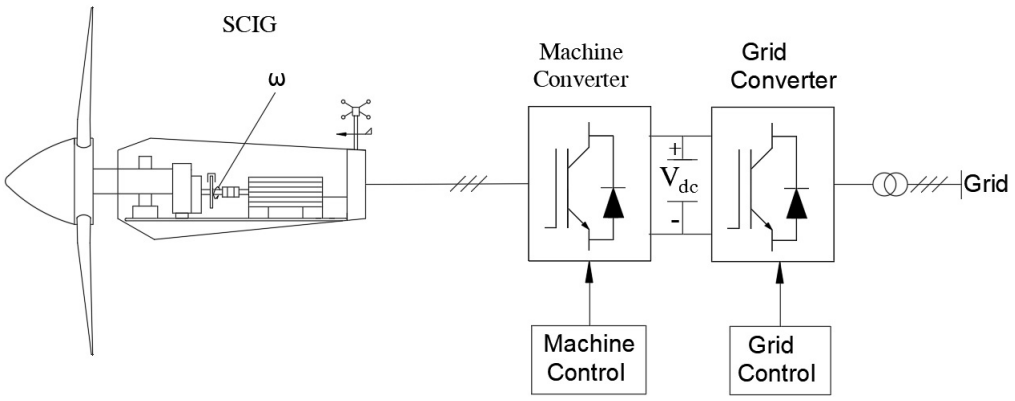

Figure 2.13: Squirrel cage induction generator control.

For DFIG wind turbine, the TSR MPPT control requires a different configuration compared to the PMSG and the SCIG. The back to back converter is connected to the rotor windings only which allows the converter using PWM to reduce the amount of power to be driven in order to allow the power extraction maximization for the overall system. The general scheme is presented in Figure 2.14 and the control strategy is presented in Figure 3.4.

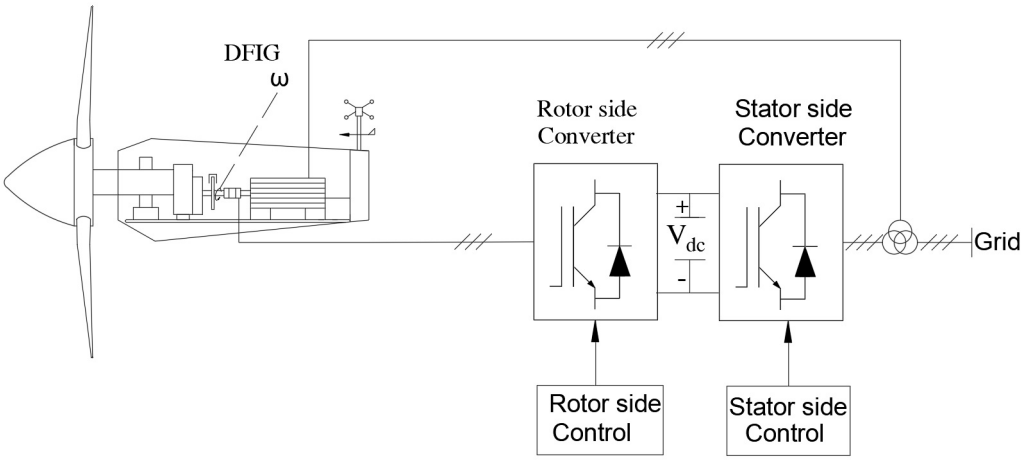

Figure 2.14: DFIG wind turbine general scheme.

2.3.2 Power Signal Feedback Control

The PSF control is another technique used in order to perform MPPT for wind turbines. For this technique, the simulations are required to obtain off

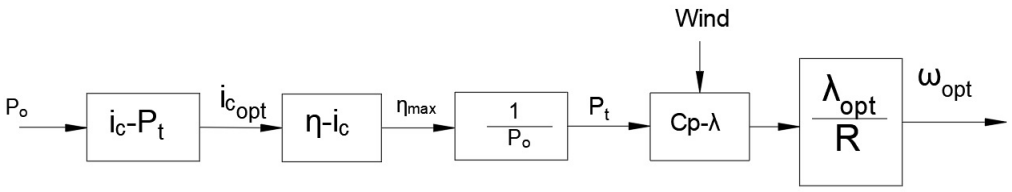

Figure 2.15: Optimum speed command control block diagram.

line tests in order to generate the $C_p$vs TSR curves in terms of output power and angular speed. The general scheme for PSF is presented in Figure 2.16.

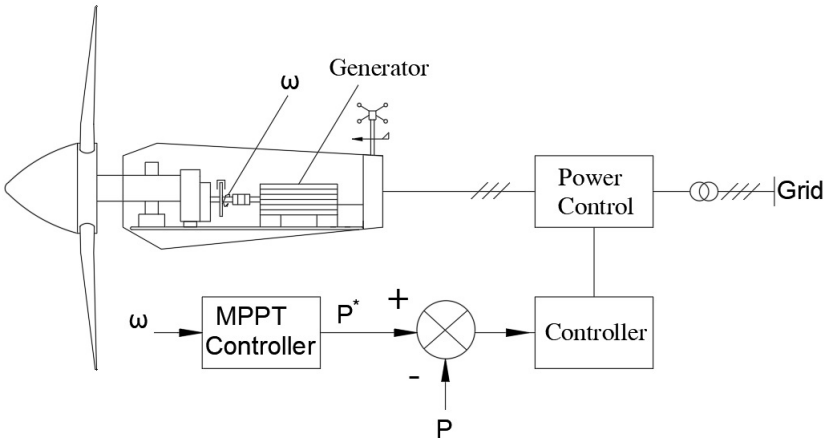

Figure 2.16: Power signal feedback control strategy.

For PMSG based wind turbines, the control follows a general scheme based on the calculation of the optimal power P_{opt} which depends only on an optimal constant K_{opt} and the rotor speed w_r as shown in Eq. 2.33 and Figure 2.17. The power electronics converter configuration applied for a PMSG is presented in Figure 2.18:

$$P_{opt} = (K_{opt})({w_r}^3) \tag{2.33}$$

For DFIG wind turbine, the PSF MPPT control requires a different configuration compared to the PMSG and the SCIG. The back to back is connected to the rotor windings only which allows the converter using PWM to reduce the amount of power to be driven so as to allow the power extraction maximization for the overall system. The control strategy has been presented in [Thongam and Ouhrouche, 2011] using a Takagi-Sugeno-Kang

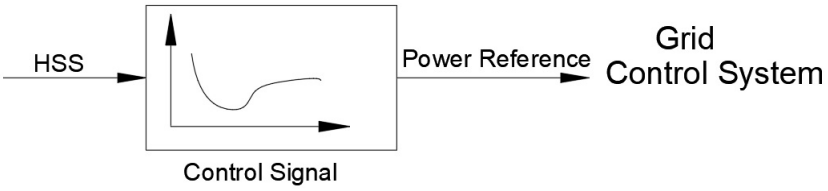

Figure 2.17: Power signal feedback control reference.

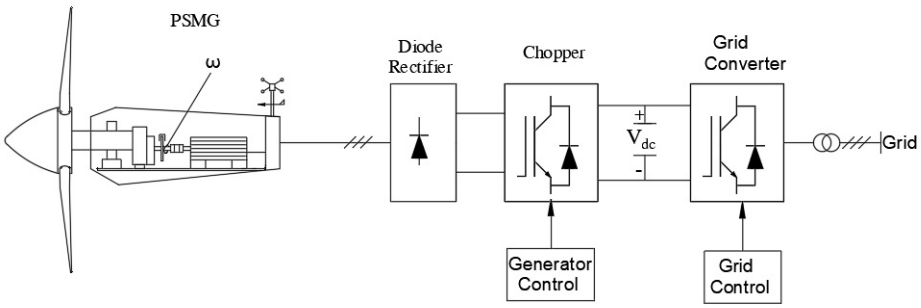

Figure 2.18: PMSG wind energy conversion system control.

(TSK) fuzzy model for maximum power extraction including two inputs such as the generated power, the HSS and the output is the power reference signal. The general scheme is presented in Figure 2.14 and the control strategy is presented in Figure 2.19. The controller tracks the variations starting at a specific point A, and then point B is calculated in order to provide the corresponding angular speed. The Turbine Power vs the Rotor Speed is presented in Figure 2.20.

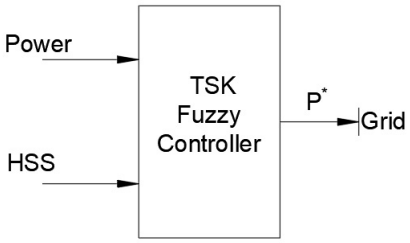

Figure 2.19: Takagi-Sugeno-Kang (TSK) MPPT control fuzzy model.

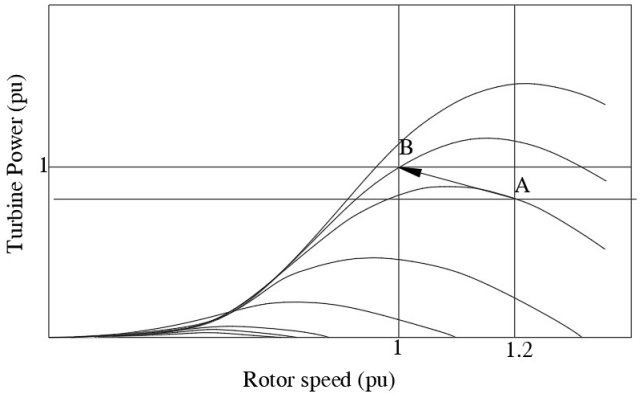

Figure 2.20: Turbine power curves.

2.3.3 Hill Climb Search Control

The MPPT control using P&O algorithm is a technique based on the derivative of the output power curve. In [Ayala and Simani, 2019] a PMSG low inertia HCS MPPT control is proposed. This method is similar to the hill climb searching algorithm proposed in [Wang and Chang, 2004]. The P&O method is implemented using a state machine as shown in Figure 2.27 where the initial values are updated each cycle. The general scheme is presented in Figure 2.21 and 2.23 where the HCS tracks the MPPT based on time dependent perturbations generated by the algorithm. The power electronics converter configuration applied for a PMSG is presented in Figure 2.22 and the control block diagram is presented in Figure 2.24.

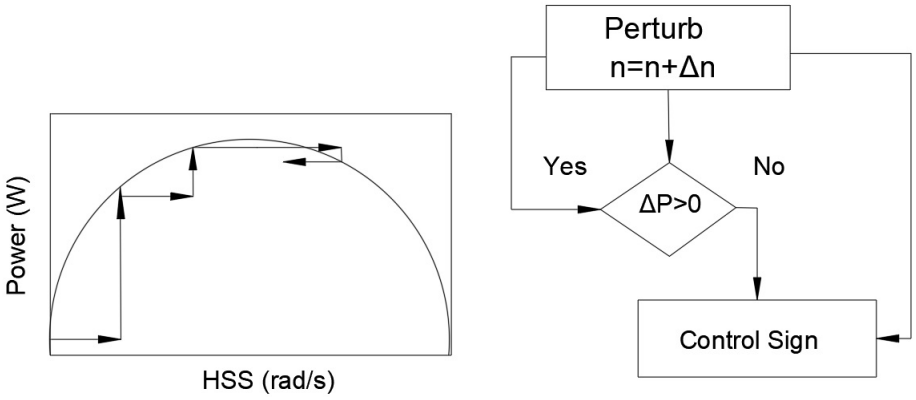

Figure 2.21: Hill climb search control strategy.

First of all, the algorithm verifies if the MPPT algorithm is activated

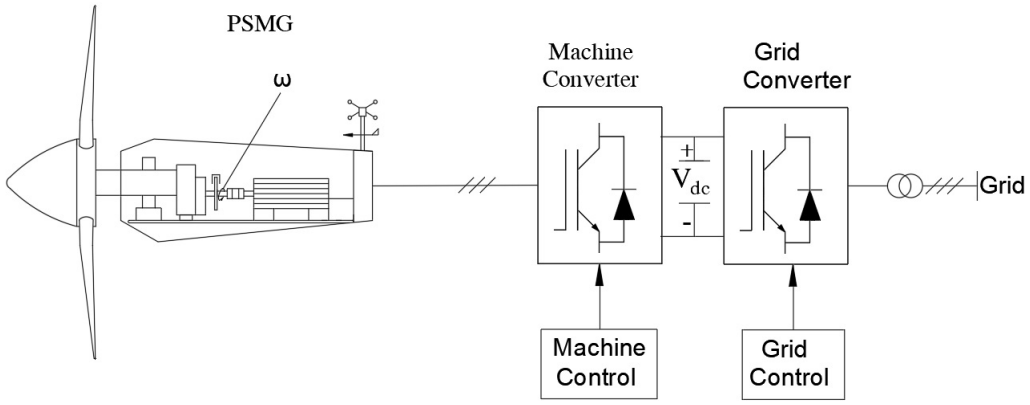

Figure 2.22: PMSG wind energy conversion system control.

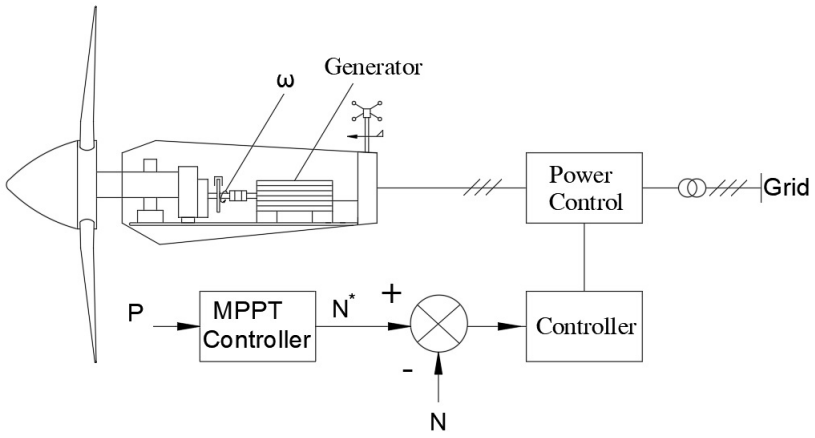

Figure 2.23: Hill climb search control strategy.

by selecting a bit that is set to 1 or 0. Then, in the next stage the initial voltage parameters are defined to initiate the controller. In the next stage, the algorithm proceeds to calculate the power by multiplying the measured voltage and current. The derivative of the power and voltage are calculated and then the algorithm decides if the actual value is increased or decreased based on the reference value of voltage. These values are stored for establishing the maximum and minimum limit of reference voltage that the controller can reach [MathWorks, 2017].

For a SCIG, the $C_p$response improves when using a fuzzy logic controller as presented in [Thongam and Ouhrouche, 2011]. The control block diagrams and the logic converter are presented in Figure 2.25 HCS control strategy for

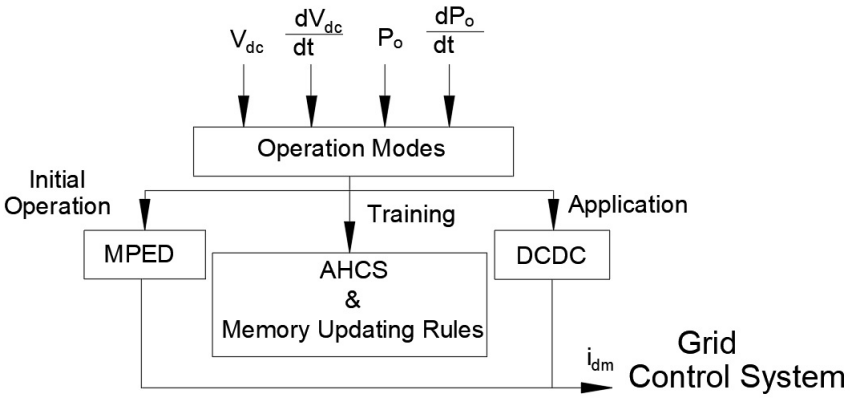

Figure 2.24: Hill climb search control architecture .

low inertial wind turbines. This is because the increase of $C_p$depends on the wind speed and the capability of correcting the mechanical losses.

Moreover, the $C_p$decreases progressively when the wind speed is reduced drastically which does not depend on the MPPT strategy purely [Mohammadi et al., 2014]. It is important to note that initial power and voltage values, ΔV, ΔP are considered null but after the system starts to measure values, the register stores data which is updated continuously every clock cycle. This method is widely applied for solar applications. For instance, a similar algorithm can be found in [Banu and Istrate, 2017] for solar panels MPPT control.

For the DFIG, the converter power system is then configured using Space Vector Control (SVC) considering the voltage grid signal characteristics. The system also allows for synchronization of the generator frequency and the grid. It is important to consider that constant wind speeds produce a more reliable $C_p$since the algorithm is not required to make multiple iterations. In other words, the more stable the wind speed that is present at the blades, the more power can be extracted from the generator using this technique. The sliding mode for MPPT control has been proposed in [Thongam and Ouhrouche, 2011] and the general block diagram is presented in Figure 2.26. For these simulations, the presented control diagram are displayed in Figure 2.26.

On the other hand, another methodology is presented in Figure 2.27 which is a particular case of study for HCS presented in [Thongam et al., 2009b].

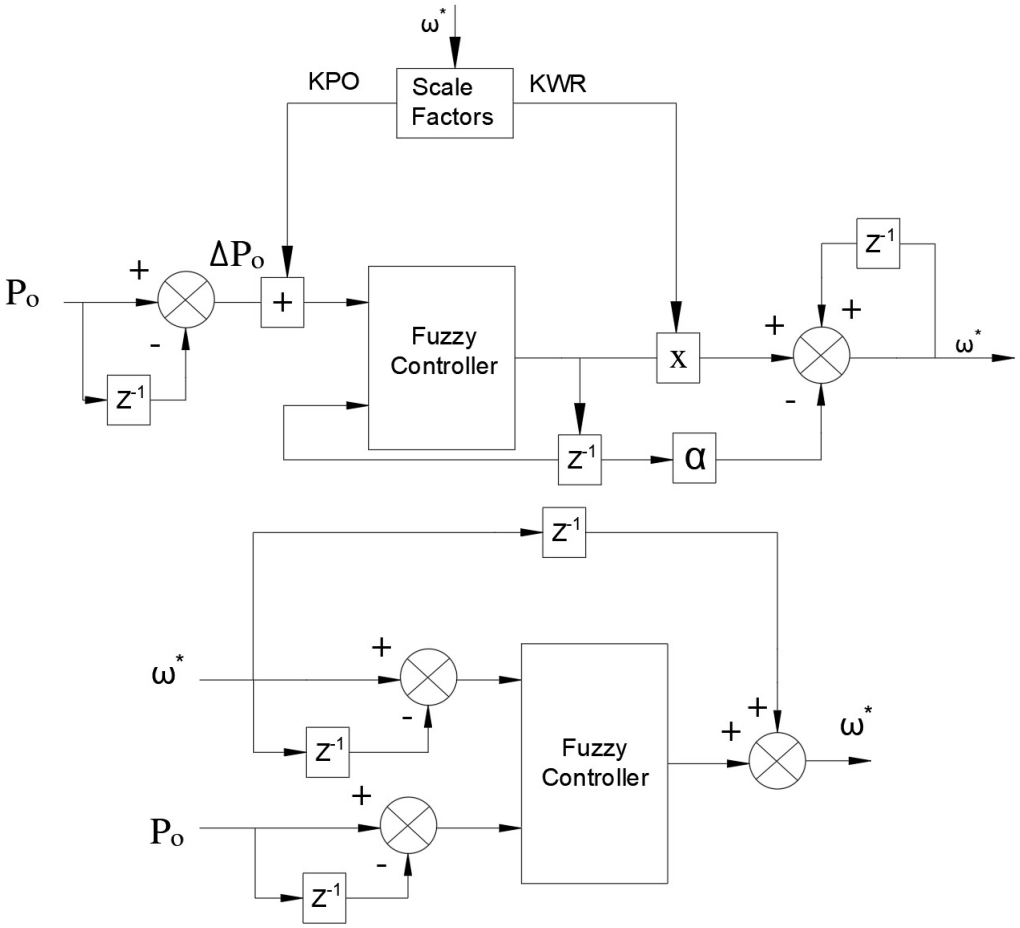

Figure 2.25: Control block diagram of fuzzy logic MPPT controller.

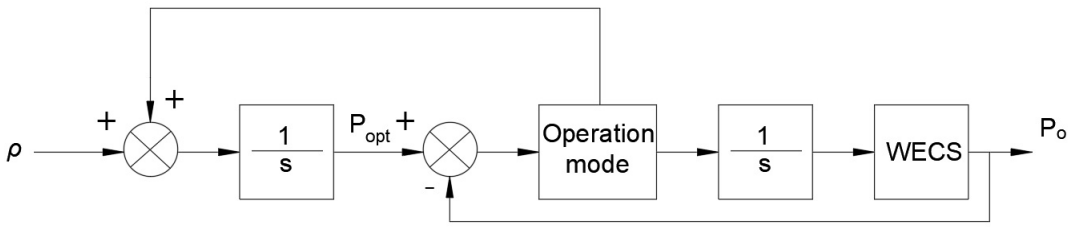

Figure 2.26: Sliding mode HCS MPPT control for a DFIG wind turbine.

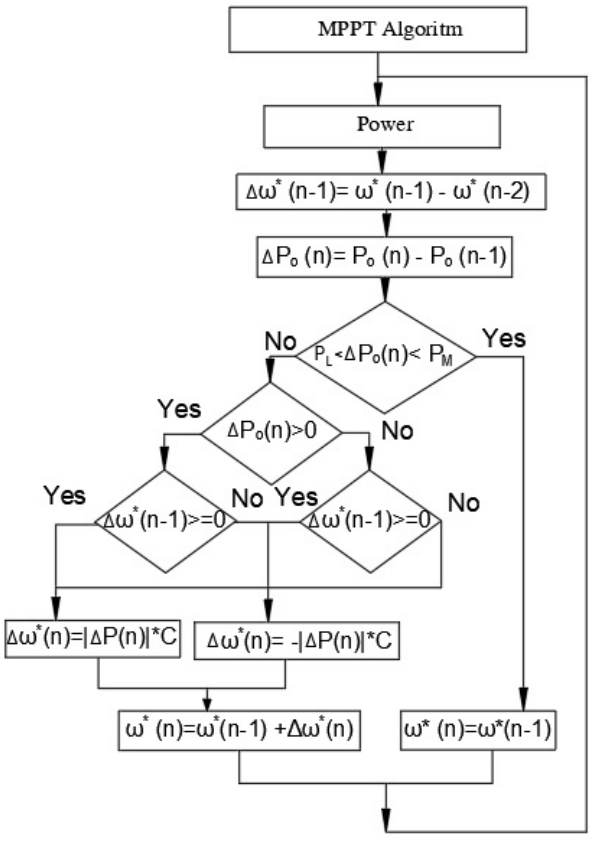

Figure 2.27: Hill climb search control for PMSG wind energy conversion system.

Chapter 3

Doubly Fed Induction Generator System

Wind turbines with DFIG configurations are very popular nowadays because the electric generator is able to produce high amounts of energy controlled by the rotor through slip rings. According to M. Rashid, the DIFG also known as Wound-Rotor Induction Generator (WRIG) is a type of induction generator which requires a small slip speed range allowing the cost reduction of power electronic converters for wind turbines. This is one of the most important advantages of this configuration as well as its ability to output power without overheating when the nominal power is exceeded. Moreover, the MPPT can be tracked over sub and super synchronous speeds making it suitable for high power applications. The general diagram of a DFIG is presented in Figure 3.1 where it can be seen how the rotor can be accessed externally in order to control the entire system.

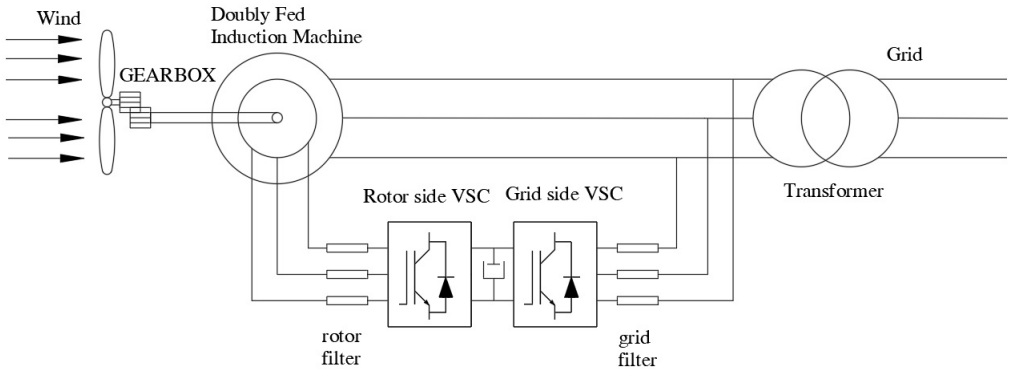

Figure 3.1: Doubly fed induction generator general diagram.

3.1 DFIG Overview

The DFIG generator has two three-phase winding arrangements: one placed on the stator and the other on the rotor. These two three-phase windings must be fed independently; however, they can be powered bidirectionally. The three-phase rotor windings can be connected in a star or delta configuration and are fed by the brushes and the collector assembly. The DFIG rotor requires a proper maintenance plan due to deterioration of the brushes and slip rings [Abad et al., 2011].

Therefore, the stator is made up of three windings at 120 degrees each. When these three stator windings are fed by a frequency balanced three-phase voltage f_s, the stator flux is induced. This stator flow rotates at a constant speed. That is, the synchronous speed n_s is given by Eq. 3.1:

$$n_s = \frac{60 f_s}{\rho} (rev/min) \tag{3.1}$$

According to Faraday's law, the stationary rotational flux induces an electromagnetic field in the rotor windings as described in Eq. 3.2:

$$e_{ind} = (v \times B) \cdot L \tag{3.2}$$

where:

e_{ind} Electromagnetic field induced in the rotor windings
v Difference between rotor speed and stator electromagnetic field
B Stator flux density vector
L Conductor length

A current is induced in the rotor windings due to the induced voltage in them, as well as, the voltage that can be supplied externally by the brushes. According to Laplace's law, this rotor current creates an induced force transformed in electrical output power as described in Eq. 3.3:

$$F = i \cdot (L \times B) \tag{3.3}$$

where:

F Electromagnetic field induced in the rotor windings

i Difference between the Rotor speed and the stator electromagnetic field

L Conductor length
B Stator flux density vector

The control principle of the DFIG consists in connecting the grid or load directly to the stator windings and the rotor windings to the AC/DC/AC converter, thus allowing the controllability of all currents in the machine. This is very useful because the rotor speed can freely vary without affecting the output voltage frequency. The control strategy can be oriented to control either the current vector control or the Direct Torque Control (DTC) which is the most popular for electric motors because of it's stability especially for high reactive generator demands. The rotor usually has more turns of winding compared to the stator which cause the rotor voltage to increase while reducing the currents. The rotor speed then can be ±30% of the synchronous speed allowing flexibility during operations. On the other hand, the low the low current requirements are helpful for the converter cost reduction because about a quarter of the total produced power is fed to the grid or load through the converter and the rest is fed directly from the stator. Moreover, the conversion rate for other machines is 1 $p.u.$ which demands a complex and costly EMI filter system. There are multiple techniques that can be applied for DFIG MPPT control described in the following subsections. The general scheme for the MPPT control strategy is shown in Figure 2.10.

3.2 DFIG Electric Characteristics

The DFIG state equivalent electrical circuit can be ideally simplified by assuming that both the stator and rotor are connected in star (Y) configuration; however, only one phase of the three-phase stator and rotor windings is depicted. The stator is mainly powered at a constant and balanced three-phase AC voltage amplitude and frequency, the rotor is also powered at a constant and balanced AC voltage independent of the stator. Finally, in order to represent the magnitudes of voltage and current in steady state, the analysis is carried out using classical phasor theory.

3.2.1 DFIG Electrical Model

The DIFG electrical model can be obtained from the general induction machine model represented in Figure 3.3 including the inductance and resistances in the stator and the rotor. From this scheme, it is possible to establish the input impedance which is very important for determining the currents and voltages in the entire system as detailed in Eq. 3.5. Moreover, the power

factor angle is represented in Eq. 3.6.The output power can be controlled by the variations in the rotor resistance as shown in Eq. 3.4 [Rashid, 2014]:

$$P_d = \frac{3R'_r V_s^2}{s[(R_s + \frac{R'_r}{s})^2 + (X_s + X'_r)^2]} \tag{3.4}$$

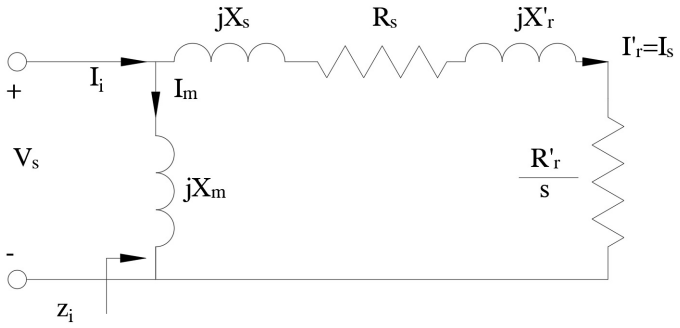

Figure 3.2: Approximate per-phase equivalent circuit of a general induction generator.

$$Z_i = \frac{-X_m(X_s + X'_r) + jX_m(R_s + \frac{R'_r}{s})}{R_s + \frac{R'_r}{s} + j(X_m + X_s + X'_r)} \tag{3.5}$$

$$\Omega_m = \pi - tan^-1\frac{R_s + \frac{R'_s}{s}}{X_s + X'_r} + tan^-1\frac{X_m + X_s + X'_r}{R_s + \frac{R'_r}{s}} \tag{3.6}$$

The DFIG electrical model considers not only the stator side but also the rotor side as shown in Figure 3.3 where the inductances, resistances, currents, voltages and fluxes are calculated based on the circuit analysis as explained in Eq. 3.7, 3.9, and 3.11:

$$\underline{\psi_s} = L_m(\underline{I_s} + \underline{I_r}) + L_{\sigma s}\underline{I_s} = L_s\underline{I_s} + L_m\underline{I_r} \tag{3.7}$$
$$\underline{\psi_r} = L_m(\underline{I_s} + \underline{I_r}) + L_{\sigma r}\underline{I_r} = L_m\underline{I_s} + L_r\underline{I_r} \tag{3.8}$$

$$L_s = L_m + L\sigma s \tag{3.9}$$
$$L_r = L_m + L\sigma r \tag{3.10}$$

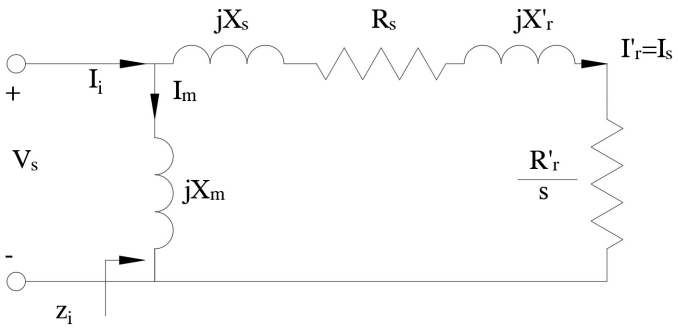

Figure 3.3: Approximate per-phase equivalent circuit of a DFIG.

$$\underline{V_s} - R_s\underline{I_s} = j\omega_s\underline{\psi_s} \tag{3.11}$$

$$\underline{V_r} - R_r\underline{I_r} = js\omega_s\underline{\psi_r} \tag{3.12}$$

In order to obtain the stator and rotor currents and voltages it is important simply to analyse the electric characteristics of the electric model, and applying Kirchhoff's current and voltages laws it is possible to determine the relations presented in Eqs. 3.13, 3.14 and 3.15:

$$\underline{V_s} - \underline{E_s} = (R_s + X_{\sigma s})\underline{I_s} \tag{3.13}$$

$$\underline{V'_r} - \underline{E'_{rs}} = (R'_r + X'_{\sigma r})\underline{I'_r} \tag{3.14}$$

$$I'_r = \frac{V_s}{[(R_s + \frac{R'_s}{s})^2 + (X_s + X'_r)^2]^{\frac{1}{2}}} \tag{3.15}$$

Once the rotor current is calculated, the output torque is determined in terms of output power (considering that mechanical and electrical power are equal). This output power in terms of angular rotor speed is shown in Eq. 3.16:

$$T_d = \frac{w_r}{P_m} \tag{3.16}$$

$$T_d = \frac{3R'_r V_s^2}{s\omega_s[(R_s + \frac{R'_r}{s})^2 + (X_s + X'_r)^2]} \tag{3.17}$$

3.3 Power Electronic DFIG Control

This section describes the most important features of a converter which is based on a two-level device. The converters are described developing models considering ideal switches. Additionally, various pulse generation strategies are analyzed. One of the most common MPPT control techniques used for DFIG is the optimum torque control which basically allows for control of the output torque based on the track of the angular speed and the corresponding torque. The torque is also recomputed following the dynamic system including an optimal constant for the case of ISC and a dynamic value for the DSC strategy. The general control scheme for optimum torque control is sketched in Figure 3.4.

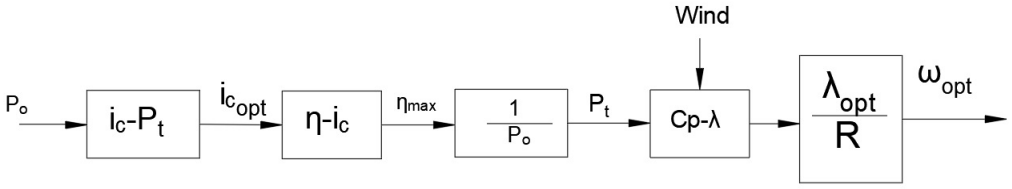

Figure 3.4: Optimum torque control block diagram.

3.3.1 Machine and Grid Side Control

The grid-connected system is composed of the grid-side converter, the grid-side filter and the grid voltage signals. The operating diagram is shown in Figure 3.1. The grid-side converter is modelled by ideal bi-directional switches, which convert voltage and currents from DC to AC, while the power exchange can be in both directions from AC to DC (rectifier mode) and from DC to AC (inverter mode).

It should be emphasized again that this chapter treats the controlled switches in an ideal way, without considering losses or efficiencies of the elements (such as switching time or voltage drops). When a more robust filter is needed, the implemented one includes capacitors which guarantees better filtering. The mains voltage is normally supplied through a transformer. This AC voltage is assumed to be balanced and sinusoidal.

3.3.2 Gate Controlled Semiconductors Switching

The electronic converter requires a versatile switching semiconductor. For simulation analysis the switching element is considered ideal which means

that no critical loses are included for analysis. Moreover, as described in the previous sections, the rotor power drives about a quarter of the total output power. For the simulation in this thesis, the switching element used is the IGBT. The ideal switch is usually implemented via a power transistor with an anti-parallel diode to allow current to flow in both directions. The activation sequence follows a vector state allowing the conversion from DC to AC based on the grid requirements as shown in Figure 3.5. The triggering sequence depends on the control strategy. Nowadays, the space vector representation of the power converter IGBT's activation sequence is more commonly utilized because it allows to operate at high frequencies driving high amounts of power. The space vector activation sequence is displayed in Figure 3.6. Moreover, the triggering signals are shown in Figure 3.7. The activation sequence is analysed as signals in Table 3.1.

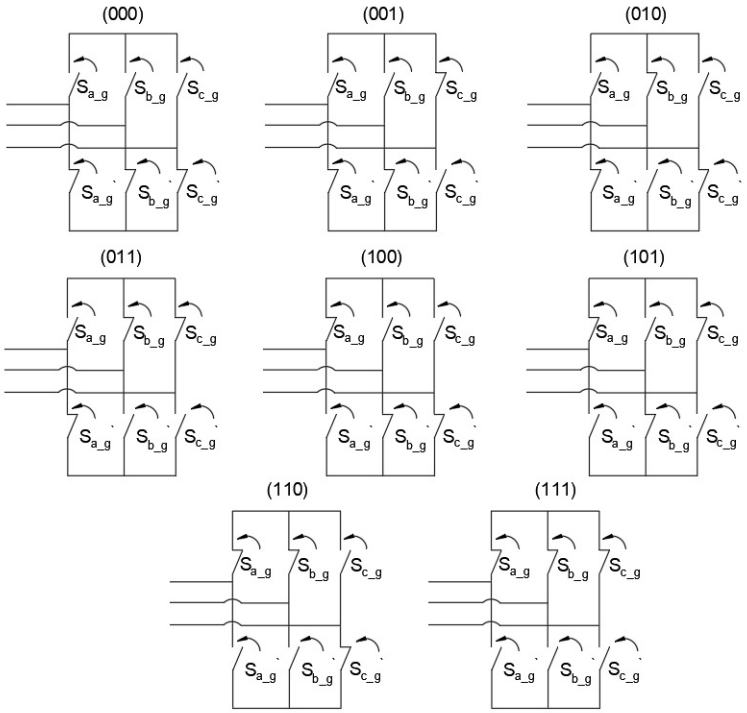

Figure 3.5: Electronic diagram of the power converter IGBT's activation sequence.

The sequence can be generated also in terms of α and β components which allows for representation of the output voltages dynamic phasors in terms of a frame for linear representation. This frame can be also represented using vectors as displayed in Figure 3.7 and the on off states as well as the voltage

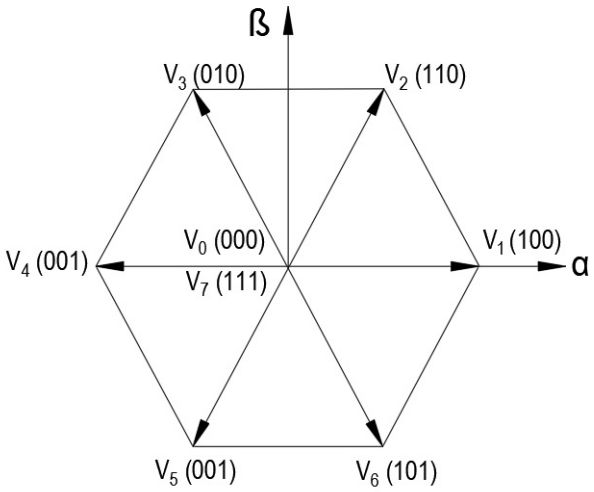

Figure 3.6: Space vector representation for the power converter.

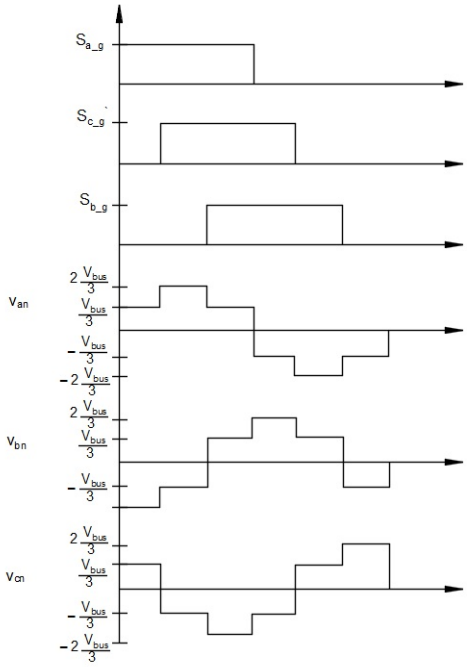

Figure 3.7: Voltage vs time gate activation of the power converter IGBT's activation sequence.

maximum values with load and non load configurations can be observed in Table 3.1.

Table 3.1: Space vector representation of the power converter IGBTs activation sequence.

S_{ag}	S_{bg}	S_{cg}	V_{ao}	V_{bo}	V_{co}	V_{an}	V_{bn}	V_{cn}
0	0	0	0	0	0	0	0	0
0	0	1	0	0	Vbus	-Vbus/3	-Vbus/3	2/3 Vbus
0	1	0	0	Vbus	0	-Vbus/3	2/3 Vbus	-Vbus/3
0	1	1	0	Vbus	Vbus	- 2/3 Vbus	Vbus/3	Vbus/3
1	0	0	Vbus	0	0	2/3 Vbus	-Vbus/3	-Vbus/3
1	0	1	Vbus	0	Vbus	Vbus/3	- 2/3 Vbus	Vbus/3
1	1	0	Vbus	Vbus	0	Vbus/3	Vbus/3	- 2/3 Vbus
1	1	1	Vbus	Vbus	Vbus	0	0	0

Chapter 4

ISC and DSC Control of the DFIG

In this section it is described the ISC and DSC strategies for the DFIG wind turbine simulations.

4.1 FAST Integration with Simulink

FAST is a software developed by NREL [NREL, 2005] which integrates aerodynamic models to control models to allow time-domain coupled nonlinear aero-hydro-servo-elastic simulation of the wind turbine elements. FAST allows the analysis of a variety of wind turbine configurations, including two or three bladed horizontal or vertical axis rotor, pitch or stall regulation, rigid or oscillating hub and downwind rotor or wind coming from different directions. Moreover, it allows the description of: the mechanical gearbox components' characteristics, torque, inertia, angular speed, and electrical variables. Thus, the wind can be modelled as a detailed signal including information of the direction, speed, and amplitude variations.

The aerodynamic model uses the wind speed signal input data allowing for computation of rotor wake effects that is very common in wind farms. It also considers loads of blade elements including dynamic stall. The electrical and control system models simulate the drivers, blade pitch sensors and actuators, generator torque, nacelle and other control devices, as well as the generator and power converter components. Structural dynamics models apply the reactions of the electrical and control system, apply aerodynamic and hydrodynamic loads, add gravitational loads, and simulate the elasticity of the rotor, transmission, and support structure. Coupling between all models is achieved through a modular interface.

FAST allows for modelling of a wind turbine as a composition of rigid and flexible elements. For example, two-blade turbines are modelled as four rigid and four flexible bodies. The rigid bodies are the ground, the nacelle, the hub, and the tip brakes (point masses) whereas the four flexible bodies comprise blades, tower, and transmission system. The components of both flexible and rigid bodies include the following variables: tower bending, blade bending, nacelle yaw, rotor position, rotor speed, and driveshaft torsional flexibility. The tower bending has two modes, each in the front-to-back and side-to-side directions, and flexible blades have two modes of rotation and one edge per blade mode. In Figure 4.1, the FAST model [Gajewski and Pienkowski, 2016] implemented in Simulink [Barbade and Kasliwal, 2012] is represented to obtain a matrix of output variables which directly interact in the proposed controller model.

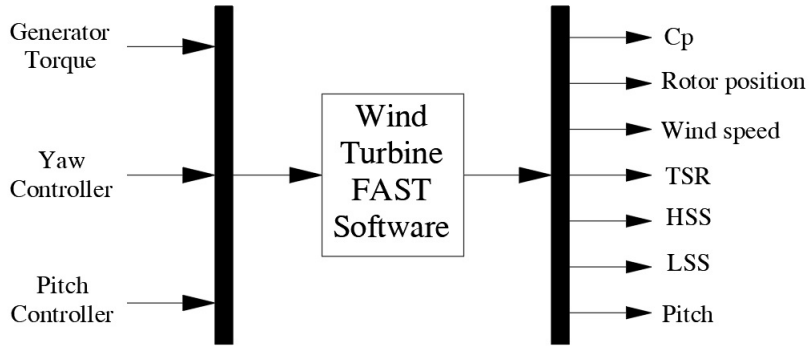

Figure 4.1: Simulink and FAST integration.

4.2 Indirect Speed Control

The ISC strategy is based on the relationship between the electromagnetic torque T_{em} and the angular velocity ω_t. Nonetheless, the relation between the electromagnetic torque and the angular velocity does not have a direct dynamic relationship due to the inertia involved. This leads to a much slower response of the system as the mechanical coupling is not cancelled [Abad et al., 2011]. The ISC modifies the dq frame currents in order to command the back to back converter allowing the controllability of the slip angle which also affects the speed and torque of the generator. The scheme to be implemented is shown in Figure 2.2.

When the wind turbine operates at optimal conditions, the parameters allow finding a constant value called K_{opt} which is used for the optimal electromagnetic torque reference calculation. The general description can be found in Eq. 4.1. According to [Abad et al., 2011], the ISC can be achieved by measuring the LSS and subtracting the mechanical losses as shown in Figure 2.2. The reference electromagnetic torque T_{em} is calculated in terms of K_{opt} and the LSS Ω_m. In Eqs. 4.2 and 4.3, it is shown how the K_{opt} is determined. The ISC strategy also considers the mechanical losses at the gearbox established including friction and damping factors [Wang and Chang, 2004], [Muller and Deicke, 2014]:

$$\lambda_{opt} = \frac{R\omega_m}{V_v}; C_p = C_{pmax}; C_t = C_{tmax} \tag{4.1}$$

$$T_{em} = \frac{1}{2}\rho\pi\frac{R^5}{\lambda_{opt}^3}C_{pmax}\Omega_m^2 = k_{opt}\Omega_m^2 \tag{4.2}$$

$$k_{opt} = \frac{1}{2}\rho\pi\frac{R^5}{\lambda_{opt}^3}C_{pmax} \tag{4.3}$$

For K_{opt} calculation it is necessary to establish the optimal TSR λ_{opt} and the corresponding C_{pmax}. These parameters can be either calculated experimentally or provided by the manufacturer. In this work, multiple simulations using Matlab-Simulink and FAST have been exploited to estimate λ_{opt}, C_{pmax} and compared to manufacturers specifications found in [Carrillo et al., 2013].

For the implementation of the proposed control algorithm, the angular velocity at low speed is initially considered, and together with Eq.4.3, the control module is carried out carried out, while importing the variables calculated in FAST [Bedoud et al., 2015]. It is worth noting that the controller has been designed in Matlab-Simulink. The implementation of the control loop is depicted in Figure 4.2.

For the calculation of i_{qr}, which feeds the PI control block, the expression of Eq. 4.4 is used. This expression is calculated from the generated electromagnetic torque [Mohammadi et al., 2014]:

$$T_{em} = -\frac{3}{2}\rho\frac{L_m}{L_s}\Psi_s i_{qr} \tag{4.4}$$

where, ρ = Generator pair of poles, Ψ_s = Stator frame flux, L_m = Mutual inductance and L_s = Stator inductance.

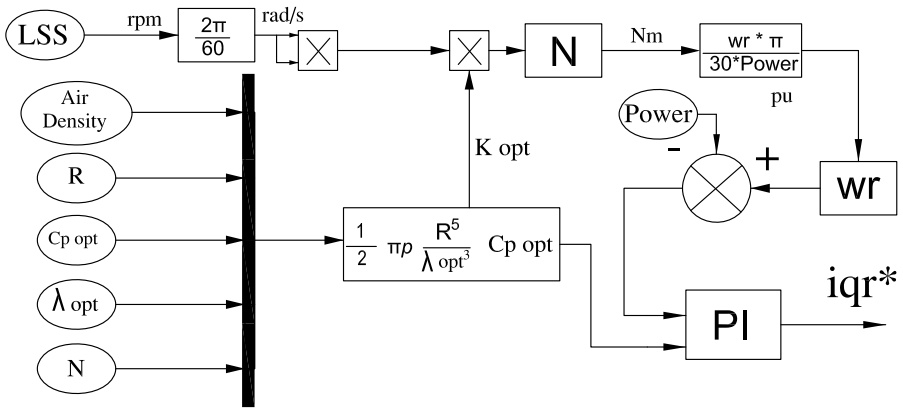

Figure 4.2: Indirect speed controller.

4.3 Direct Speed Control

In this section, the DSC MPPT strategies used for the thesis simulations are described.

4.3.1 System Dynamics and Control Model

The controller presented in the following considers the angular velocity of the rotor as input, and together with expression of Eq. 4.6, the electromagnetic torque is calculated. This calculated torque, by means of a state observer block, allows the generation of the estimated electromagnetic torque control signal to regulate the wind turbine output power [MathWorks., 2018], [Singh et al., 2014]. The dynamic system has internal conditions at determined points that are monitored by the state observer based on Luenberger structure. In order to define the control strategy, the observer may have a complete or reduced order depending on the monitored states. Once the estimated state data are computed, the signal error is calculated by the gain of the estimator which depends on the system. For these simulations, the gain is unitary as shown in Figure 4.3.

4.3.2 Luenberger Observer Control

The DSC has an advantage over other control methods that allows to follow the power curve with a much faster response. Knowing the TSR λ, the optimum wind turbine rotation speed ω_{opt} can be found from the wind speed v. Unfortunately, for the dynamic control model, v cannot be measured

because it is a fictitious variable or a representation of the total wind speed.

However, the optimum value of the rotational speed can be obtained from an estimate of the aerodynamic torque. A state observer and using magnitudes such as the electromagnetic torque T_{em} and the turbine rotation speed ω_t, directly linked to the measured signals, can be easily designed to calculate the estimated aerodynamic torque of the turbine [Abad et al., 2011]. Thus, from Eq. 4.5, at the optimal operating point has the following form:

$$\omega_m = N\sqrt{\frac{T_{est}}{k_{opt}}} \tag{4.5}$$

Once the rotational speed reference is generated, an MPPT controller regulates ω_t using the electromagnetic torque value T_{em}. The scheme to be implemented is shown in Figure 4.3.

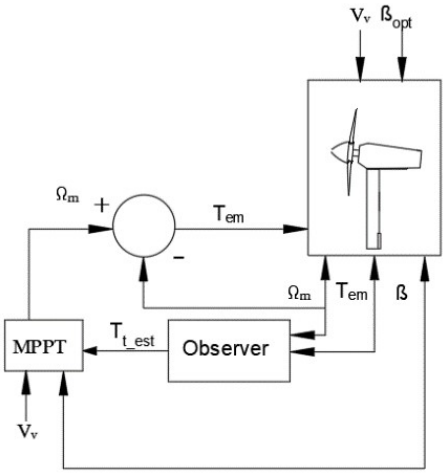

Figure 4.3: Direct speed control strategy

.

In this document the observer is implemented in an MPPT controller. When the C_{pmax} is at its maximum power point, the torque is calculated as shown in Eq. 4.6 [Abad et al., 2011]:

$$T_{est} = \frac{1}{2}\rho\pi\frac{R^5}{\lambda_{opt}^3}C_{pmax}\omega_t^2 = k_{opt}\omega_t^2 \tag{4.6}$$

Finally, we manipulate the above expression to have a relationship in terms of k_{opt}, as shown in Eq. 4.7:

$$k_{opt} = \frac{1}{2}\rho\pi\frac{R^5}{\lambda_{opt}^3}C_{pmax} \tag{4.7}$$

All the above expressions have been simulated in Matlab-Simulink, and for the aeroelastic wind model. On the other hand, the software FAST has been used for modelling a wind turbine as a combination of mechanical elements and their interactions. For this work, a three bladed turbine has been modelled as the combination of rigid and flexible elements [Hofmann and Okafor, 2001], [Singh et al., 2014].

The controller presented in Figure 4.4 considers the angular velocity of the rotor as input, and together with expression of Eq. 4.6, the T_{est} is calculated. This low shaft torque, by means of a state observer block, allows the generation of the estimated electromagnetic torque control signal to regulate the wind turbine output power [(NREL), 2020], [Singh et al., 2014].

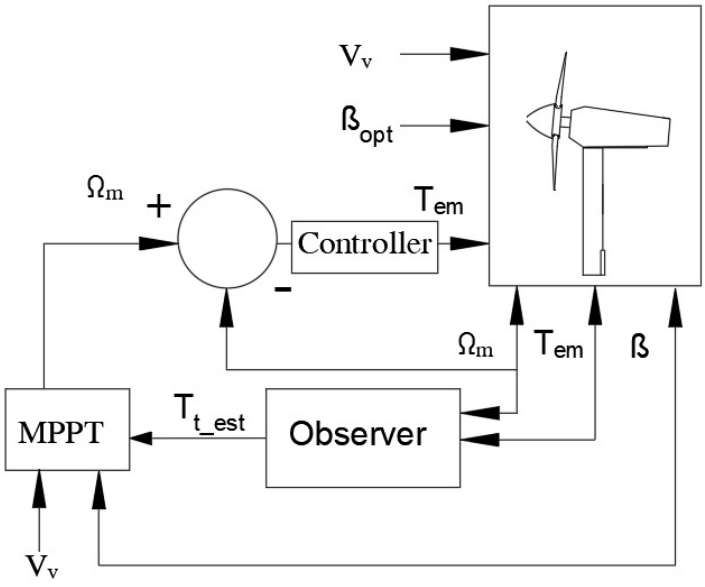

Figure 4.4: Direct speed control block diagram.

The dynamic system has internal conditions at determined points that are monitored by the state observer based on Luenberger structure. In order to define the control strategy, the observer may have a complete or reduced order depending on the monitored states. Once the estimated state data are computed, the signal error is calculated by the gain of the estimator which depends on the system. For these simulations, the gain is unitary

as shown in Figure 4.5, whilst in Figure 4.6 the implementation of the controller in Matlab-Simulink is illustrated. For the calculation of the current reference i_{qr} which feeds the PI control block, the following the expression of Eq. 4.8 is used and calculated from the generated electromagnetic torque [Mohammadi et al., 2014]:

$$T_{em} = -\frac{3}{2}\rho\frac{L_m}{L_s}\varphi_s i_{qr} \tag{4.8}$$

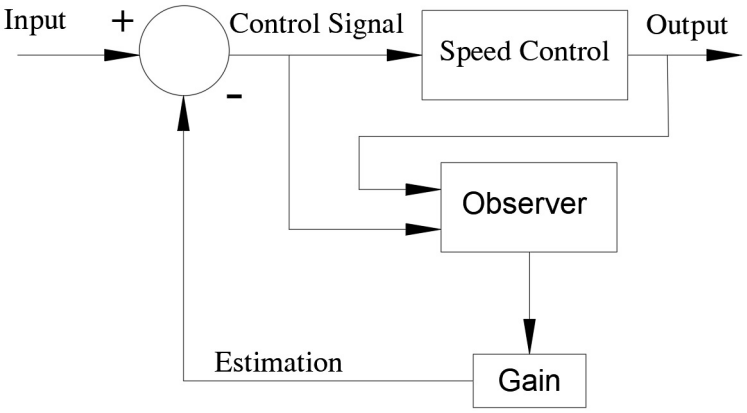

Figure 4.5: Feedback of observed states block diagram.

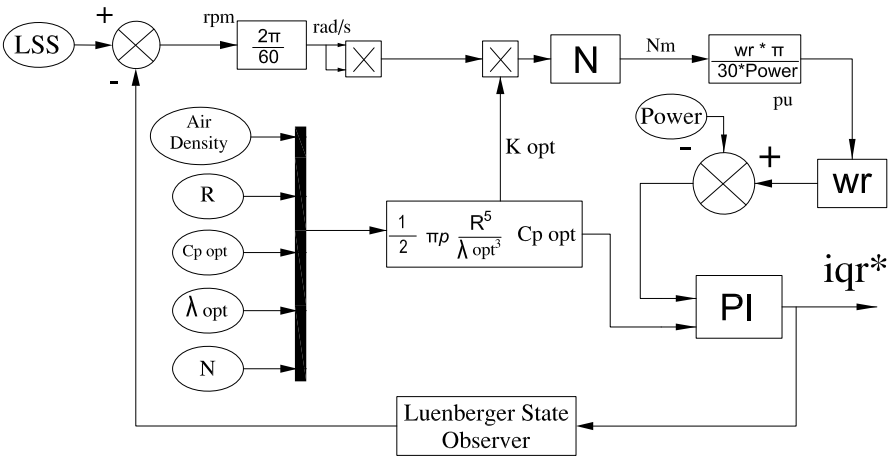

Figure 4.6: Direct speed controller implementation block diagram.

4.3.3 Takagi-Sugeno PI Controller

In many cases, due to the complex dynamics of the system to be controlled or the nature of the system, this methodology may not be the most appropriate, as it does not provide good results in the desired control. Therefore, as shown in this research, it should be replaced by a more effective method, to achieve a response that better satisfies the actual control.

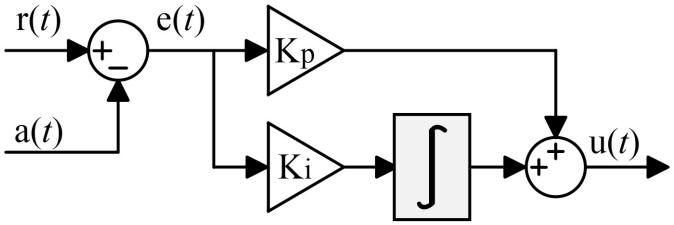

Figure 4.7: Digital PI controller block diagram

.

The PI control whose generic structure is shown in Figure 4.7 is continuously used in industrial processes and renewable energies. Moreover, it is exploited in the control of mechanical and electrical parameters of wind turbines such as TSR, pitch angle, currents, torques, speeds, voltages, powers and others. However, when considering the fluctuations of the wind speed, these parameters vary significantly, highlighting that the PI alone may not guarantee the stability of the system [Tahiri et al., 2018] and [Semrau et al., 2015].

The proposed control technique follows the operating principle of the DSC strategy. This methodology seeks to keep the TSR at its optimal value λ_{opt} in order to guarantee that the reference Ω_g is also the appropriate one. This allows the monitoring of the C_{pmax} with an estimate of the wind speed measurement through the behaviour of the electromagnetic torque and the power train. With this result, a new value of electromagnetic torque that controls Ω_g acting on the power and current references iq_{ref}, defined in the traditional DFIG control model [Abu-Rub et al., 2014]:

$$T_{opt} = K_{opt}\Omega_r^2 \tag{4.9}$$

Solving for Ω_r from Eq. 4.9 and translating this into the high-speed side, the reference Ω_g is obtained:

$$\Omega_g = N\sqrt{\frac{T_{opt}}{k_{opt}}} \tag{4.10}$$

In Eq. 4.10 it is evaluated the real torque value of the rotor, which depends on the dynamic conditions of the turbine and represents the optimum torque to be applied at each instant of time. Once the reference value of the generator speed is defined, it must be controlled therefore, a fuzzy controller is incorporated to change the value of the required T_{em} and acts on the PI power control. In this way, a new current reference i_{qr} is established, and the monitoring of C_{pmax} guarantees the maximum power extraction.

Following the operation process of the fuzzy control in order to guarantee an improvement in the extraction of maximum power, the design of the Mamdani controller model is defined as follows:

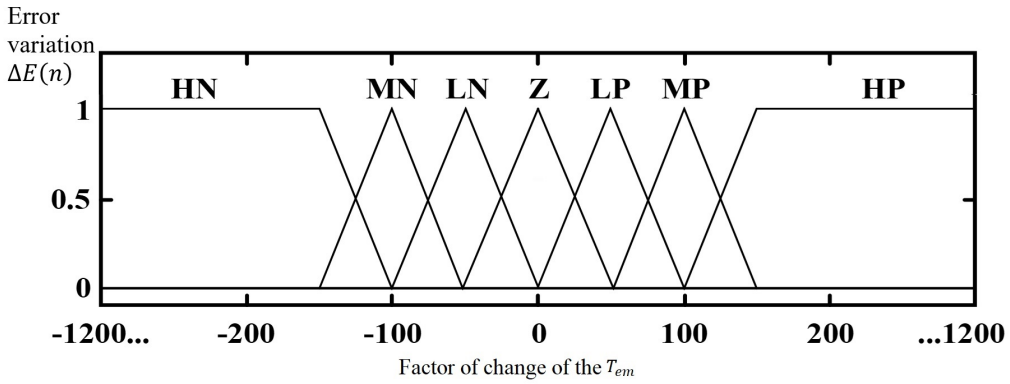

Figure 4.8: E(n) speed error membership functions.

Fuzzification: The numeric input variables are converted into the nomenclature of fuzzy logic called linguistic terms. In the control, the linguistic variables used as inputs are the speed error $E(n)$ of the generator (Figure 4.8) and the variation of the error $\triangle E(n)$, and, as output, a factor of change of the electromagnetic torque. For the 3 variables, 7 linguistic terms such as BN (Big Negative), MN (Medium Negative), SN (Small Negative), Z (Zero), SP (Small Positive), MP (Medium Positive), and BP (Big Positive) have been selected.

As membership functions, for each of the variables involved, triangular functions have been denoted for the linguistic terms MN, SN, Z, SP and MP; on the other hand, open trapezoidal functions at their ends for the linguistic terms BN and BP are used in order to complete the overall range of values from start to finish. After these these considerations, the degree of membership of each associated linguistic term is established.

Inference: Once defined the rules to control the system based on the designated inputs and outputs, the control response to the data is selected. Each rule is evaluated by following an $IF-THEN$ logic. By working with

Table 4.1: Fuzzy control rules

		Error variation E(n)						
		BN	**MN**	**SN**	**Z**	**SP**	**MP**	**BP**
Error E(n)	BN	BP	BP	MP	MP	MP	SP	Z
	MN	MP	MP	SP	SP	SP	Z	SN
	SN	MP	SP	Z	Z	Z	SN	SN
	Z	MP	SP	Z	Z	Z	Z	SN
	SP	MP	SP	Z	Z	SN	SN	MN
	MP	MP	Z	SN	SN	SN	MN	MN
	BP	SP	SN	MN	MN	MN	BN	BN

two input variables of 7 linguistic terms each, a set of 49 control rules is generated as shown in Table 4.1. For each entered group of data in the controller, a specific output, which is established through a control surface is obtained. The control surface is defined by the values of each rule representing the membership degrees and the linguistic terms.

Defuzzification: The final stage calculates the numerical output value for the system, such as the change in torque, by converting the linguistic terms obtained from the inference process. The present work exploits the centroid defuzzification method has been used as it is one of the most commonly used options. The new electromagnetic torque reference then acts on the power PI controller; in this way, this solution integrates the two controllers, *i.e.* the fuzzy logic and the PI structure for power control. Together, they generate the reference iq_{ref}, within the established limits in the function of the found electromagnetic torque.

Chapter 5

Simulations and Results

In this section, the dynamic response of the three proposed MPPT controllers is detailed using three types of wind input signals in order to validate the obtained results. In all cases, the wind turbine reaches the optimal operating point but there some considerations depending on the input signal and also the controller response. The following outputs are considered in order to evaluate the system dynamic response: reference signal i_{qr} in $p.u.$, the electromagnetic torque in Nm, the active output power in $Watt$, the wind input in m/s, the generator speed in rpm, the pitch angle in degrees, and the power coefficient id dimensionless. The tests input signals are referenced from [Jafarnejadsani and Pieper, 2015], [Palejiya and Chen, 2016] and [Ma et al., 2015].

Three different wind speed signals have been configured for analysis and validation in this research. These signals have been generated and imported into FAST where the outputs are calculated considering mainly partial load operations. The signals are generated considering different dynamic responses such as step, triangular and realistic oscillatory functions. All the signals have been created for evaluation purposes considering real ranges such as levels or slopes. Furthermore, there are some considerations for defining the wind speed profiles.

For instance, according to [Abad et al., 2011], the low speed region oscillates between 3.5 and 5.5 m/s. Partial load operations where the MPPT ISC controller acts from a input wind speed of 5.5 to 11 m/s and the constant or nominal speed is defined between 11 and 12 m/s. The C_p is plotted from time zero. Besides, the initial inertia, wind, and rotor speed cause the C_p start from an unrealistic value; however, after ten seconds, the C_p swings between 0.4 and 0.5 which is desirable for this wind turbine (see Table 5.1). The simulations presented in this section compare a traditional PI with the ISC controller.

Table 5.1: Wind turbine characteristic values.

1.5 MW Wind turbine parameters	
Parameter	**Value**
Synchronism	1200 rpm
Rated Power	1.5 MW
Rated Stator Voltage	575 V_{rms}
Rated Torque	10 KNm
ρ	3 pairs
R	41.25 m
Rs	0.006352 pu
Lm	2.613233 pu
Rr	0.004496 pu
Ls	0.154253 pu
Lr	0.1406427 pu
NI	49.103 e+03 Kgm^2
GI	960 Kgm^2

5.1 Indirect Speed Control Test

ISC-MPPT simulation strategy is based on a DFIG electric machine of $1.5MW$ output power at nominal speed. The main wind turbine parameters used in FAST and Matlab-Simulink are displayed in Table 5.1. The ISC-MPPT technique depends deeply on the system dynamics because the optimal value calculated in Eq. 4.3 remains constant for all possible wind variations. The advantage of this method consists in its implementation simplicity and conceptually it is easier to understand its behaviour. This method requires accurate characteristics of the wind turbine and evidently can be improved using DSC methods based on advanced observers. It is important to note that ISC does not require to measure the wind speed directly for the control strategy. Wind speed can be calculated, predicted or estimated for DSC if it is necessary. However, the wind turbine system dynamics and the corresponding ISC-MPPT controller need to be tested for multiple wind conditions.

5.1.1 Multilevel Wind Speed Tests

The first wind speed signal used for simulations consists of different levels of steady wind speed with ramp type transitions. The idea, is to provide a realistic signal to evaluate the controller response. It is well known that step shape functions are often used in order to determine the system response for

abrupt input variations. The wind speed input signal varies from 8 to 10 m/s and it is depicted in Figure 5.4. For the study's purpose, 100 seconds of simulation have been tested. Thereupon, the following outcomes have been obtained. First, the output power remains at an average value of 1.275 MW.

It is important to note that even though the wind turbine is at a rated speed of 11 m/s, the simulation considers only the partial load. When the rated speed is achieved, the output power reaches about 1.5 MW, and these wind speed profiles generate a stable C_p near 0.5. In terms of the pitch controller, it also operates, but the simulations are intended to reduce its direct influence over the MPPT controller.

In this test, the main achievement is the stability of the C_p signal in Figure 5.7, the ISC-MPPT is reported, even though the C_p average value slightly increases. However, the output power shown in Figure 5.3 also increases, as well as the stability characteristics. Figure 5.1 shows the i_{qr} reference current which is similar for both controllers; however, for the ISC the current is saturated between 50 and 70 seconds because the wind speed exceeds the partial load limit.

For these simulations, the pitch angle controller is activated when the magnitude of the wind is above 9.5 m/s which corresponds to the manufacturer specifications. The pitch angle is represented in Figure 5.6 where the pitch angle shows three corrections before it reaches the steady state for traditional PI control; on the other hand, two corrections for the case of the ISC are highlighted. This leads to limit the pitch variations, thus reducing the stress of the components of the overall system.

Figure 5.1 shows the difference of the current reference i_{qr} between the proposed control strategy and a traditional PI control; for this case, the response speed improves, thus allowing to reach the speed reference of the generator faster. A saturation is observed after 50 seconds, this is because the pitch control has to be activated; however, after few seconds the i_{qr} is maintained around 0.8.

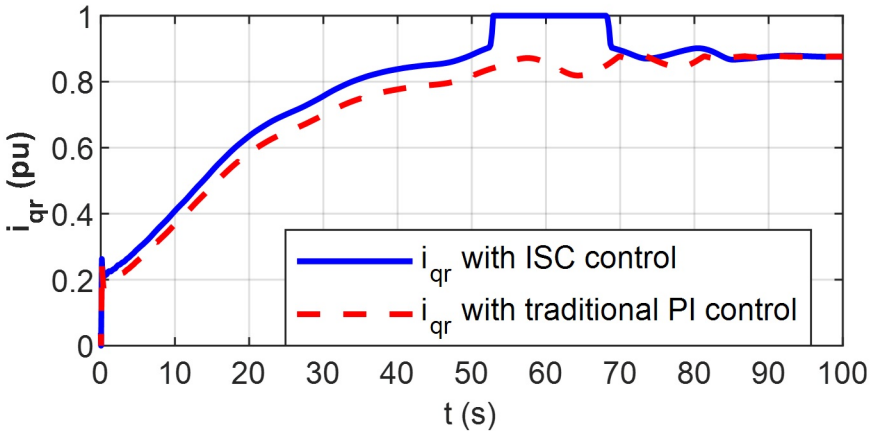

Figure 5.1: Reference signal i_{qr} in $p.u.$

Figure 5.2 shows the electromagnetic torque T_{em} is presented. It is important to note how the torque reaches its nominal value. In this simulation, it can be seen how the torque presents fewer oscillations compared to a traditional PI controller which means better dynamic control.

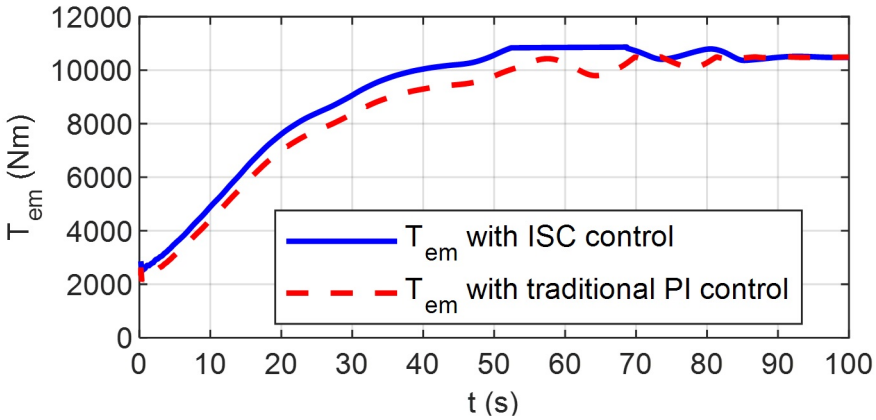

Figure 5.2: Electromagnetic torque in Nm.

In Figure 5.3 the output power is reported. It is important to mention that with the proposed control strategy the extracted power is achieved in the same time when compared to a PI; however, there are fewer oscillations when it reaches its nominal value.

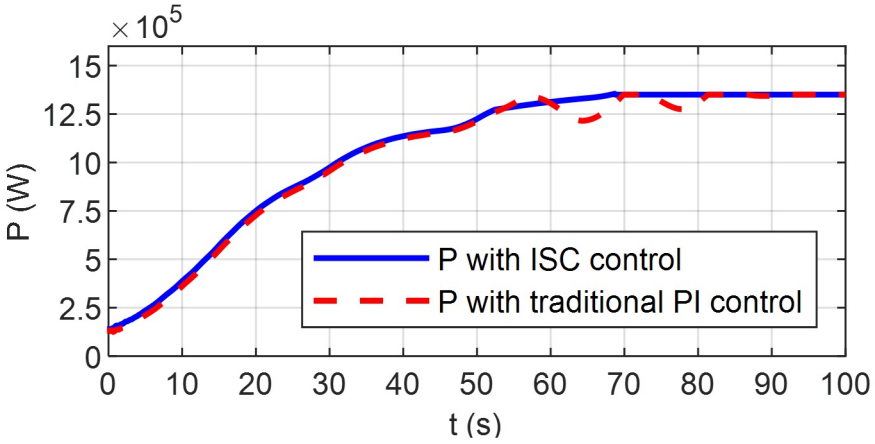

Figure 5.3: Active output power in $Watt$.

In Figure 5.4 the wind speed input is shown. The signal is composed of progressive transitions with positive slopes from 8 to 10.5 m/s. In this case it can be seen a progressive transitions until the wind reaches the nominal value of 10.5 m/s which is also limited by the current i_{qr}, while the MPPT is activated.

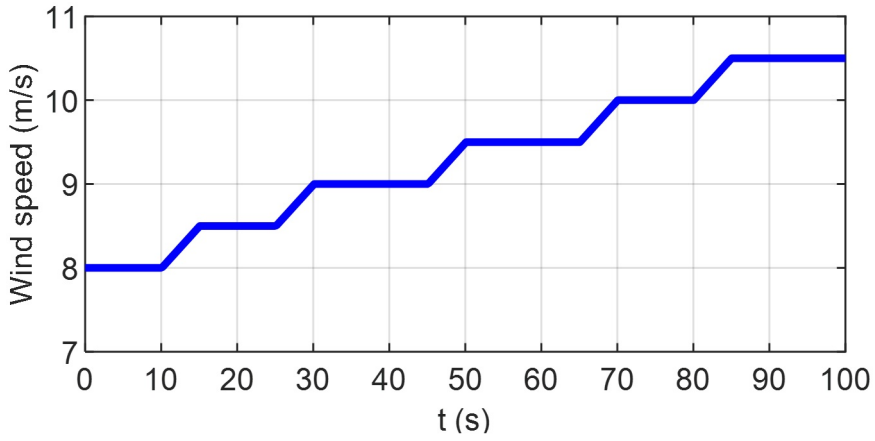

Figure 5.4: Wind input in m/s.

In Figure 5.5 the rotor speed is depicted. For the proposed control strategy during these tests a lower speed is needed to achieve the same amount of generated power compared to traditional controllers although the response is very similar.

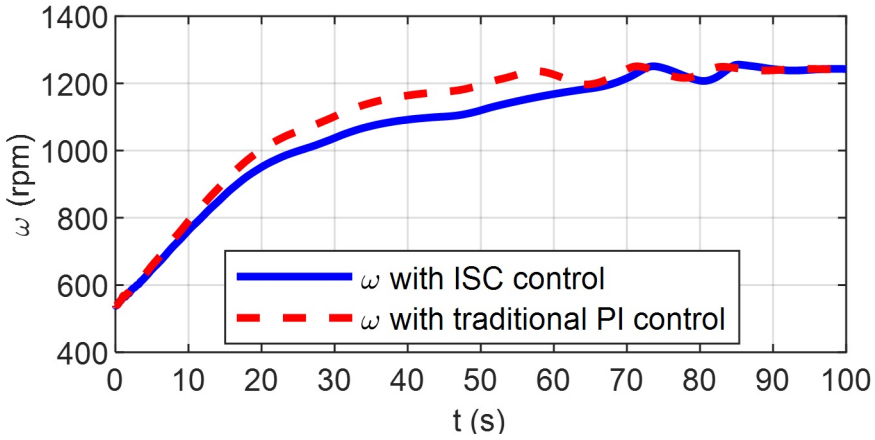

Figure 5.5: Generator speed in *rpm*.

In Figure 5.6 shows the variations of the pitch angle. There is a faster response of the pitch controller to the proposed ISC method compared to the traditional PI. In fact, in the traditional control a higher speed is needed to extract about the same amount of power.

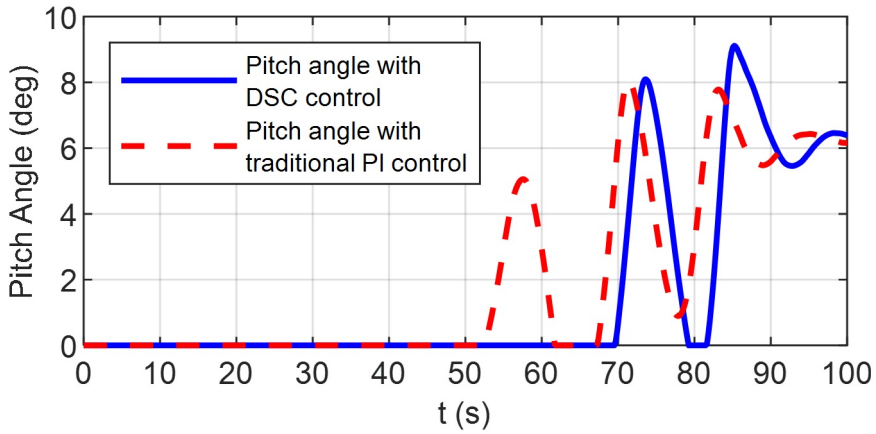

Figure 5.6: Pitch angle in degrees.

In Figure 5.7 shows the power coefficient C_p where the behaviour is similar in both cases. However, for the case of the ISC controller, there are smaller oscillations when the turbine reaches its nominal speed.

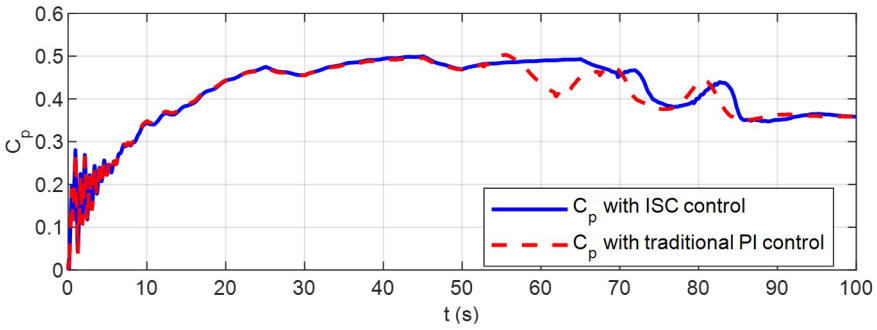

Figure 5.7: Power coefficient C_p.

5.1.2 Triangular Wind Speed Test

The second wind speed signal used for the system test consists of a triangular type input. The idea is to test the system with positive and negative slopes in order to evaluate the dynamic response which allows for understanding of the wind turbine response over progressive increments and decrements of winds. This signal simulates an increasing wind speed profile which varies between 6.5 and 8.5 m/s.

In this simulations time has been set in 100 seconds. The power has an average value of 0.9 MW when the MPPT is used. It is fundamental to emphasize that even though the wind turbine has been configured at the rated speed of 11 m/s, the simulation evaluates the dynamic response during more variations of the wind. Moreover, the initial inertia and torque are low for testing the dynamics during partial load. Some oscillations occur at the beginning of the simulation corresponding to the initial inertia configuration in FAST.

In the results, it can be seen when the rated speed is attained, the output power reaches near 0.75 MW, and the wind speed profiles generate a stable C_p near to 0.5 which corresponds to a desirable value. With respect to the pitch controller, it also acts when the wind speed increases, and because of this, the system is tested mainly during partial load without a straight impact on the pitch control. Figure 5.8 shows the triangular input signal with small slopes stating at 7 m/s speed. For these simulations the pitch angle does not actually work because the wind speed is low as shown in Figure 5.13.

The output power clearly increases after 80 seconds and remains higher for a steady state condition after 90 seconds as shown in Figure 5.10. i_{qr} shows smooth variations in Figure 5.8; however, it is able to produce changes also in the C_p which also has rapid variations following the response of the wind with triangular shape function.

In Figure 5.8 it is possible to observe the behaviour of the current i_{qr} between the proposed control strategy and a traditional PI control. In this case, it can be seen that the current in its first instants starts with a smaller nominal value; however, due to the controller activity, this current generates a larger signal with respect to traditional PI control.

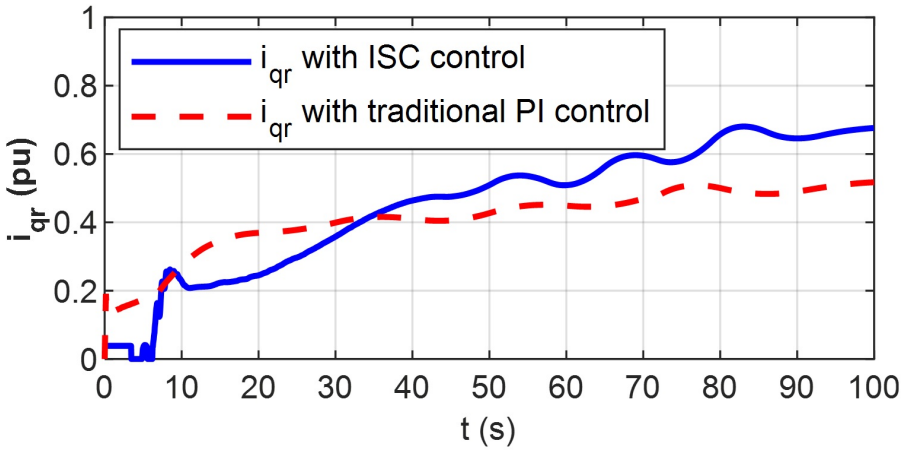

Figure 5.8: Reference signal i_{qr} in $p.u.$

In Figure 5.9 the behaviour of T_{em} is shown. It can be seen that the ISC controller generates a greater torque compared to the traditional PI control.

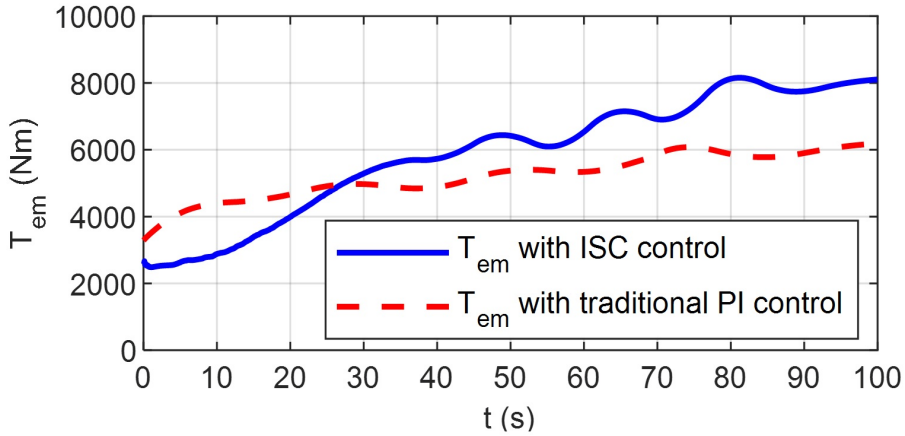

Figure 5.9: Electromagnetic torque in Nm.

In Figure 5.10 the output power is shown; it is important to mention that the wind turbine is able to produce more output power with the proposed ISC control strategy than the traditional PI control.

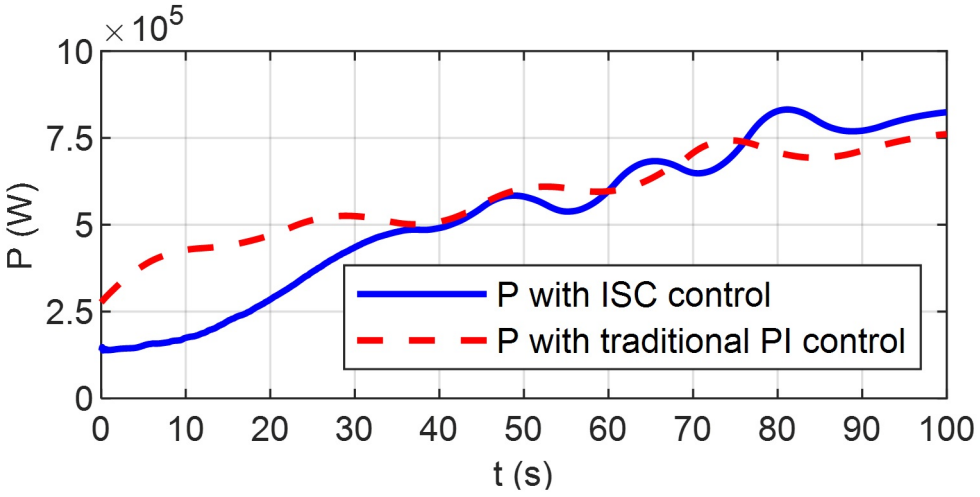

Figure 5.10: Active output power in $Watt$.

In Figure 5.11 the wind speed input is shown; in this case, positive and negative transitions are presented to evaluate the performance of the control using a triangular shaped signal between 6.5 and 8.5 m/s.

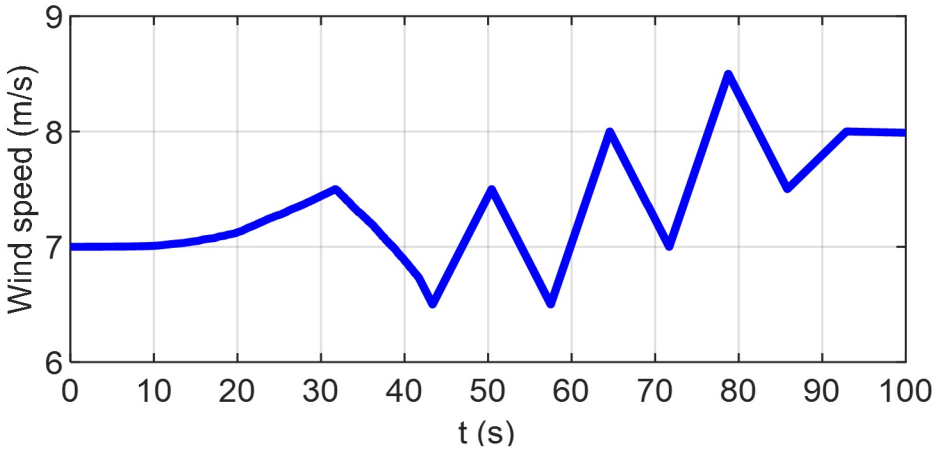

Figure 5.11: Wind input in m/s.

In Figure 5.12 the speed of the turbine is depicted. It can be seen that the proposed control strategy requires a lower speed to extract the same amount of power.

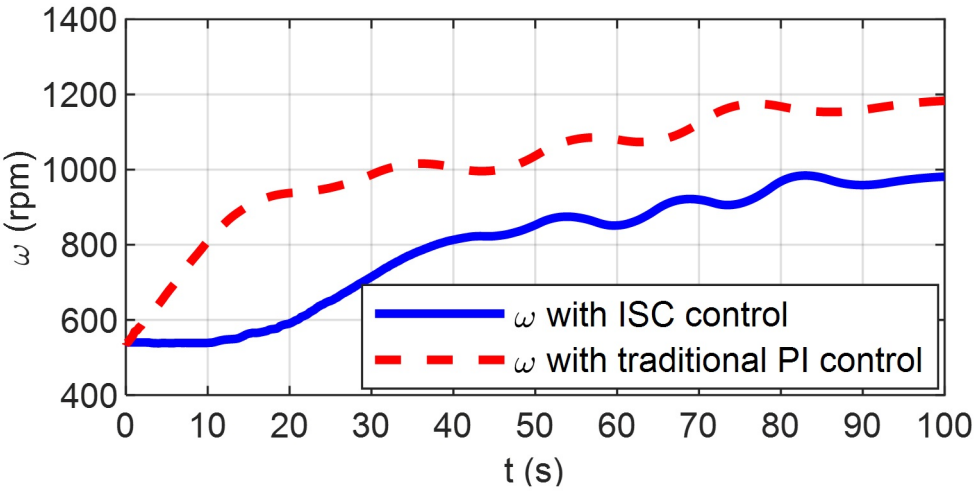

Figure 5.12: Generator speed in *rpm*.

In Figure 5.13 the performance of the pitch control are highlighted where there is no variation since the speed of the turbine remains below its nominal value. It means that, for both controllers there is no need to activate the pitch angle positioning system.

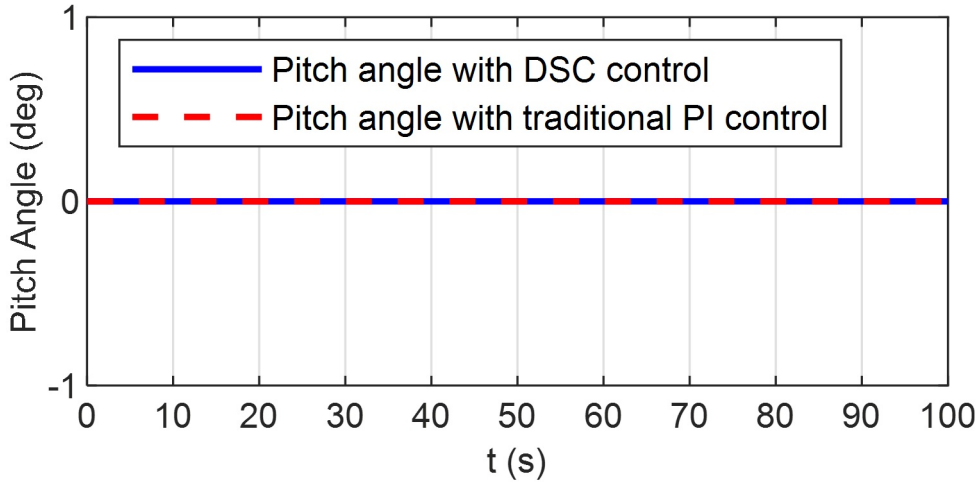

Figure 5.13: Pitch angle in degrees.

In Figure 5.14 it is depicted the power coefficient C_p. For both controllers the behaviour is similar. However, for the case of the ISC proposed controller, the C_p presents a greater amount of oscillations in the first interval of simulation with respect to the traditional control and after 40 seconds the C_p is higher with ISC.

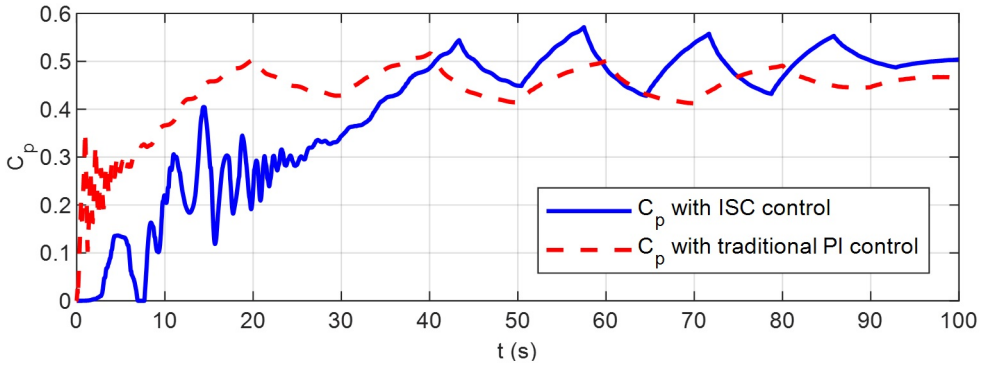

Figure 5.14: Power coefficient C_p.

5.1.3 Wind Speed Realistic Tests

The third wind speed signal used for simulations consists of a variable wind speed with transitions. The idea is to validate the system with a more realistic oscillatory signal in order to evaluate the dynamic response. The oscillatory signal simulates an increasing wind speed profile which varies from 7 to 10 m/s. Moreover, 100 seconds of simulation have been tested. Under these assumptions, the following results have been obtained. First, the output power has an average value of 0.9 MW when the MPPT is active.

Therefore, it is important to highlight that even though the wind turbine is at rated speed of 11 m/s, the simulation considers only the partial load and the initial conditions. Moreover, the initial inertia and torque are low for testing the dynamics during partial load. When the rated speed is reached, the output power is near to 1.25 MW due to the slip, and these wind speed profiles generate a stable C_p near 0.5. Regarding the pitch controller, it also acts when the wind speed increases, and therefore the system is tested mainly during partial load without a straight impact of pitch control.

The generated realistic input wind speed is shown in Figure 5.18. The improvements of the C_p are highlighted in Figure 5.21 basically along all the curve. The pitch angle also remains zero because of the range of the wind speed as shown in Figure 5.20. The most important achievement consists in the improvement of the output power along the curve following the variations of the driving wind sequence.

In Figure 5.15 it is possible to observe the comparison of the current i_{qr} between the proposed control strategy and a traditional PI control. Moreover, it can be noted a higher response speed in the case of the proposed ISC controller.

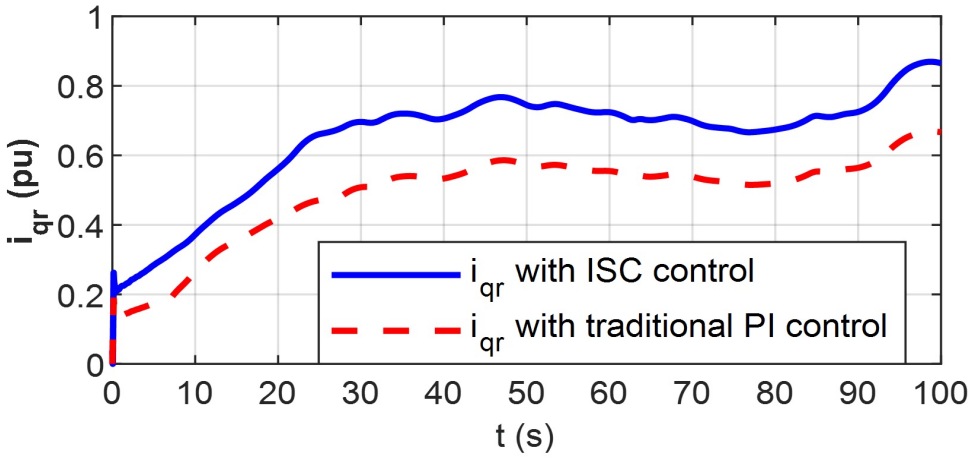

Figure 5.15: Reference signal i_{qr} in $p.u.$

In Figure 5.16 the behavior of T_{em} is shown. It can be seen that the ISC controller generates a greater torque than the traditional control.

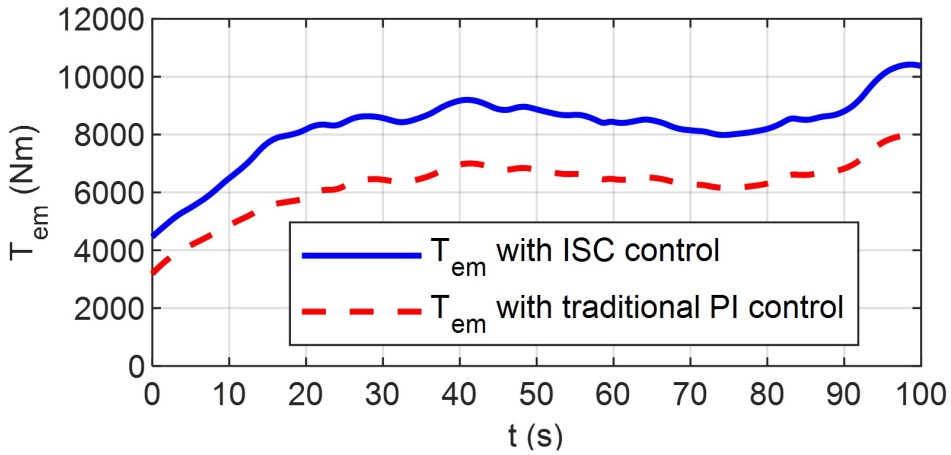

Figure 5.16: Electromagnetic torque in Nm.

In Figure 5.17 the output power is reported. It is important to mention that the proposed ISC control strategy allowed the generation of more power output than the traditional PI control.

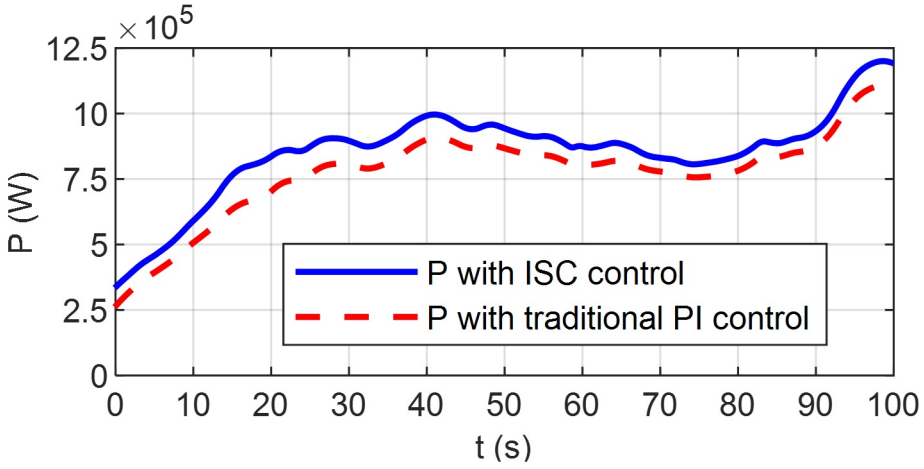

Figure 5.17: Active output power in $Watt$.

In Figure 5.18 the wind speed input is shown. In this case, a realistic signal is presented in order to evaluate the performance of the control. The wind varies between 7 and 10 m/s.

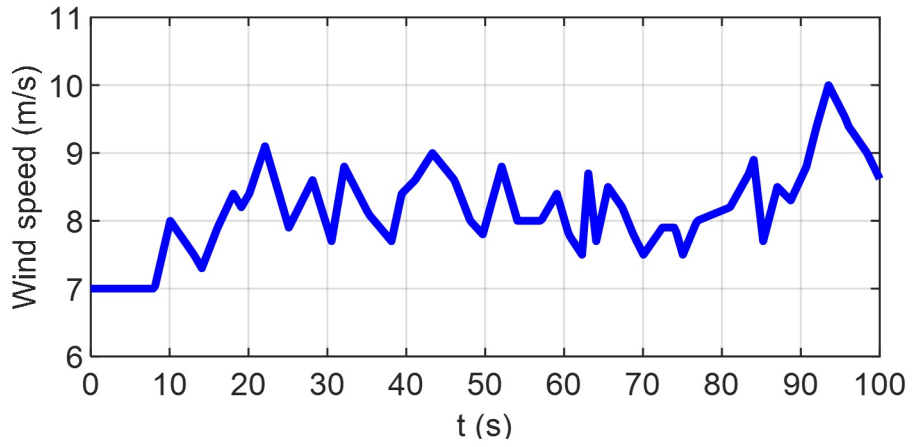

Figure 5.18: Wind input in m/s.

In Figure 5.19 the speed of the turbine is depicted. It can be seen that in the proposed control strategy requires a lower while the output power remains almost the same for both cases.

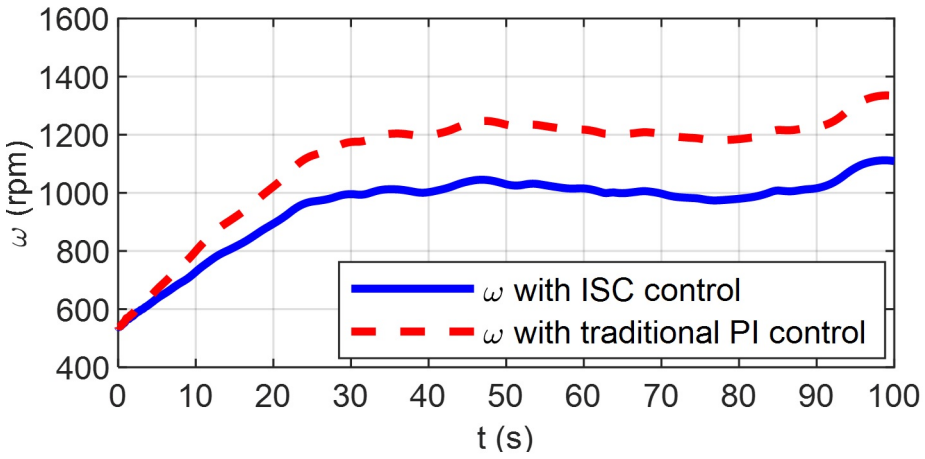

Figure 5.19: Generator speed in *rpm*.

In Figure 5.20 the performance of the pitch controls shown almost constant since the speed of the turbine remains below its nominal value. Therefore, for both controllers there is no need of activating the pitch angle positioning system.

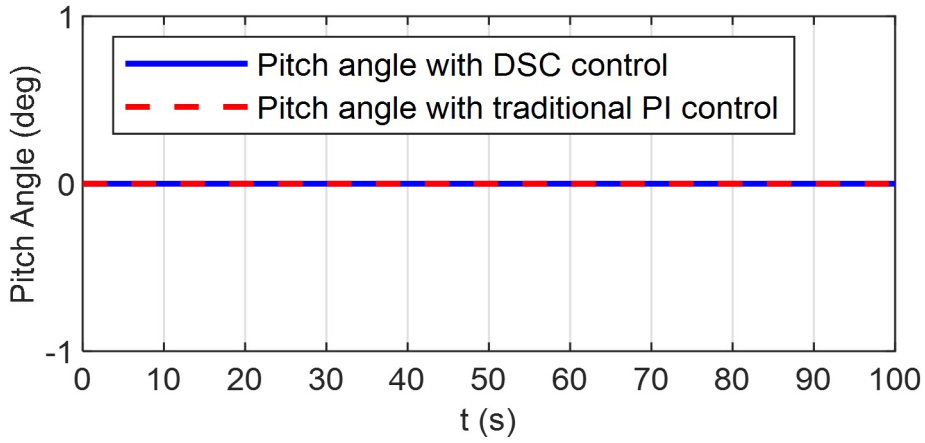

Figure 5.20: Pitch angle in degrees.

In Figure 5.21 it can be seen the power coefficient C_p. For both controllers the behaviour is similar. However, for the case of the proposed ISC controller, the C_p presents a greater amount of oscillations at the beginning, with respect to the traditional control and after 25 seconds the C_p is higher with ISC.

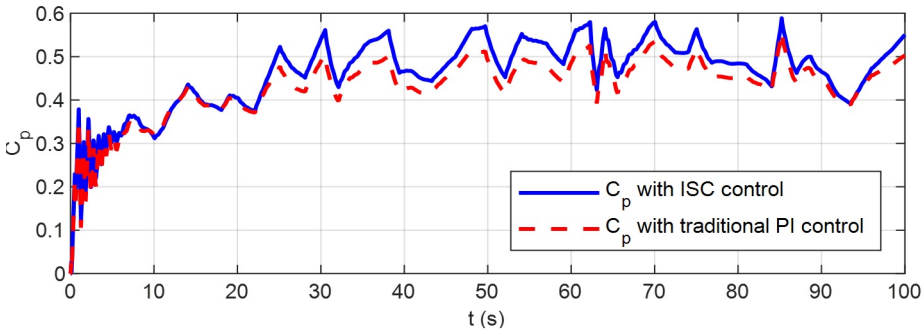

Figure 5.21: Power coefficient C_p.

5.2 Direct Speed Control via Luenberger Observer

As in the previous cases, the DSC MPPT simulation strategy is based on a DFIG electric machine of $1.5MW$ output power at nominal speed. Some wind turbine parameters in the FAST and Matlab-Simulink configurations determine the system dynamics; moreover, the optimal constant calculated in Eq. 4.3 remains steady for all possible wind variations. Moreover, the observer based on the Luenberger structure allows to estimate the torque input value. This method leads to an internal state variable that is observed, thus allowing to improve the C_p response. It is important to note that DSC requires the measurement of the ISC, which represents an internal variable in the AC/DC/AC converter. In can be sen as an improved version of the ISC considering that the wind turbine system needs a robust controller.

5.2.1 Multilevel Wind Speed Tests

The results of these tests are summarised in this section by using steady wind speed input signal including ramp type transitions. The DSC Luenberger state observer tracks the C_p value with a more rapid response. The C_p dynamics in this case are improved compared to the PI controller in Figure 5.28. The produced output power using this DSC strategy in comparison with the classical PI controller is also more stable, as shown in Figure 5.23.

In Figure 5.22 the i_{qr} current between the proposed DSC control strategy and a classic PI control is compared. The performance of the control strategy has a similar behaviour; however, the response of the DSC controller shows less oscillation than the classic controller.

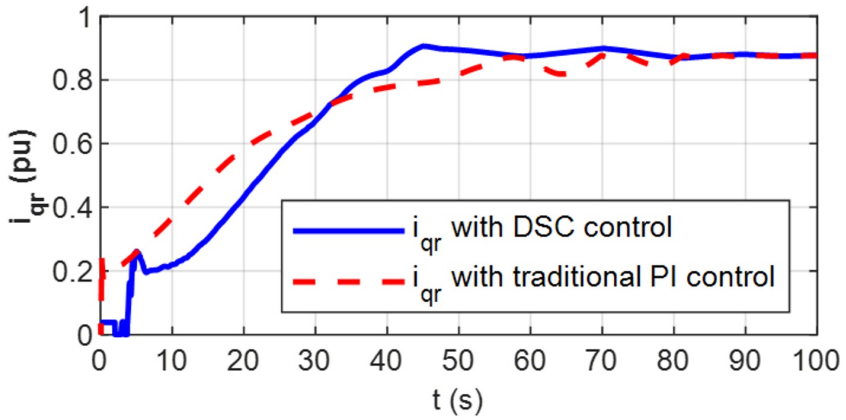

Figure 5.22: Reference signal i_{qr} in $p.u.$

In Figure 5.23 the performance of the electromagnetic torque T_{em} is depicted. It can be seen a similar behaviour for both cases; it is important to note that the proposed DSC controller generates a more stable signal. The DSC itself does not produce more electromagnetic torque but regulates with better dynamics.

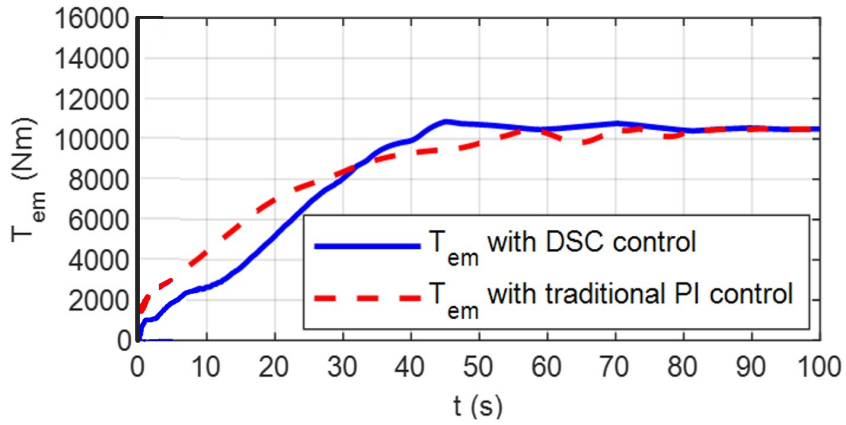

Figure 5.23: Electromagnetic torque in Nm.

In Figure 5.24 the extracted power is is depicted; in this situation, the proposed control strategy and the classical PI control have similar performances; however, for the case of the DSC control less oscillations are generated before reaching the nominal value.

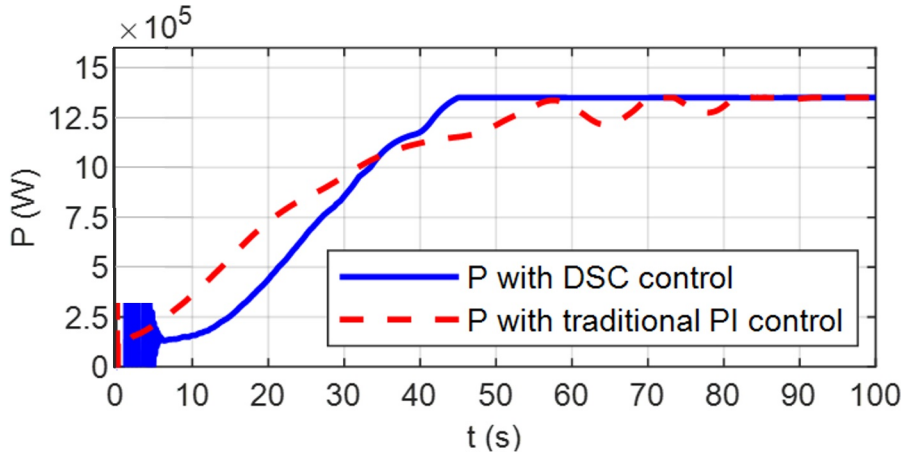

Figure 5.24: Active output power in $Watt$.

In Figure 5.25 the wind speed input signal is shown; in this case, progressive transitions are used in order to test the controller performance.

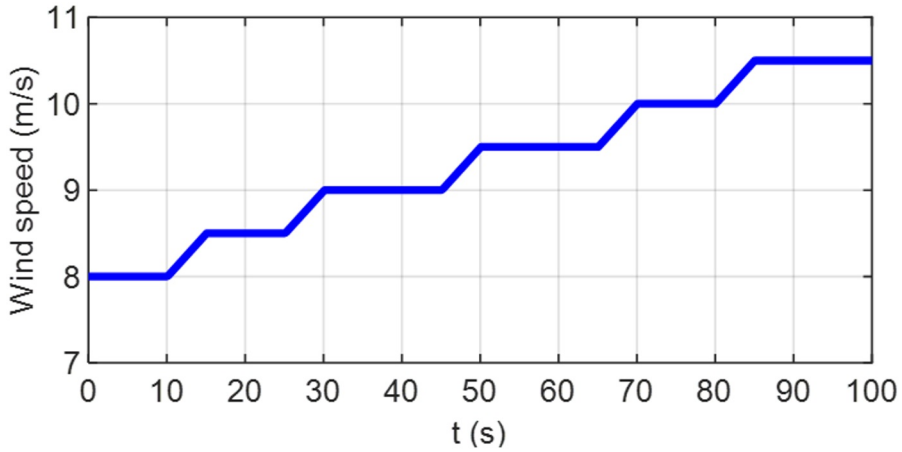

Figure 5.25: Wind input in m/s.

Figure 5.26 shows the wind turbine rotor speed where it can be seen that the DSC and the PI controller produce similar behaviors. For the proposed DSC controller it is important to note that in the first 30 seconds the rotor speed is significantly lower compared to the PI controller. This represents less fatigue and friction losses which is an advantage also for the proposed method.

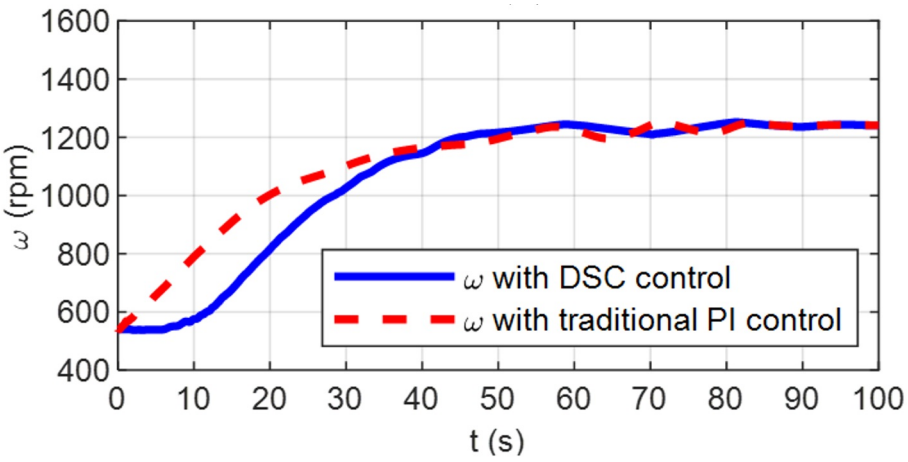

Figure 5.26: Generator speed in *rpm*.

Figure 5.27 shows the behaviour of the wind turbine's pitch angle control. In this case the proposed DSC controller presents fewer oscillations in the turbine. This is because the rotor speed has been also reduced and less inertial forces are produced, thus enhancing the pitch control to reduce action over the system.

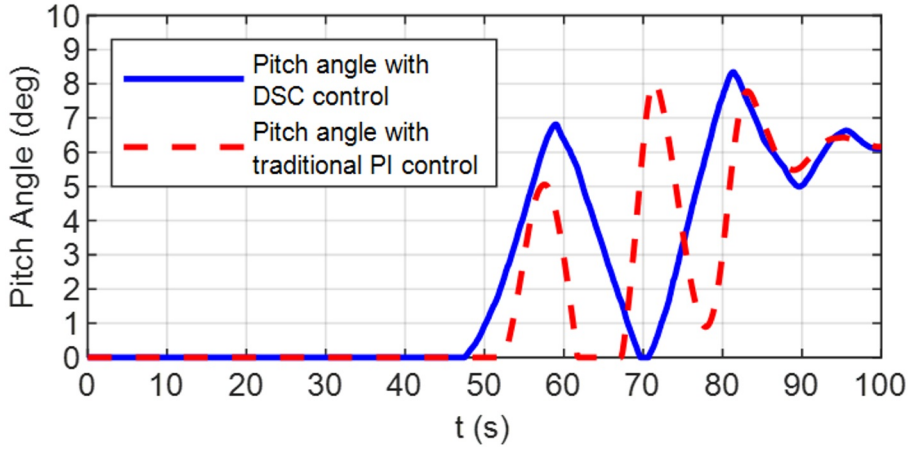

Figure 5.27: Pitch angle in degrees.

In Figure 5.28 the behaviour of the power coefficient is depicted. In this case, it can be seen that the response is similar for both cases which guarantees maximum power extraction during the simulated operating conditions. However, the DSC controlled system presents better dynamics and more power, whilst the PI controller generates some oscillations.

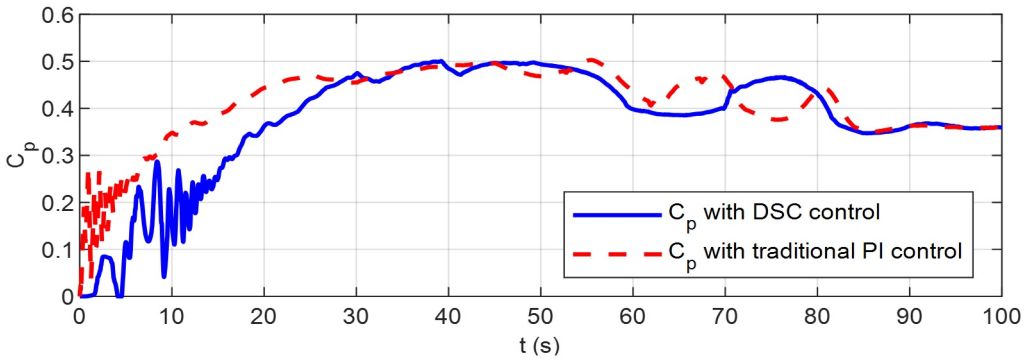

Figure 5.28: Power coefficient C_p.

5.2.2 Triangular Wind Speed Tests

Positive and negative slope wind speed input signals have been used during these tests to validate the efficacy of the considered control approaches. The results will be shown at the end of this section. The DSC state observer tracks the C_p value with a more quick dynamics. The C_p response, in this case, is better than the PI controller shown in Figure 5.35. The MPPT rapidly responds to wind changes, thus achieving a better response in the optimal operating parameters.

In Figure 5.29 the behaviour of the current i_{qr} is shown: in the case of the proposed DSC controller the current signal has a slightly higher amplitude, however the behaviour is similar in both cases.

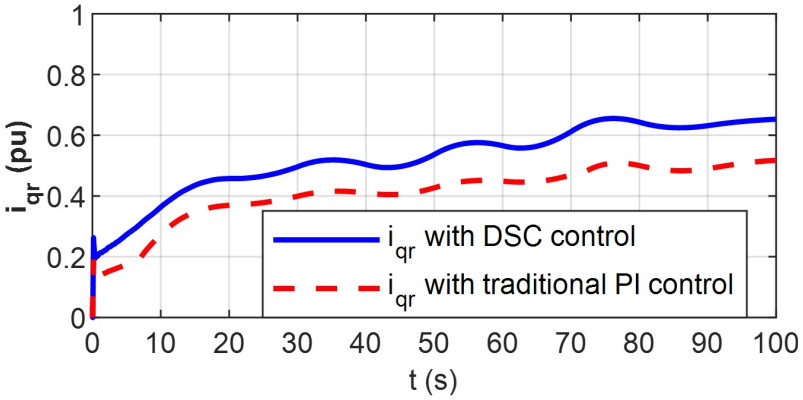

Figure 5.29: Reference signal i_{qr} in $p.u.$

In Figure 5.30 it can be seen the behaviour of T_{em} where it is shown that the signals present the same behaviour; however, the signal of the proposed

controller has a slight variation in its amplitude which corresponds to a higher i_{qr} current.

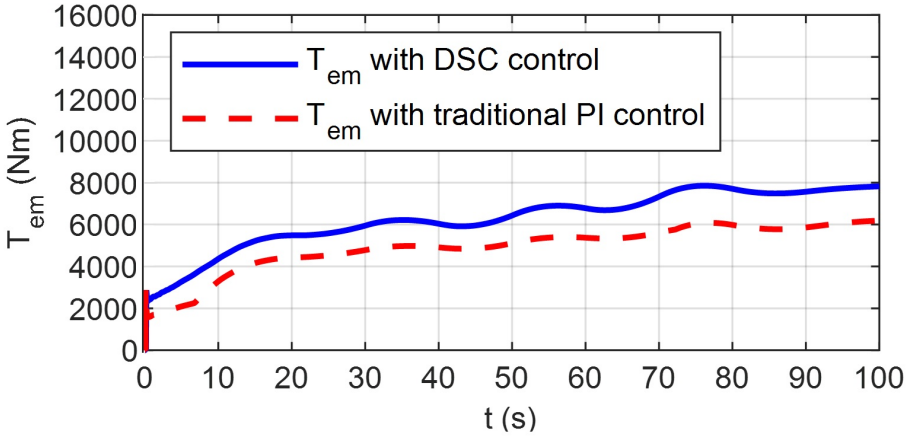

Figure 5.30: Electromagnetic torque in Nm.

In Figure 5.31 the power extraction for the proposed scenario is depicted, and for both cases the behaviour is similar. An increase in the extracted power is present in the proposed DSC controller output power.

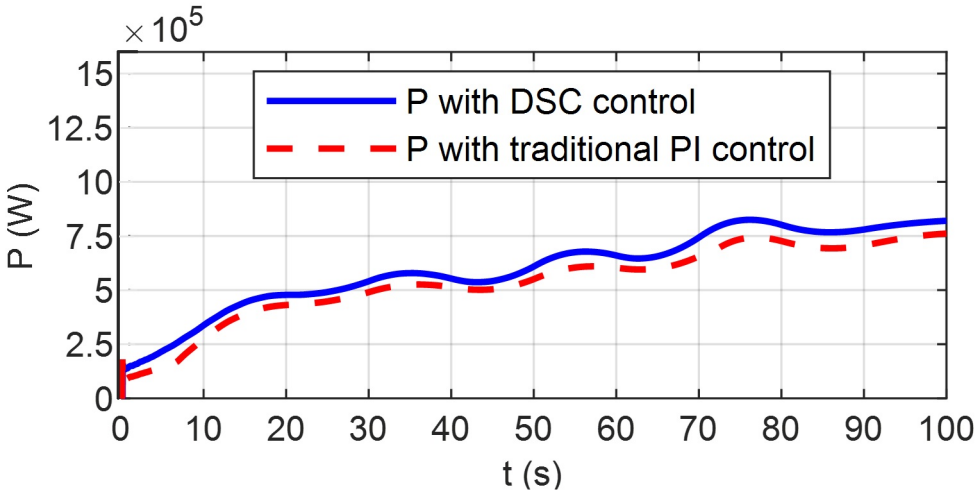

Figure 5.31: Active output power in $Watt$.

In Figure 5.32 the rotation speed of the wind turbine is shown; in particular, in the case of the proposed controller it is observed that the system requires less angular speed to extract the same amount of power. This is also highlighted by the torque and current in these simulations.

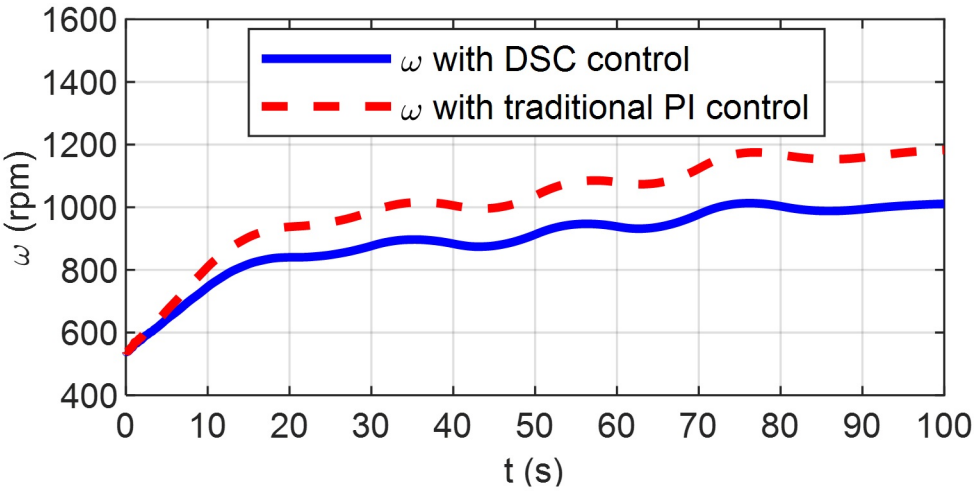

Figure 5.32: Wind input in m/s.

In Figure 5.33 the input signal used in the simulation is shown; the reason for this type of input is to evaluate the behaviour of the controller at sudden progressive changes in speed with positive and negative slopes.

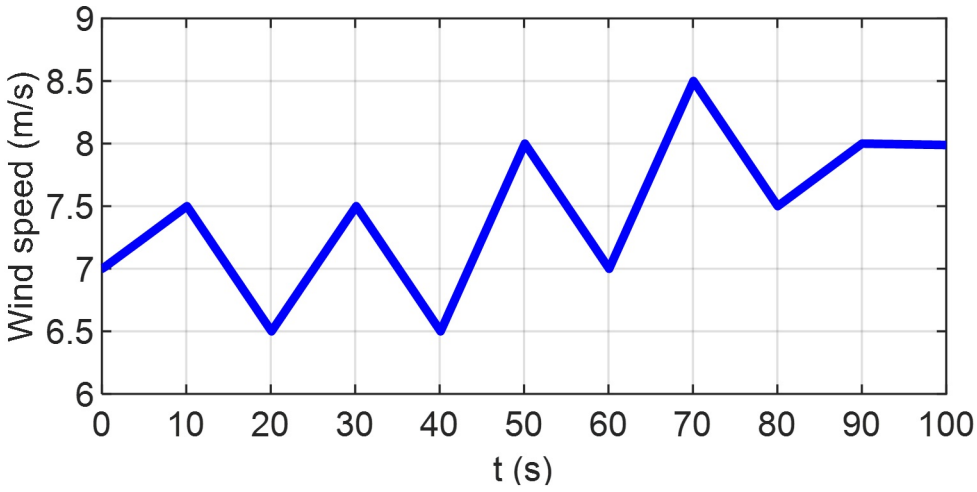

Figure 5.33: Generator speed in rpm.

Figure 5.34 shows the behaviour of the pitch angle for the proposed operating scenario. For both cases there is no variation since the turbine does not reach its nominal speed value. This means that there is no need to activate the pitch controller during this simulation.

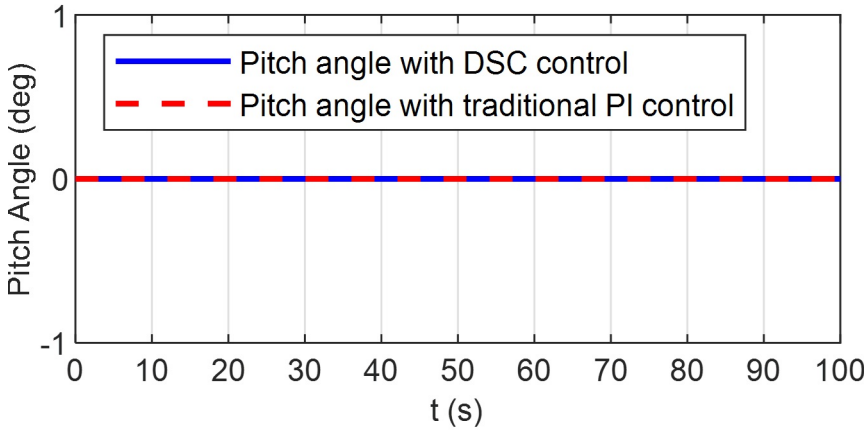

Figure 5.34: Pitch angle in degrees.

In Figure 5.35 the power coefficient is shown where a similar behaviour is observed. However, for the case of the proposed controller there is a slight increase in the amplitude of the C_p.

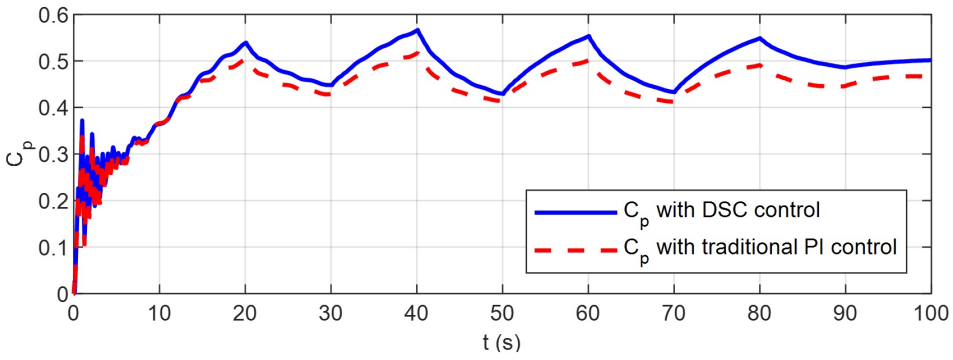

Figure 5.35: Power coefficient C_p.

5.2.3 Variable Wind Speed Realistic Input

A realistic wind speed has been used in this test to validate the dynamic response. The results are shown in this section. The DSC state observer tracks the C_p value with a more quickly dynamics. The C_p response, in this case, is better than the PI controller of Figure 5.42. The MPPT rapidly responds to wind changes, thus achieving a better response in the optimal operating parameters.

Figure 5.36 shows the behaviour of the current i_{qr} where a similar behaviour is observed but with an increase in the amplitude of the signal corresponding to the proposed controller.

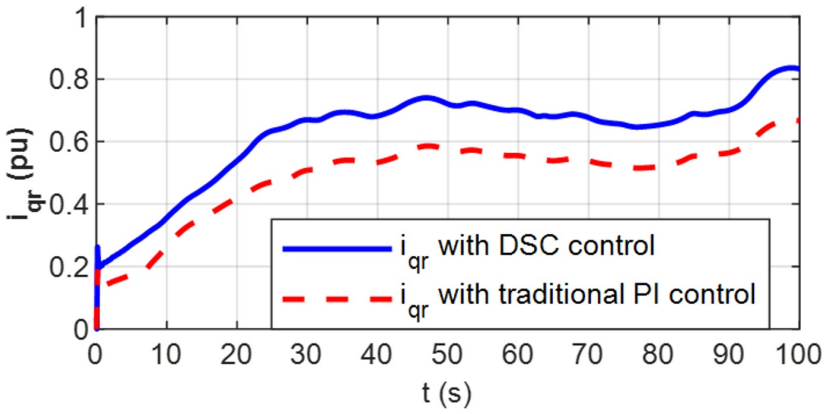

Figure 5.36: Reference signal i_{qr} in $p.u.$

In Figure 5.37 the behaviour of T_{em} is shown. For the case of the proposed controller, an increase in the torque amplitude can be observed although both continue to maintain the same behaviour; however, the DSC controlled system produces slightly higher torque in comparison.

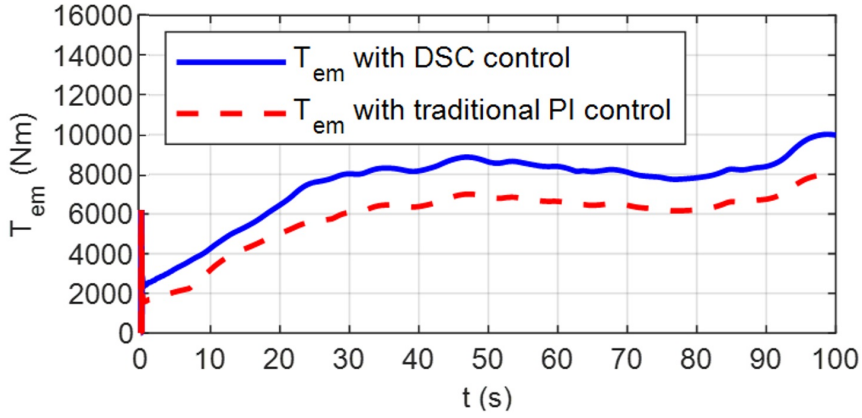

Figure 5.37: Electromagnetic torque in Nm.

In Figure 5.38 the power extracted by the wind turbine is shown. It can be seen that the proposed controller is more efficient since it extracts slightly more power.

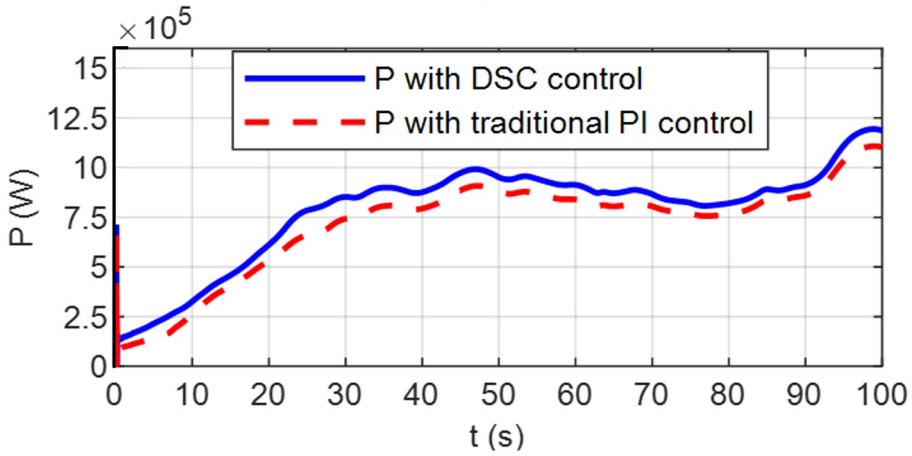

Figure 5.38: Active output power in $Watt$.

Figure 5.39 shows the simulation of the speed of the wind turbine. For the case of the proposed controller it can be clearly seen that the system is capable of extracting more power at lower speed.

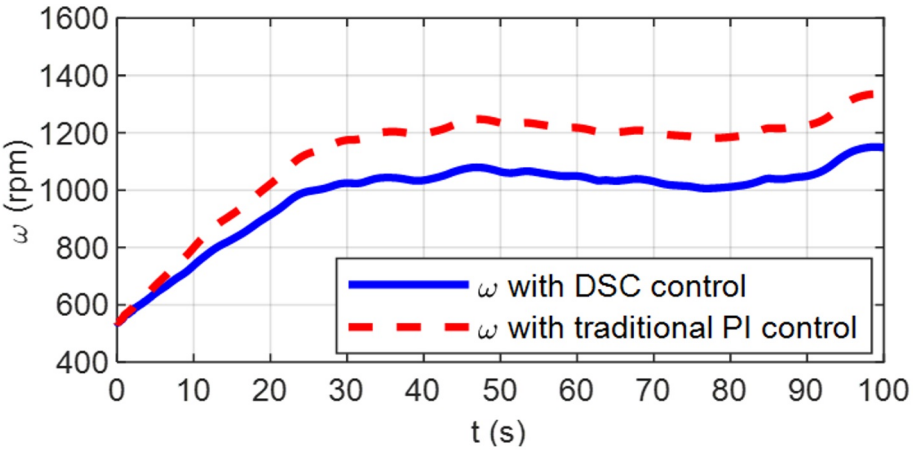

Figure 5.39: Wind input in m/s.

In Figure 5.40 the wind speed input signal used is represented; in this case, a realistic signal is depicted to evaluate the performance of the controller under real operating conditions ranges.

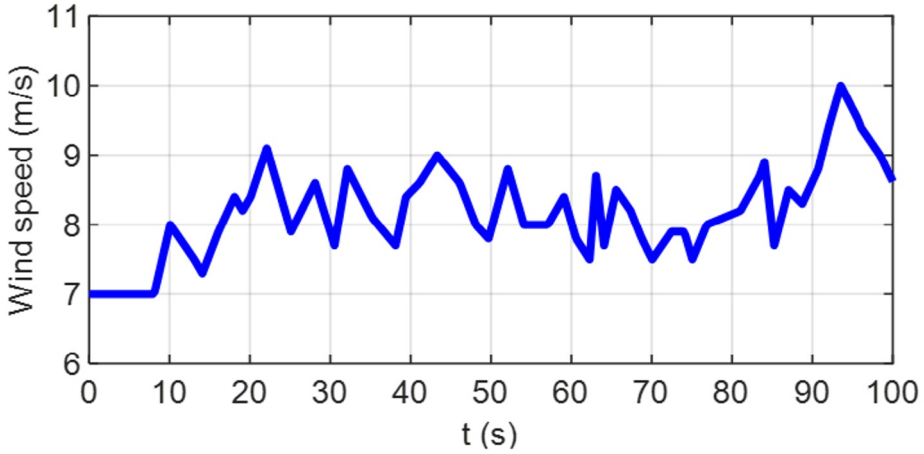

Figure 5.40: Generator speed in *rpm*.

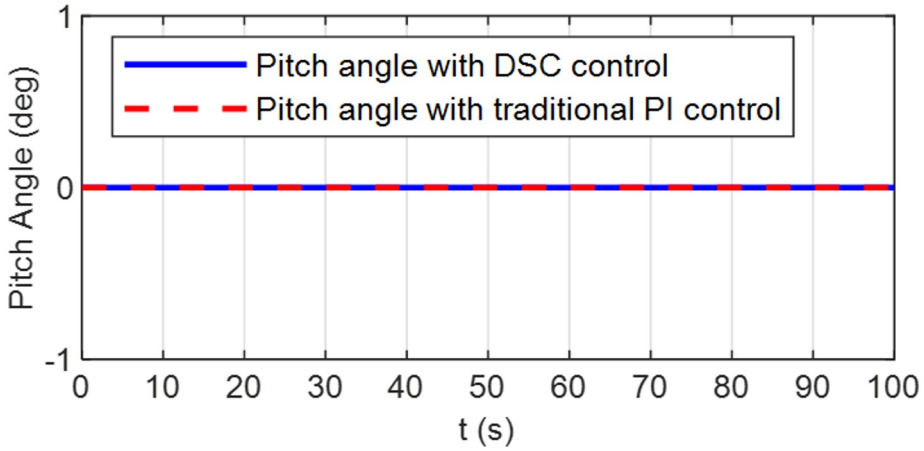

Figure 5.41: Pitch angle in degrees.

Figure 5.41 shows the behaviour of the pitch angle for the proposed operating scenario: in both cases, there is no variation since the turbine does not reach its nominal speed value.

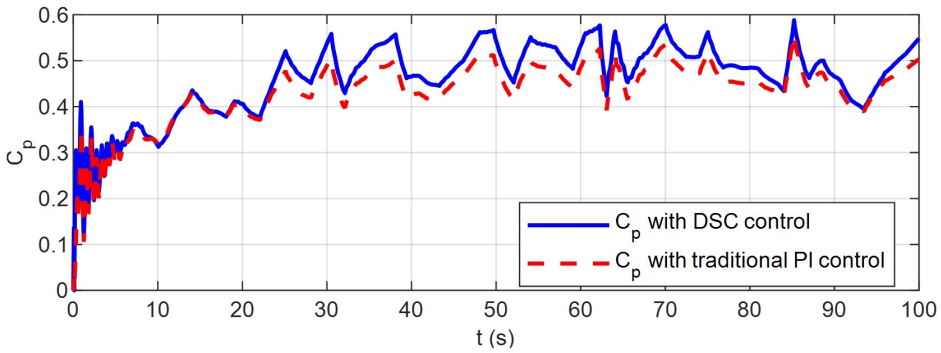

Figure 5.42: Power coefficient C_p.

In Figure 5.42 the behaviour of the power coefficient is shown, which which presents similar dynamics in both cases.

5.3 DSC using Takagi-Sugeno PI and Fuzzy Controllers

The results achieved by the proposed strategy has been carried out by using the FAST, as described in [Hilloowala and Sharaf, 1996], and Matlab-Simulink, along with the technical data reported in Table 5.1.

With the use of FAST, the modelling of the mechanical, electrical and control subsystems of the wind turbine has led to a high-fidelity description of the total system by considering the influence of various factors and components. FAST uses files that define the input of the aerodynamic parts by which it calculates the different required variables.

The results obtained are presented in the simulations of two different wind speed behaviours. First, step inputs have been used to establish the fundamental response of the system, and then a second input to describe the behaviour due to wind oscillations. The comparison of the validity of the designed solution is carried out with the classic PI controller. This control uses a table describing the link between power and rotor speed, which does not always correspond to the real performance of the turbine, blades, or the system in general.

This situation is due to several reasons such as uncertainties in the aerodynamic calculations or measurements, structural or construction defects, variation of aerodynamic parameters over time, wear of the elements, materials on the blades, and any other changes in the parameters [Calderaro et al., 2008].

5.3.1 Multilevel Wind Speed Tests

The results of the system response are shown in this section where the wind turbine reaches the optimal operating values rapidly and accurately with the proposed control. A more effective and efficient monitoring of the maximum power is performed as shown in Figure 5.43. The C_p function responds to rapid changes and achieves stability in the optimal operating values. The electromagnetic torque tracks the corresponding reference with the developed controller; on the other hand, the classic PI controller does not precisely track the electromagnetic torque as shown in Figure 5.44.

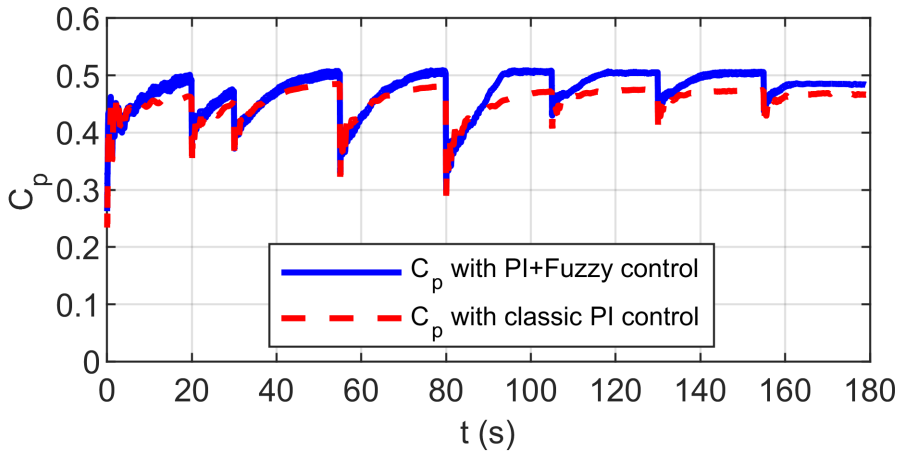

Figure 5.43: Power coefficient C_p.

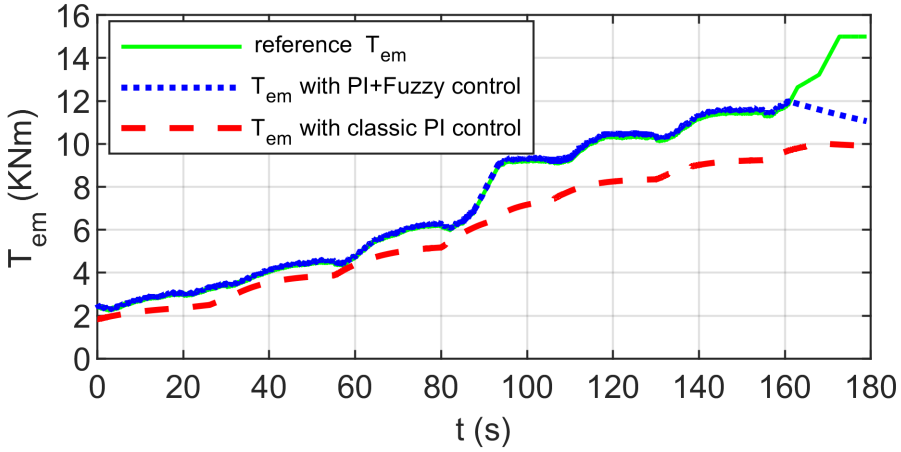

Figure 5.44: Electromagnetic torque in Nm.

5.3.2 Variable Wind Speed Realistic Input

Considering wind driving sequences closer to reality, the outputs of the system are analysed by using the proposed control. It is evident that the involved variables, as shown in this section, react with higher sensitivity to constant changes in the wind speed, thus reaching their ideal values rapidly. It should be clarified that in this case there is also a correct tracking of the electromagnetic torque with respect to its reference by means of the considered control with respect to PI governor. This is indicated in Figure 5.45.

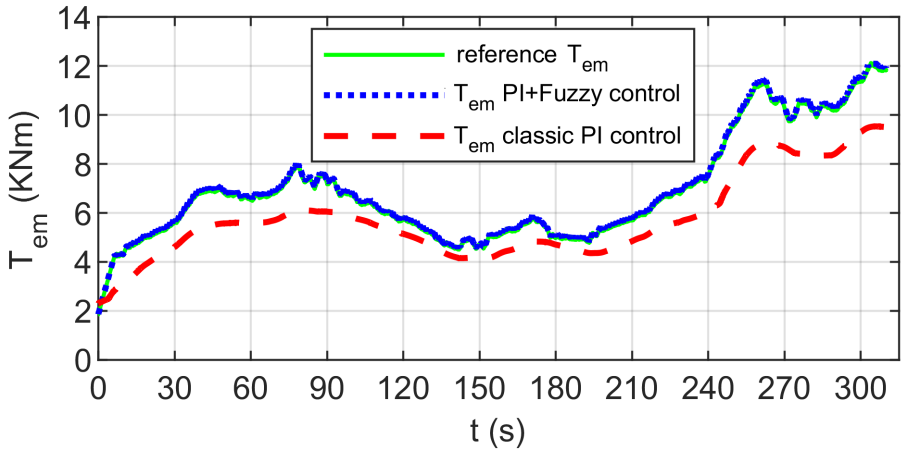

Figure 5.45: Electromagnetic torque in Nm.

Figure 5.46 depicts the power coefficient which demonstrates the effect of the built-in control. At this point, it is important to note that the response shows improvements in almost all the performed simulations. However, during large drops of the wind speed, the response of the system does not show a considerable improvement due to the inertia of the turbine and the generator. Therefore, it is difficult for the wind turbine to overcome this effect and achieve the optimum speed and power operating values. Despite this situation, the control leads to some improvements with respect to the MPPT technique.

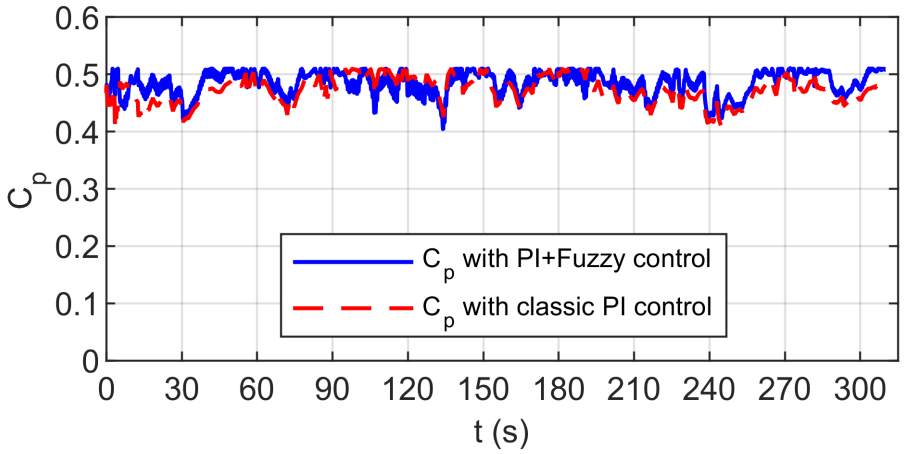

Figure 5.46: Power coefficient C_p.

5.4 ISC Analysis with Disturbances

The following subsection presents a set of simulations including uncorrelated white noise added to the input wind speed signal in order to test the robustness of the system to oscillations produced naturally or due to the electronic wind speed sensor. The following subsections include this analysis for different conditions based on [Pozo et al., 2021a], and [Pozo et al., 2021b].

5.4.1 Steps Wind Speed Including Disturbances

The presented tests in this subsection are important because they include different signals tested including Non Correlated White Noise (NCWN) in order to perform more accurate analysis and comparison.

Figure 5.47 shows the input signal affected by the noise to evaluate the performance of the controller.

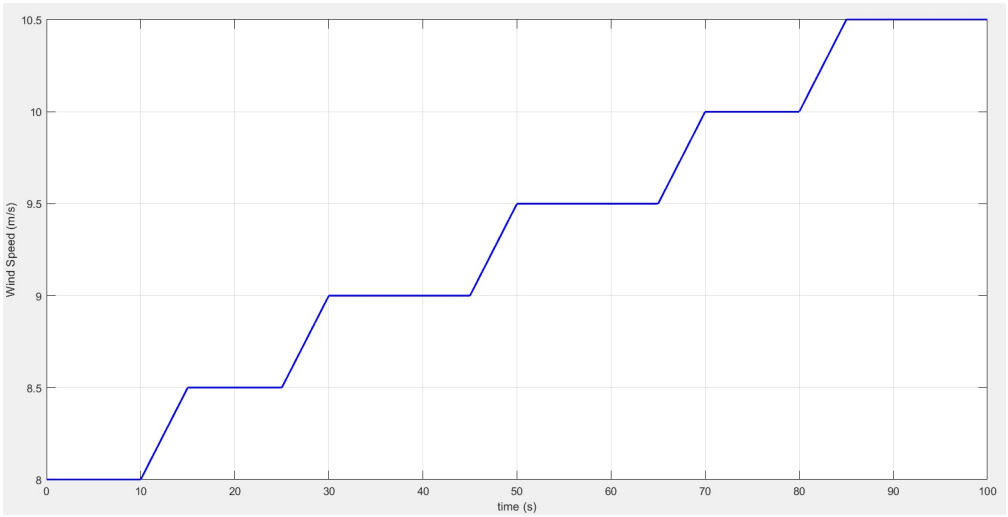

Figure 5.47: Wind input in m/s.

In Figure 5.48 the behaviour of the current i_{qr} is shown when a white noise signal is considered, whose amplitude is 10% of the input wind speed. It can be seen that the performances in both cases are quite close.

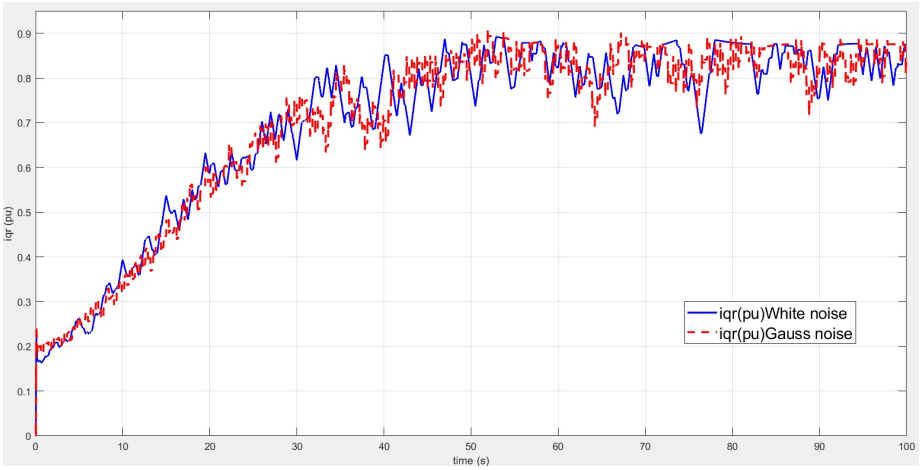

Figure 5.48: Reference signal i_{qr} in $p.u.$

In Figure 5.49 the behaviour of T_{em} is shown with noise signals. Note that the performance in both cases is similar.

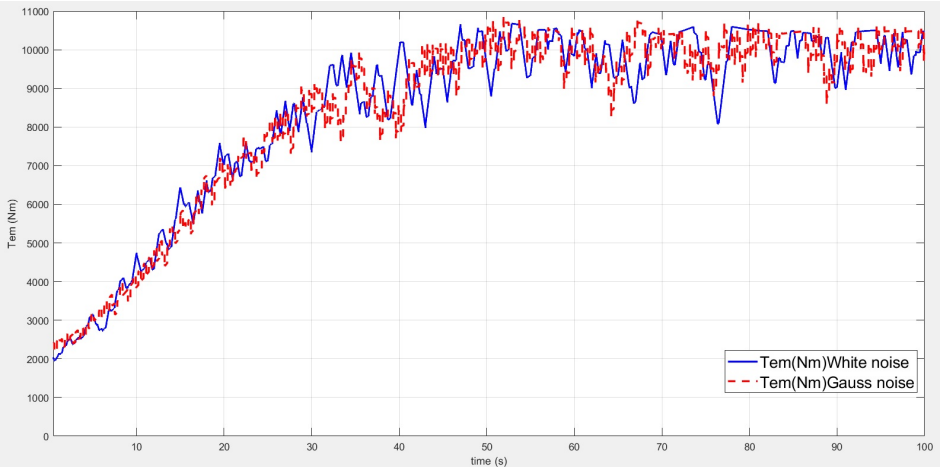

Figure 5.49: Electromagnetic torque in Nm.

In Figure 5.50 the power extracted by the wind turbine is shown with noise signals, where it can be seen that for both cases the behaviour is similar.

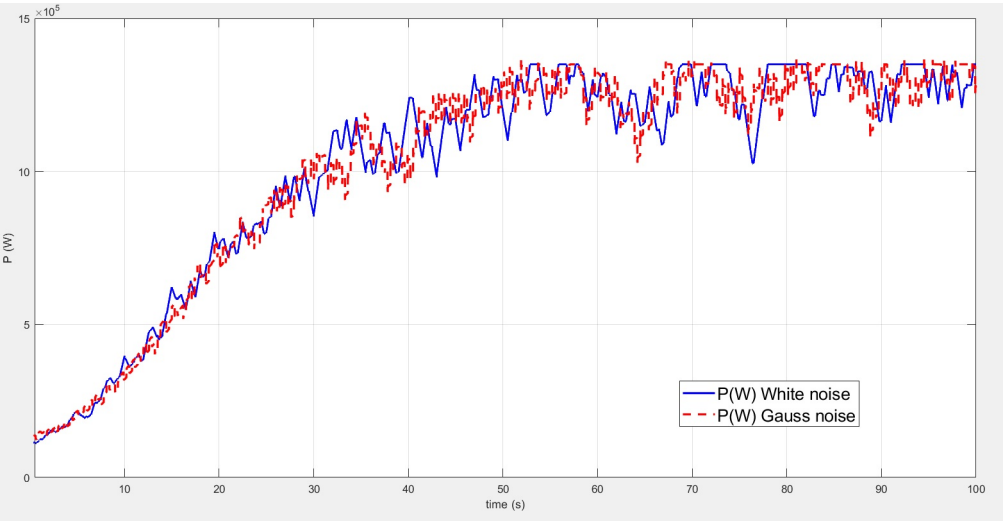

Figure 5.50: Active output power in $Watt$.

In Figure 5.51 the behaviour of the pitch angle is shown by considering the noise. In the case of the proposed DSC controller system, it can be seen that the pitch controller produces fewer transitions to maintain the speed of the turbine at its nominal value.

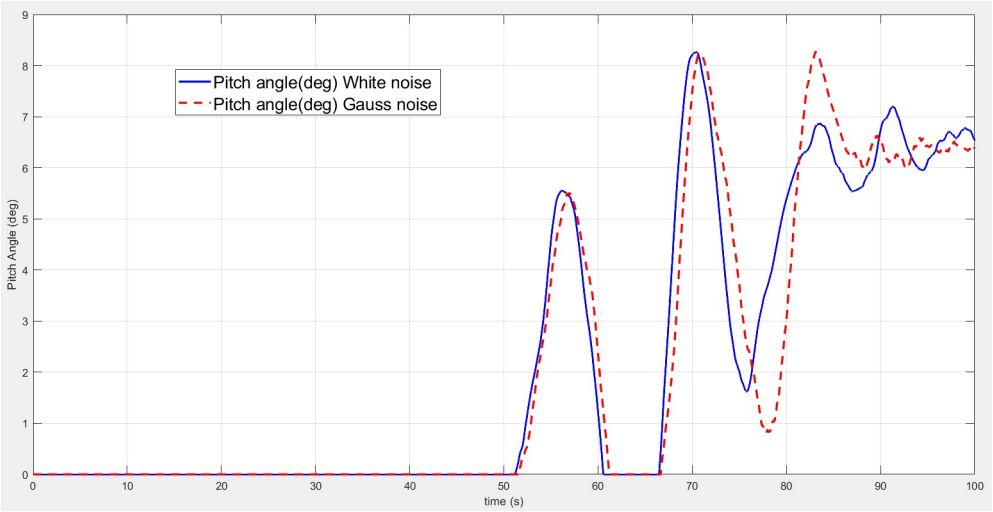

Figure 5.51: Pitch angle in degrees.

Figure 5.52 shows the power coefficient with the noise. In both cases the same behaviour is observed.

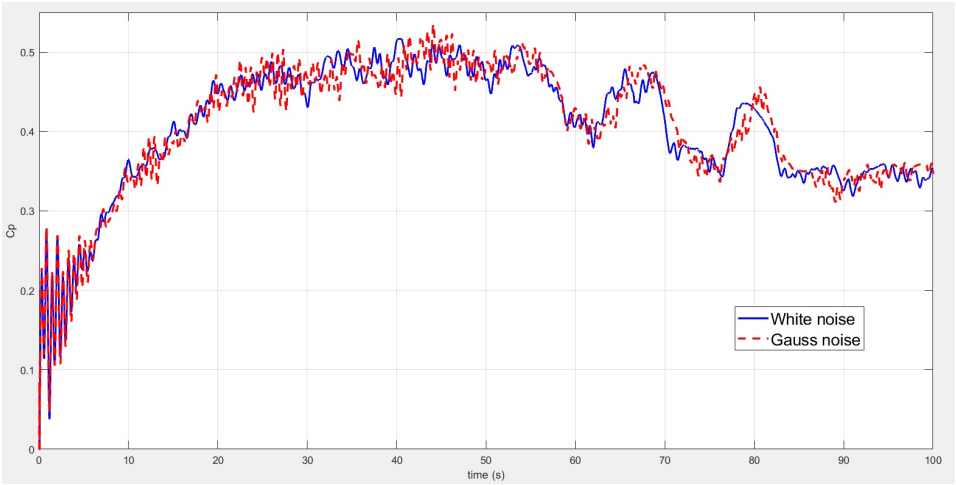

Figure 5.52: Power coefficient C_p.

Figure 5.53 shows the noise processes affecting the input signal that are exploited for evaluating the performance of the controller.

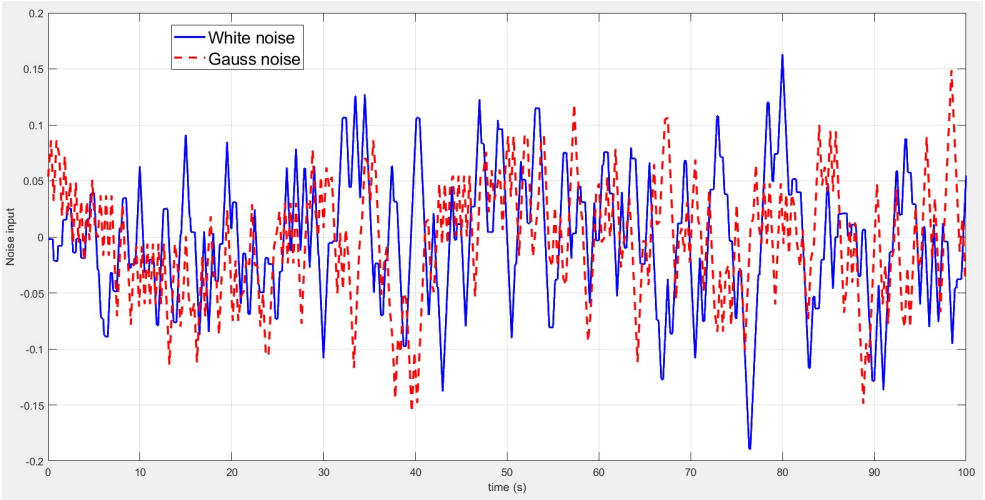

Figure 5.53: Noise input signal.

5.4.2 Triangular Wind Speed Including Disturbances

The following simulation include 10% white noise added to the input wind speed signal in order to test the robustness features. In Figure 5.55 the behaviour of the current i_{qr} is shown in the presence of noise; note that the performance for both cases is similar. During these simulations, the behaviour of the pitch angle via the introduction of noise remains constantly zero with no variations. This is because the wind turbine does not reach its nominal speed during these tests.

In Figure 5.54 the noise processes used in the simulations the input signal are shown. They are used for evaluating the performance of the controller.

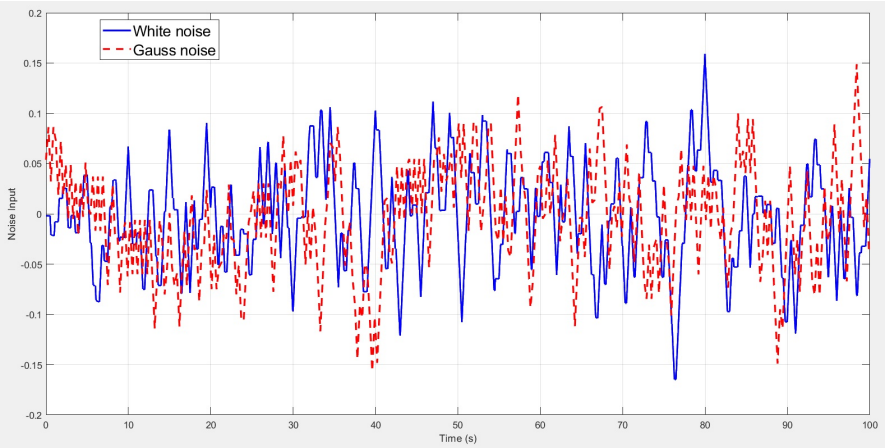

Figure 5.54: Noise signal input.

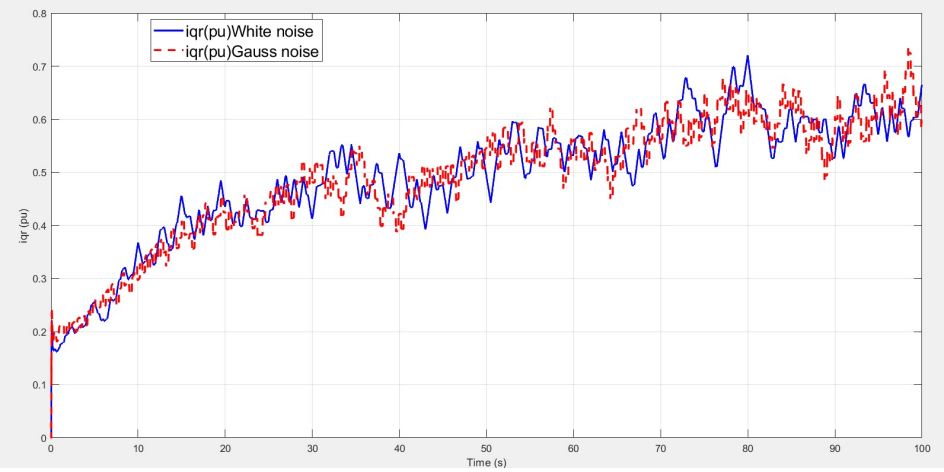

Figure 5.55: Reference signal i_{qr} in $p.u.$

In Figure 5.56 the behavior of T_{em} is is shown in the presence of noise; note that the performance for both cases is similar.

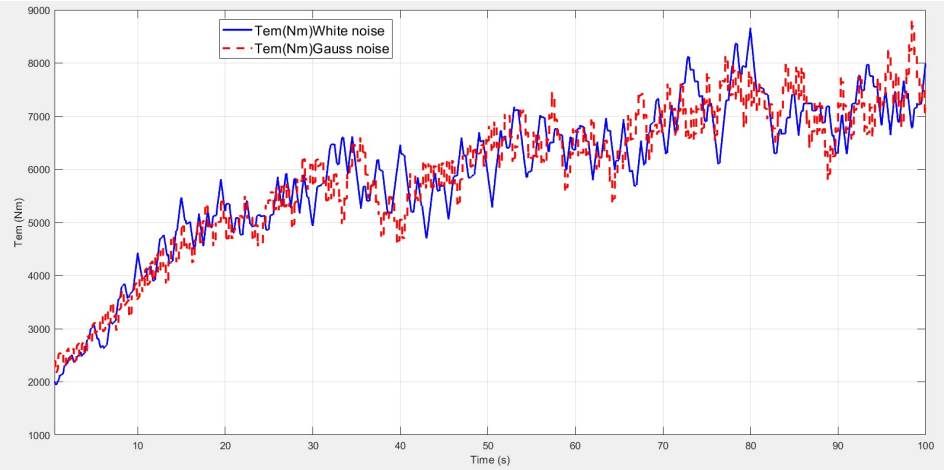

Figure 5.56: Electromagnetic torque in Nm.

In Figure 5.57 the power extracted by the wind turbine is shown with noise signals, where it can be seen that the behaviour is similar in both cases.

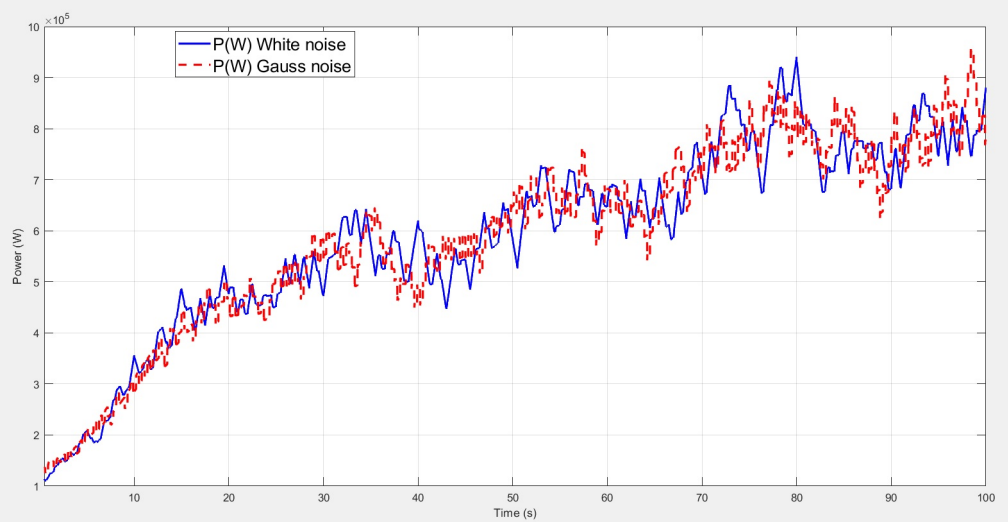

Figure 5.57: Active output power in $Watt$.

Figure 5.58 depicts the input signal including the additive noise considered to evaluate the performance of the controller.

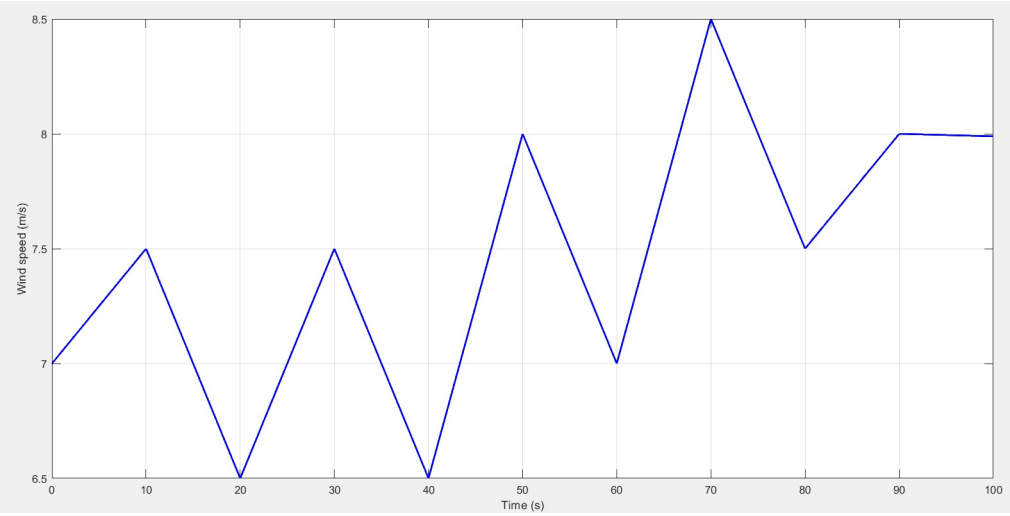

Figure 5.58: Wind input in m/s.

Figure 5.59 shows the simulation of the power coefficient with the noise signals; for both cases the same behaviour is observed.

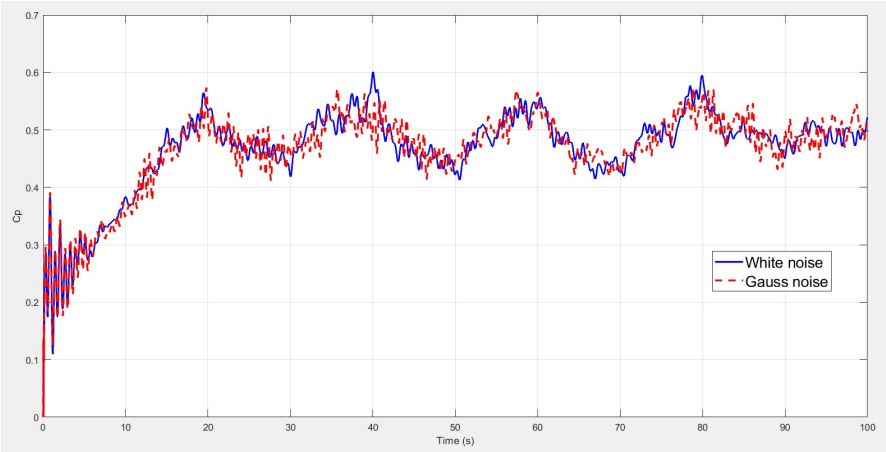

Figure 5.59: Power coefficient C_p.

5.4.3 Realistic Wind Speed Including Disturbances

In Figure 5.60 the behaviour of the current reference i_{qr} is shown in the presence of noise. Note that the performance for both cases is similar. During these simulations, the behaviour of the pitch angle via the introduction of noise remains constantly zero with no variations. This is because the wind turbine does not reach its nominal speed during these tests.

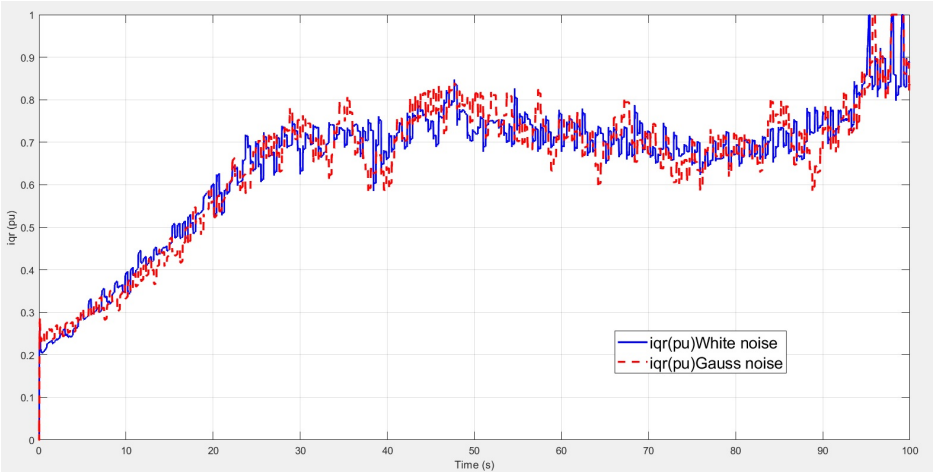

Figure 5.60: Reference signal i_{qr} in $p.u.$

In Figure 5.61 the behaviour of T_{em} is shown in the presence of noise. Note that the performance for both cases is similar.

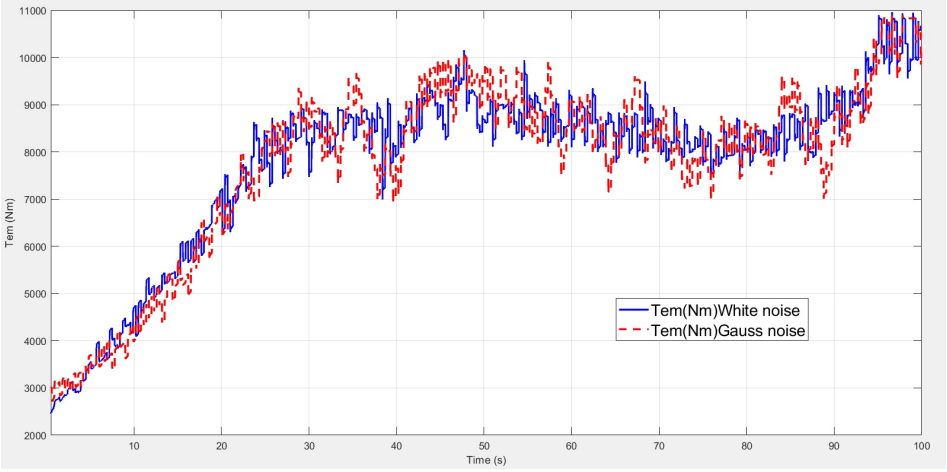

Figure 5.61: Electromagnetic torque in Nm.

In Figure 5.62 the power extracted by the wind turbine is shown with a noise signal, where it can be seen that for both cases the behaviour is similar.

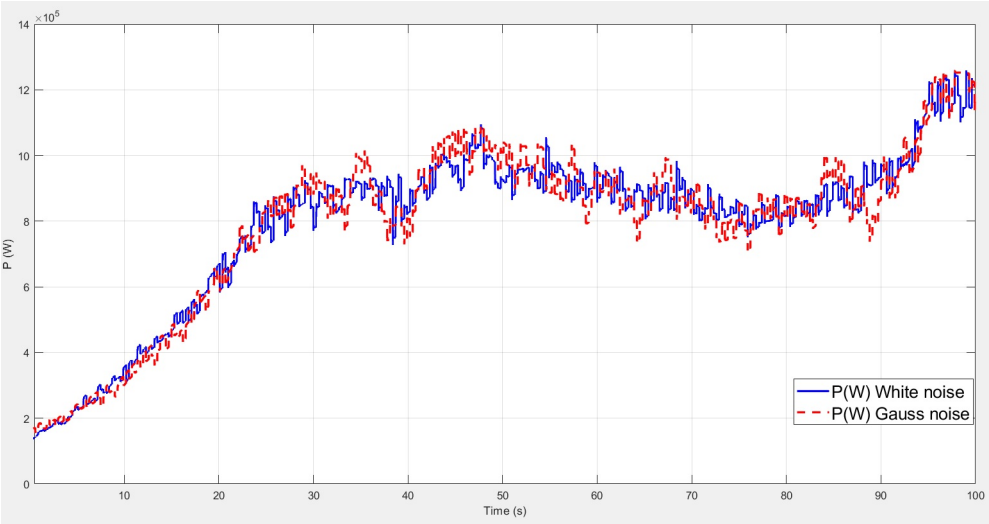

Figure 5.62: Active output power in $Watt$.

Figure 5.63 shows the noise-free input signal used to evaluate the performance of the controller.

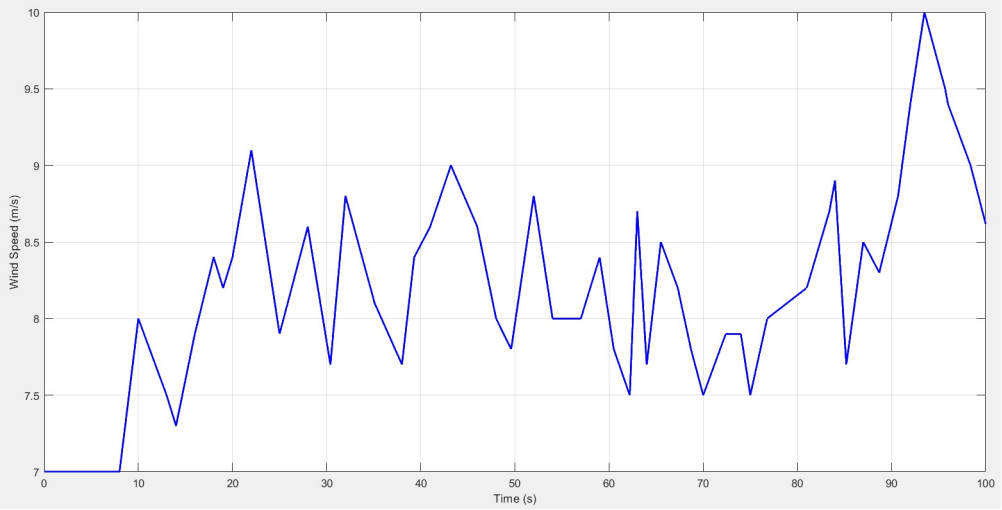

Figure 5.63: Noise-free input signal

Figure 5.64 shows the power coefficient in the presence of noise; in both cases the same behaviour is observed.

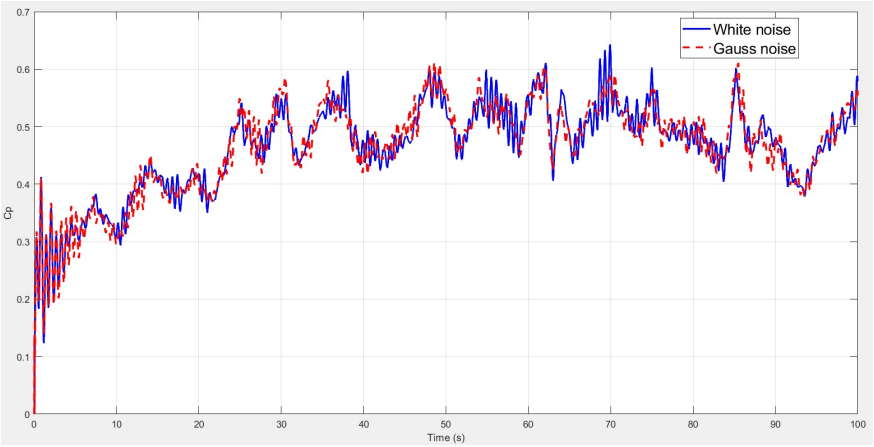

Figure 5.64: Power coefficient C_p.

Figure 5.65 shows the noise noise signals used in the simulations and for the evaluation of the controller.

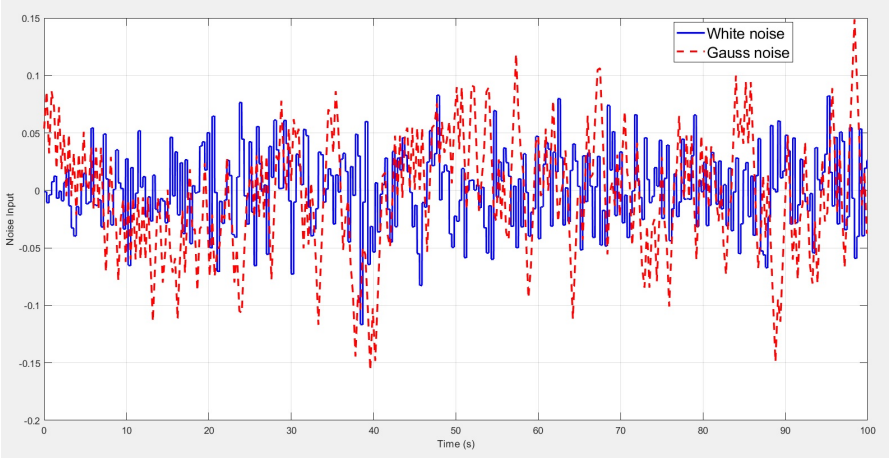

Figure 5.65: Noise signal input.

5.5 DSC Analysis with Disturbances

The DSC controller has been also tested using 10% amplitude uncorrelated white noise which has been added to the wind speed input signal. The following subsections show the simulations including the noise processes in order to evaluate the robustness features as for the ISC case.

5.5.1 Steps Wind Speed Including Disturbances

In Figure 5.66 the behaviour of the current i_{qr} is shown in the presence of noise. Note that the performance for both cases is similar.

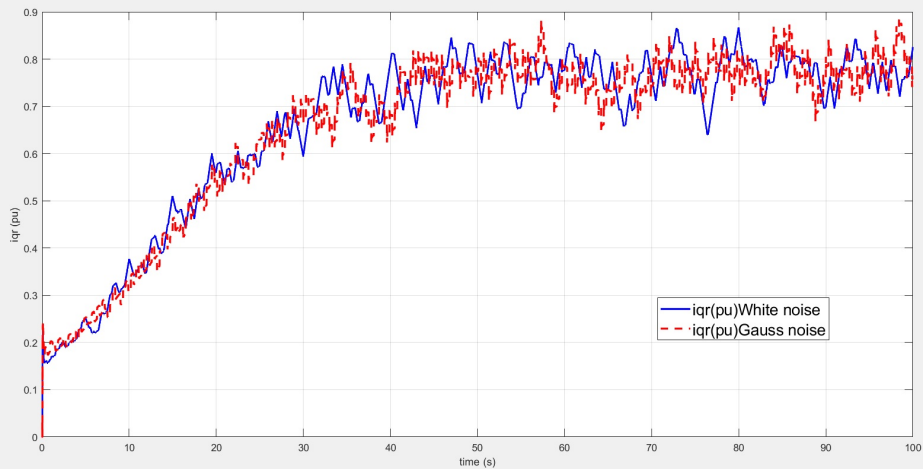

Figure 5.66: Reference signal i_{qr} in $p.u.$

In Figure 5.67 the behaviour of T_{em} is depicted in the presence of noise. Note that the performance for both cases is similar.

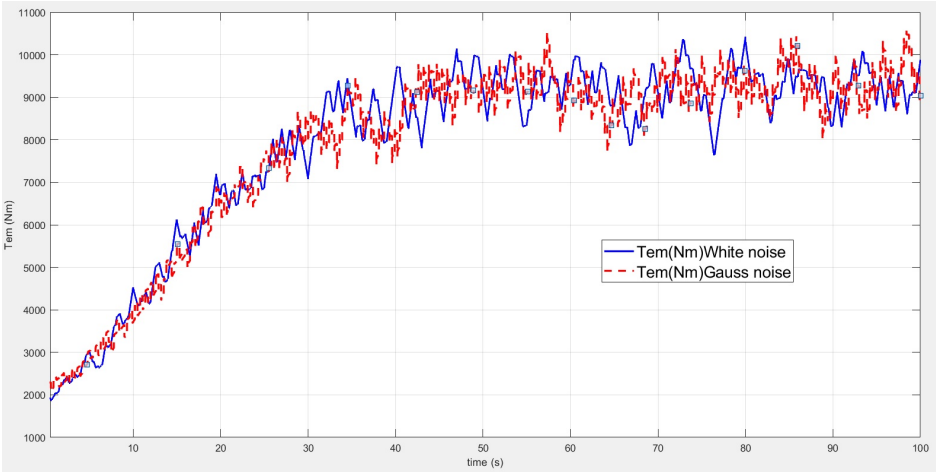

Figure 5.67: Electromagnetic torque in Nm.

In Figure 5.68 the power extracted by the wind turbine is shown in the presence of noise. Note that for both cases the behaviour is similar.

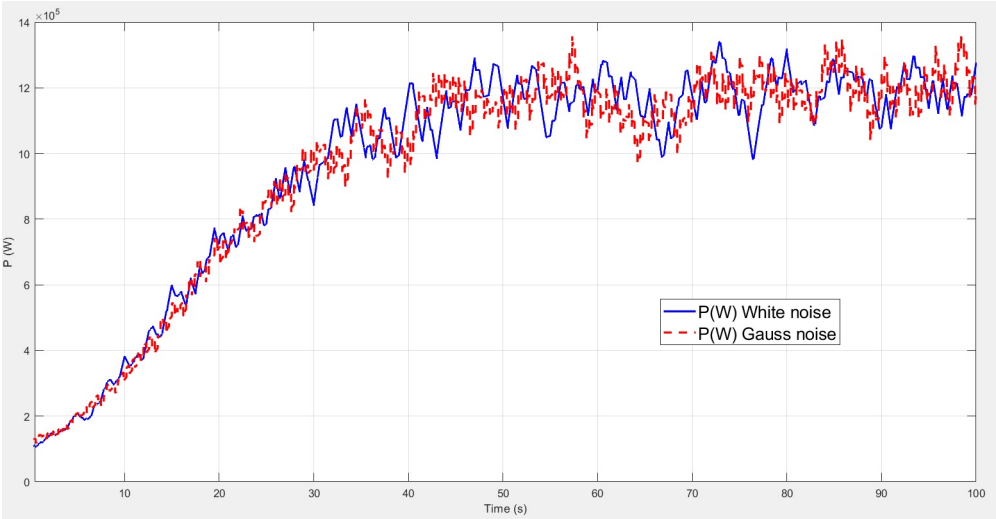

Figure 5.68: Active output power in $Watt$.

Figure 5.69 shows the noise-free input signal used to evaluate the performance of the controller.

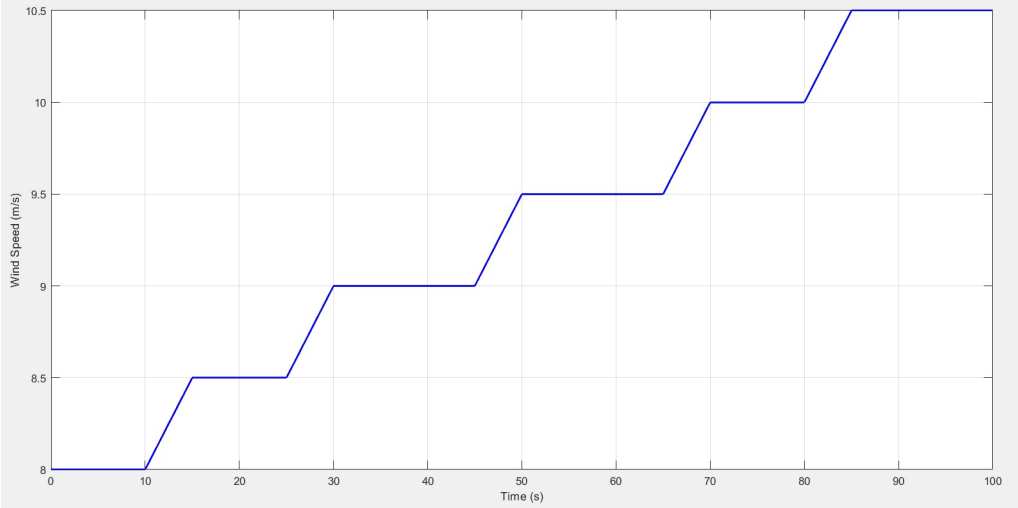

Figure 5.69: Wind input in m/s.

In Figure 5.70 the behaviour of the pitch angle is shown via the simulations with noise: similar dynamics are obtained. However, for the case of the uncorrelated white noise signal, reduced oscillations are observed.

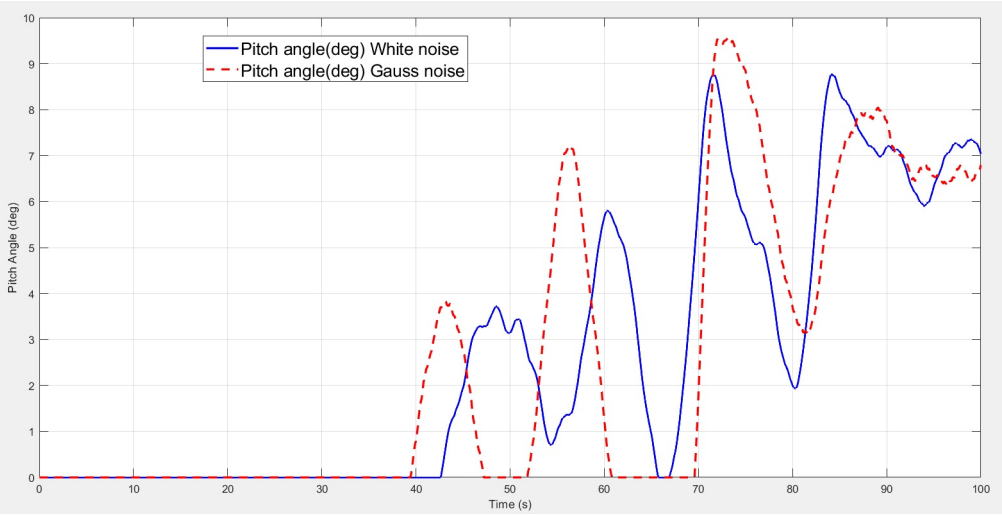

Figure 5.70: Pitch angle in degrees.

Figure 5.71 shows the power coefficient in the presence of noise. In both cases, the same behaviour is observed.

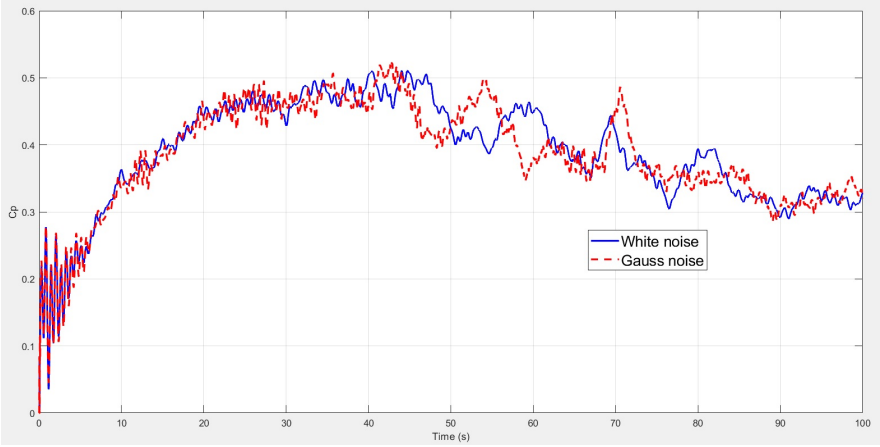

Figure 5.71: Power coefficient C_p.

Figure 5.72 shows the noise signals included into the simulations and exploited for evaluating the performance of the controller.

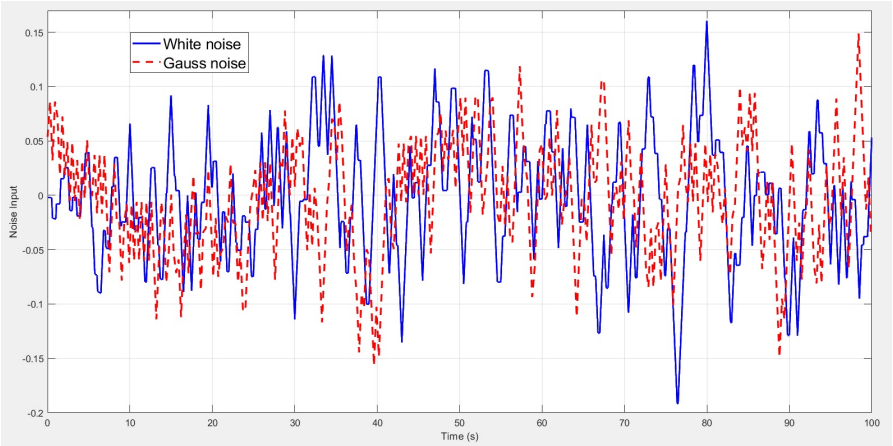

Figure 5.72: Noise input signal.

5.5.2 Triangular Wind Speed Including Disturbances

In Figure 5.73 the behaviour of the current i_{qr} in the presence of noise; it is worth noting that the performance for both cases is similar. During these simulations, the behaviour of the pitch angle via the introduction of noise remains constantly zero with no variations. This is because the wind turbine does not reach its nominal speed during these tests.

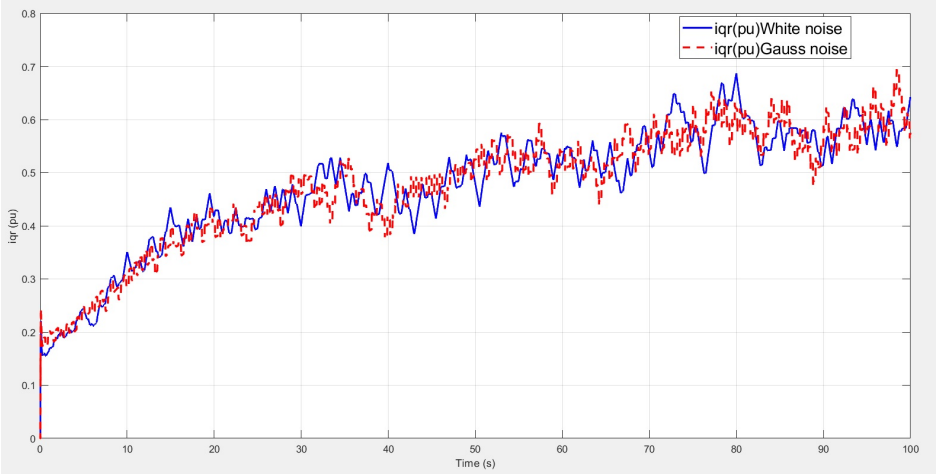

Figure 5.73: Reference signal i_{qr} in $p.u.$

In Figure 5.74 the behaviour of T_{em} is depicted in the presence of noise; note that the performance for both cases is similar.

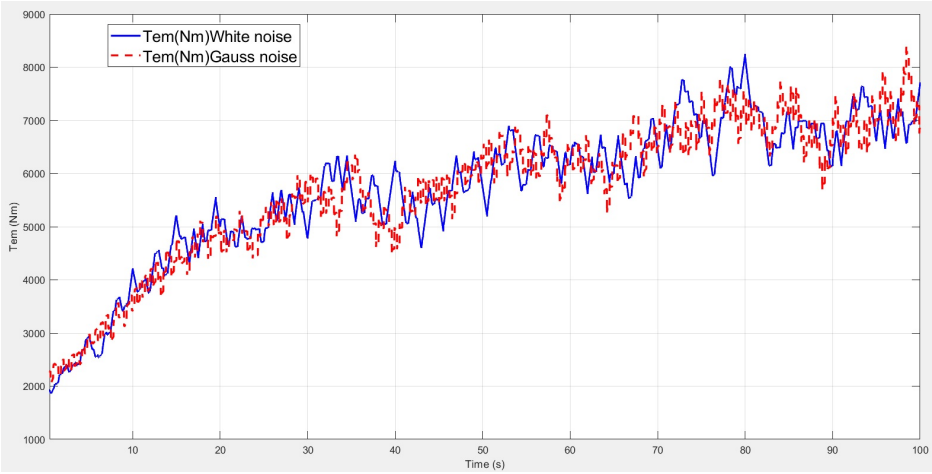

Figure 5.74: Electromagnetic torque in Nm.

In Figure 5.75 the power extracted by the wind turbine is shown with noise signals, where it can be seen that for both cases the behaviour is similar.

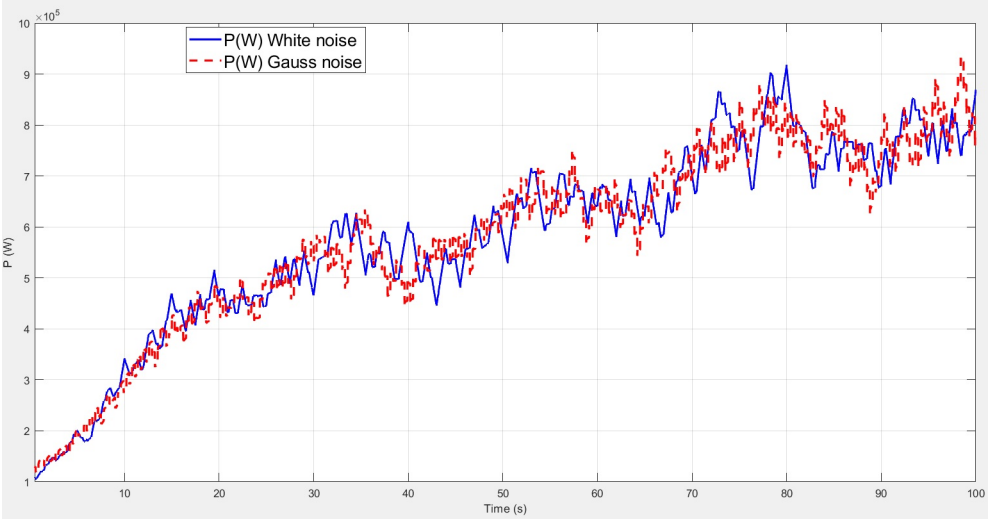

Figure 5.75: Active output power in $Watt$.

In Figure 5.76 depicts the noise-free input signal that is used to evaluate the performance of the controller.

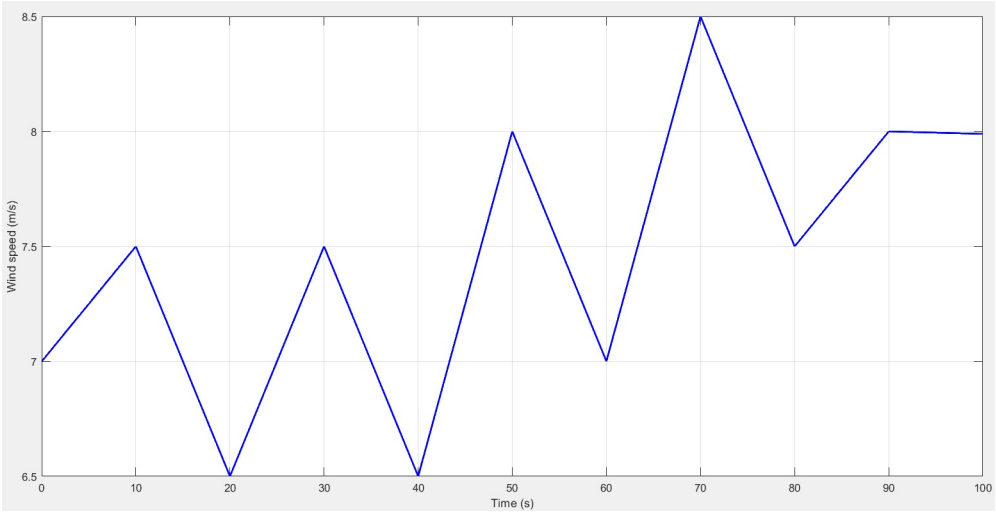

Figure 5.76: Wind input in m/s.

In Figure 5.77 the simulation of the power system in the presence of noise is shown; in both cases, the same behaviour is observed. Perhaps, a slightly better dynamics can be observed in the C_p produced by the DSC controlled system.

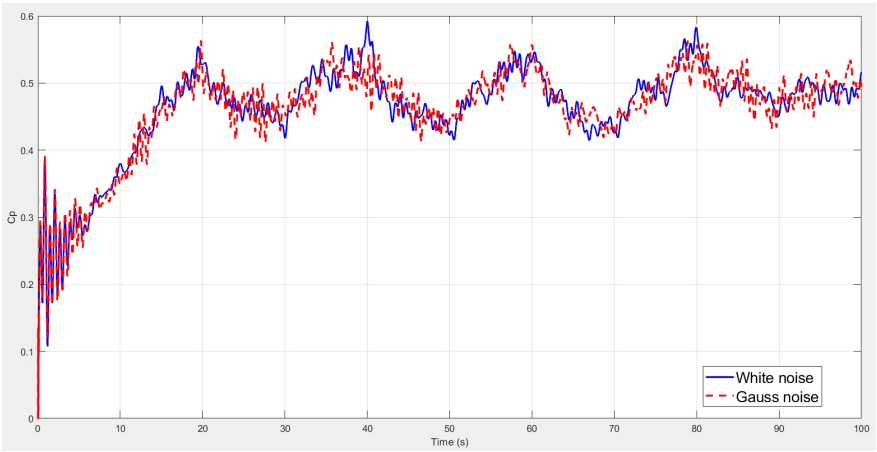

Figure 5.77: Power coefficient C_p.

In Figure 5.78 the noise processes included into the simulations are shown and exploited for evaluating the performance of the controller.

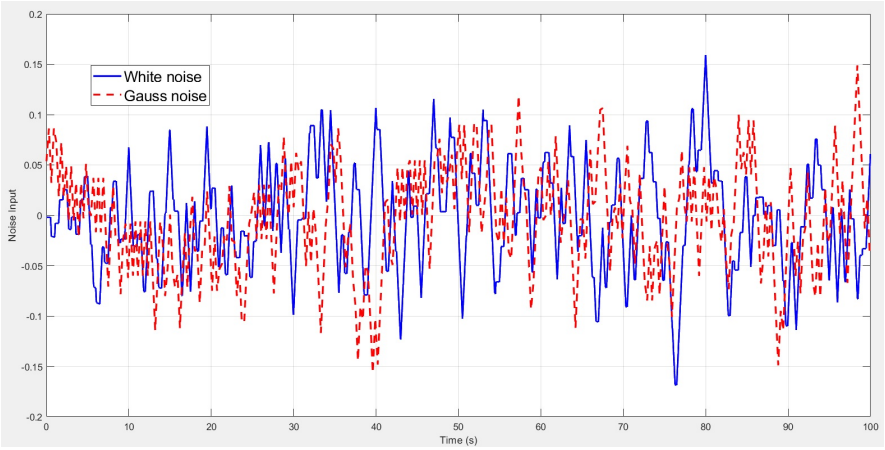

Figure 5.78: Noise input signal.

5.5.3 Realistic Wind Speed Including Disturbances

In Figure 5.79 the behaviour of the current i_{qr} is shown in the presence of noise; note that the performance for both cases is similar.

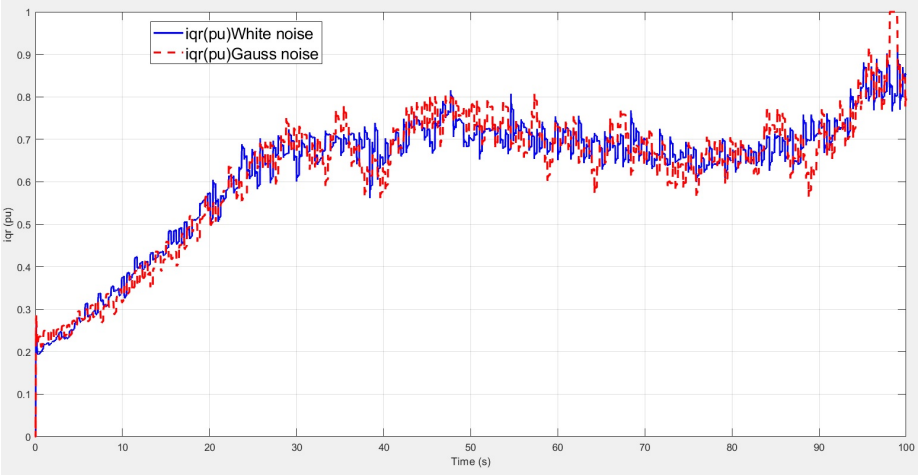

Figure 5.79: Reference signal i_{qr} in $p.u.$

In Figure 5.80 the behaviour of T_{em} is shown in the presence of noise signals; note that the performance for both cases is similar.

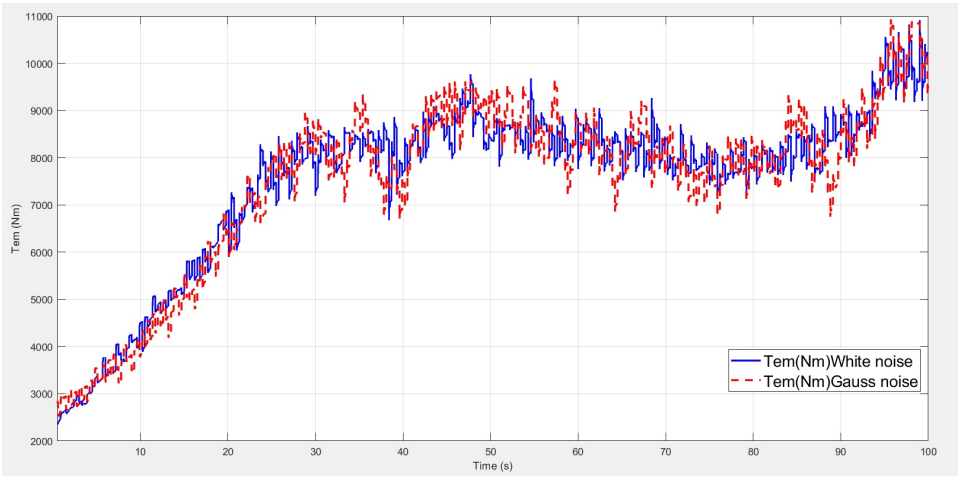

Figure 5.80: Electromagnetic torque in Nm.

In Figure 5.81 the power extracted by the wind turbine is shown with noise signals, where it can be seen that in both cases the behaviour is similar.

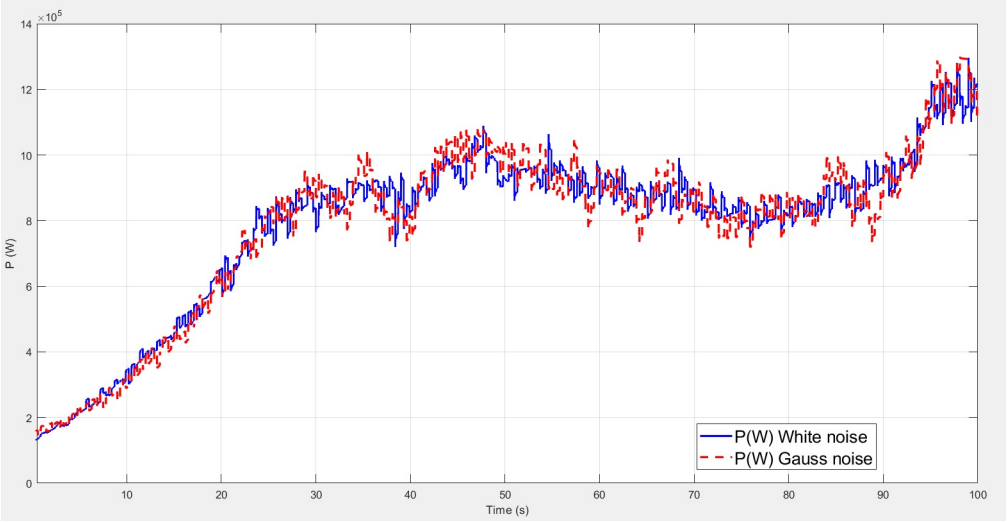

Figure 5.81: Active output power in $Watt$.

In Figure 5.82 the noise-free input signal is shown, and it is used to evaluate the performance of the controller.

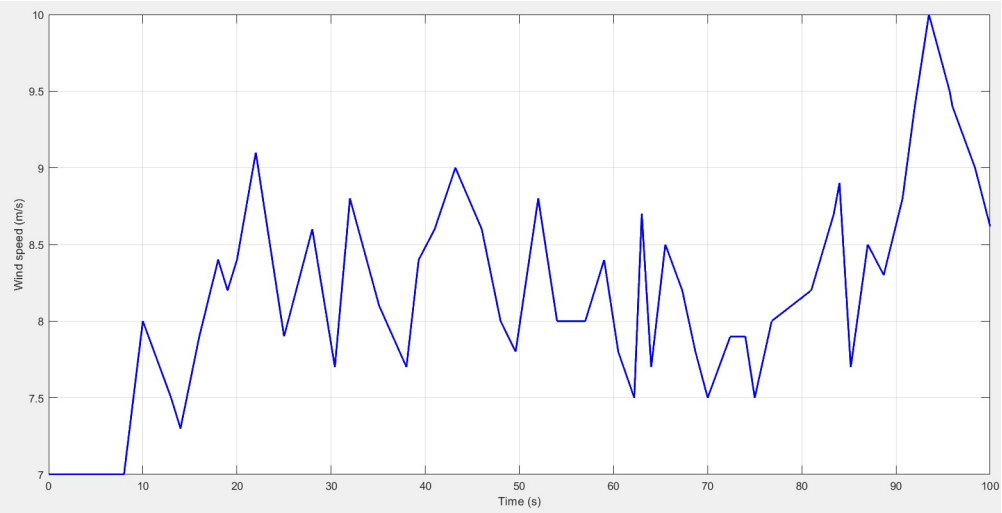

Figure 5.82: Wind input in m/s.

Figure 5.83 shows the simulation of the power coefficient in the presence of noise; in both cases, the same behaviour is observed.

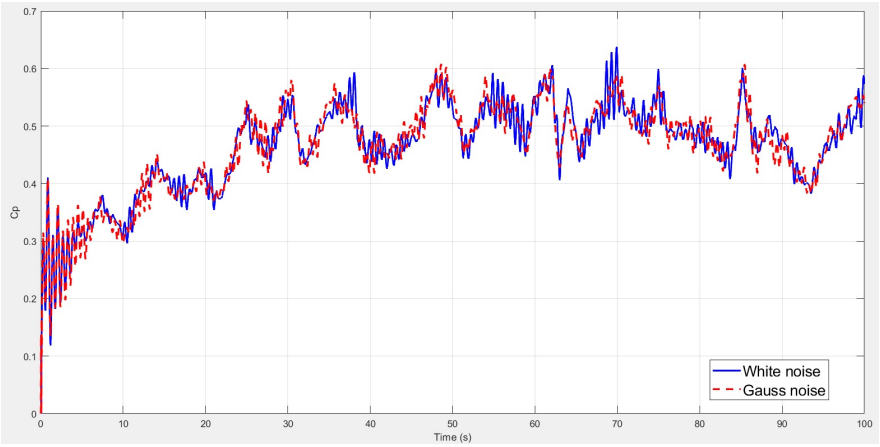

Figure 5.83: Power coefficient C_p.

Finally, in Figure 5.84 the noise signals included into the system is shown, and it is exploited for evaluating the performance of the controller.

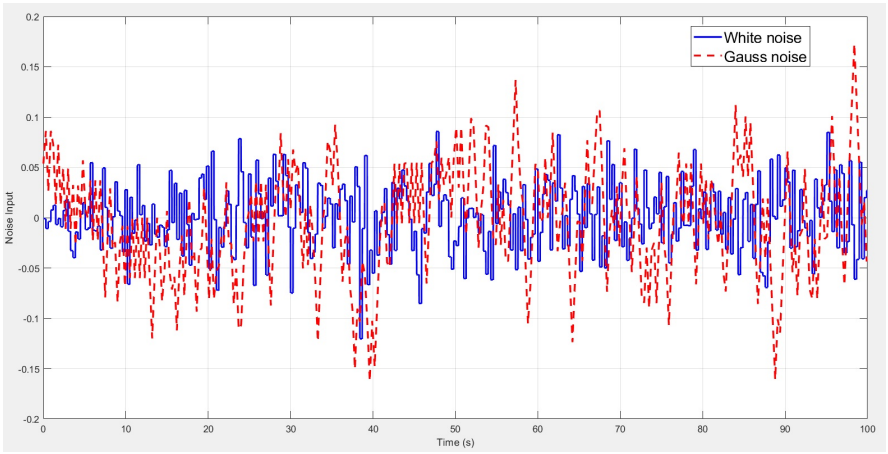

Figure 5.84: Noise input signal.

Chapter 6

Conclusions and Further Investigations

In this research, the ISC has been implemented by using FAST and Matlab for a 1.5 MW DFIG wind turbine. Compared to the classical PI control, the results highlight an important improvement because of the correct selection of optimal TSR and maximum C_p when calculating the optimal torque constant at the controller stage. This implementation also considers the initial LSS speed and inertia which produce an oscillation during the first 20 seconds of simulation. Nevertheless, after that period of time, the rotor speed becomes steady and closer to the nominal value. The considered simulations have the intention of demonstrating the capability of this technique to provide a fast response, even in the presence of disturbance in the wind input signal. Furthermore, the pitch controller is able to limit the speed of the shaft properly. This is important since the C_p performance is also affected by the pitch angle. When the simulations consider full load operations, the power and speed reach their nominal values and these simulations demonstrate the correct operation of the wind turbine in partial load conditions.

It is important to note that the DFIG can be configured for the grid or stand alone connections; therefore, any MPPT technique must allow the system to provide maximum power. These simulations have considered any standard grids. The ISC improvements compared to the traditional PI controller can be explained in terms of stability but mainly of C_p maximization. This can be observed in the results when the average output active power is measured where the ISC allows more power extraction. The wind speed is not constant for real scenarios and it is mostly an oscillatory signal which produces a complex dynamic behaviour. The ISC could be improved when the knowledge of all possible variables is available since it is very sensitive to disturbances. Therefore, the implementation of DSC methods are recommended

for better dynamic performance.

The DSC strategy based on the Luenberger state observer has allowed the system to operate with a better power extraction and C_p. Although the system is unstable during the first seconds of simulation due to the initial conditions, it rapidly reaches the optimum values. This means more active power generation and more reactive power absorption of wind turbine. The advantage of this technique is that the observer does not require any additional hardware implementation since it exploits common wind turbine signal measurements such as the HSS, the wind speed, torque, voltages and currents. For further implementations, it can be increased the number of inputs intended to improve the accuracy of the controller.

Moreover, for the Lederberg observer, it is worth noting that this technique can be implemented for most wind turbine models because the system can be adapted to different dynamic systems. An appropriate model and control design are key factors not only in terms of operation but also in terms of maintenance and durability of the elements. Although the wind speed is not always constant, MPPT is still able to track the dynamic response of the system; this feature makes it an interesting strategy. When a proper MPPT is performed, a more reliable energy system can be guaranteed. Moreover, by adding contributions of individual generators into wind farms, the influence of the controller becomes evident.

The concave shape of the C_p function is easily tracked by the observer. The complementary DSC strategy allows the wind turbine to produce more torque and power by progressive variations of i_{qr}. The HSS can not be increased drastically in order to maximize the output power because it can produce more mechanical losses. Instead, the HSS must be reduced as much as possible and this effect is achieved with this technique in comparison to the classical PI controller. This means that the mechanical components improve the performance in terms of fatigue, and the operative lifetime of the mechanical components can be thus improved. Finally, this controller is modular and mostly applied by a digital circuit that can be implemented over most wind turbines.

About the Takagi-Sugeno (T-S) PI fuzzy strategy, this technique demonstrates the influence of different subsystems over the maximum extracted power – *i.e.*, electrical, mechanical, and control – which constitute the wind turbine system. The dynamic model used for these simulations approximates real scenarios by providing relevant information on its operation. The aforementioned subsystems are the basis for generating robust control techniques. A control scheme for MPPT based on the fuzzy PI controller has been developed, deploying a feasible simulation of a 1.5 MW wind turbine model with a DFIG electric machine. This approach has demonstrated more effectiveness

in contrast to a classic PI controller. The improvement can be observed in the C_p response in terms of precision and speed. In addition, this strategy does not require an accurate description of the mathematical model or system for its configuration, showing optimal behaviour with complex dynamics. Different tests have demonstrated that, using the DSC fuzzy PI-based controllers, the electromagnetic torque, output power, rotor reference current, and rotational speed can track the effect of the variations in the wind speed more rapidly. This solution allows the system to adapt faster to input variations and, consequently, to improve the extraction of maximum power.

For future research, the incorporation of a robust pitch angle controller is recommended allowing more stability of the output variables which is desirable in order to accomplish nominal operation values. This robust controller is required, especially, in the face of wind speed drops or gusts where the rotor speed must be controlled to, consequently, overcome the inertia of the system in a shorter time. Additional investigations with real prototypes of previous industrial implementation are recommended because of multiple considerations including faults, vibrations and grid requirements.

Finally, this research includes simulations using data from manufacturers and published papers. Future research should include real implementations using hardware in the loop strategies in order to analyse the proposed scheme with a prototype. Moreover, it is necessary to include real scenarios such as real wind speed profiles in order to analyze a more accurate dynamic response. Additionally, other simulations can be performed including other electrical machine technologies such as PMSG in order to demonstrate the effectiveness of the proposed method.

Bibliography

[Abad et al., 2011] Abad, G., Lopez, J., Rodriguez, M., Marroyo, L., and Iwanski, G. (2011). *Doubly Fed Induction Machine Modeling and Control for Wind Energy Generation.* IEEE.

[Abdullah et al., 2012] Abdullah, M., Yatim, A., Tan, C., and Saidur, R. (2012). A review of maximum power point tracking algorithms for wind energy systems. *Renewable and Sustainable Energy Reviews*, 16(5):3220–3227.

[Abu-Rub et al., 2014] Abu-Rub, H., Malinowski, M., and Al-Haddad, K. (2014). Properties and control of a doubly fed induction machine. *Power Electronics for Renewable Energy Systems, Transportation and Industrial Applications.*

[AWEA, 2015] AWEA (2015). American wind energy association.

[Ayala and Simani, 2019] Ayala, E. and Simani, S. (2019). Perturb and observe maximum power point tracking algorithm for permanent magnet synchronous generator wind turbine systems.

[Bakouri et al., 2014] Bakouri, A., Mahmoudi, H., and Elyaalaoui, K. (2014). Direct torque control of a doubly fed induction generator of wind turbine for max-imum power extraction.

[Baldo, 2012] Baldo, F. (2012). Modeling of load interfaces for a drive train of a wind turbine.

[Banu and Istrate, 2017] Banu, I. and Istrate, M. (2017). Modeling of maximum power point tracking algorithm for photovoltaic systems. *IEEE Dataport.*

[Barbade and Kasliwal, 2012] Barbade, S. and Kasliwal, P. (2012). Neural network based control of doubly fed induction generator in wind power generation. issn 2278-7763. *International Journal of Advancements in Research Technology.*

[Bedoud et al., 2015] Bedoud, K., Ali-rachedic, M., Bahid, T., Lakelb, R., and Grid, A. (2015). Robust control of doubly fed induction generator for wind turbine under sub-synchronous operation model. *International Conference on Technologies and Materials for Renewable Energy, Environment and Sustainability*, page 886–899.

[Ben Amar et al., 2017] Ben Amar, A., Belkacem, S., and Mahni, T. (2017). Direct torque control of a doubly fed induction generator. *International Journal of Energetica (IJECA)*, 2(1):11–14.

[Bharti et al., 2015] Bharti, O., Saket, R., and Nagar, S. (2015). Design of pi controller for doubly fed induction generator using static output feed-back.

[Boukhezzar and Siguerdidjane, 2009] Boukhezzar, B. and Siguerdidjane, H. (2009). Nonlinear control with wind estimation of a dfig variable speed wind turbine for power capture optimization. *Energy Conversion and Management*, 50(4):885–892.

[Boukhezzar and Siguerdidjane, 2011] Boukhezzar, B. and Siguerdidjane, H. (2011). Nonlinear control of a variable-speed wind turbine using a two-mass model. *IEEE Transactions on Energy Conversion*, 26(1):149–162.

[Calderaro et al., 2008] Calderaro, V., Galdi, V., Piccolo, A., and Siano, P. (2008). A fuzzy controller for maximum energy extraction from variable speed wind power generation systems. 78(6):1109–1118.

[Carrillo et al., 2013] Carrillo, C., Obando Montaño, A., Cidrás, J., and Diaz, E. (2013). Review of power curve modelling for wind turbines. *Renewable and Sustainable Energy Reviews*, 21:572–581.

[Castellani et al., 2014] Castellani, F., Garinei, A., Terzi, L., Astolfi, D., and Gaudiosi, M. (2014). Improving windfarm operation practice through numerical modelling and supervisory control and data acquisition data analysis, issn= 1752-1416. *Transactions on Sustainable Energy, IEEE*, 8(4):367–379.

[Fu et al., 2018] Fu, C., Pan, T., Liu, H., Wu, D., Shen, Y., and Hao, Z. (2018). Mppt control based fuzzy for wind energy generating system.

[Gajewski and Pienkowski, 2016] Gajewski, P. and Pienkowski, K. (2016). Direct torque control and direct power control of wind turbine system with pmsg, issn 0033-2097. pages 249–253.

[Hallak et al., 2018] Hallak, M., Hasni, M., and Menaa, M. (2018). Modeling and control of a doubly fed induction generator base wind turbine system.

[Heier, 1988] Heier, S. (1988). *Grid Integration of Wind Energy Conversion Systems*. John Wiley Sons Ltd.

[Hilloowala and Sharaf, 1996] Hilloowala, R. and Sharaf, A. (1996). A rule-based fuzzy logic controller for a pwm inverter in a stand alone wind energy conversion scheme. *IEEE Transactions on Industry Applications*, 32(1):57–65.

[Hofmann and Okafor, 2001] Hofmann, W. and Okafor, F. (2001). Doubly-fed full-controlled induction wind generator for optimal power utilisation. *4th IEEE International Conference on Power Electronics and Drive Systems*, pages 355–361.

[Jafarnejadsani and Pieper, 2015] Jafarnejadsani, H. and Pieper, J. (2015). Gain-scheduled ℓ_1 -optimal control of variable-speed-variable-pitch wind turbines. *IEEE Transactions on Control Systems Technology*, 23(1):372–379.

[Ma et al., 2015] Ma, Z., Yan, Z., Shaltout, M., and Chen, D. (2015). Optimal real-time control of wind turbine during partial load operation. *IEEE Transactions on Control Systems Technology*, 23(6):2216–2226.

[Mahmoud and Oyedeji, 2019] Mahmoud, M. S. and Oyedeji, M. (2019). Adaptive and predictive control strategies for wind turbine systems: A survey. *Journal of Automatic Sinica, IEEE*, 6(2):364–378.

[MathWorks, 2017] MathWorks (2017). Mathworks wind turbine.

[MathWorks., 2018] MathWorks., T. (2018). Matlab.

[Meharrar et al., 2011] Meharrar, A., Tioursi, M., Hatti, M., Boudghène, A., and Stambouli, N. (2011). A variable speed wind generator maximum power tracking based on adaptative neuro-fuzzy inference system. pages 7659–7664.

[Michalke, 2008] Michalke, G. (2008). Variable speed wind turbines - modelling, control, and impact on power systems.

[Mohammadi et al., 2014] Mohammadi, J., Vaez-Zadeh, S., Afsharnia, S., and Daryabeigi, E. (2014). A combined vector and direct power control for dfig-based wind turbines. *Transactions on Sustainable Energy, IEEE*, 5(3):767–775.

[Muhamamad, 2014] Muhamamad, R. (2014). *Power Electronics, Circuits, Devices, and Applications*. Pearson.

[Muller and Deicke, 2014] Muller, S. and Deicke, M. (2014). Properties and control of a doubly fed induction machine. *Power Electronics for Renewable Energy Systems*, 8:270–318.

[NREL, 2005] NREL (2005). *FAST User Manual*. IEEE.

[(NREL), 2020] (NREL), N. R. E. L. (2020). Fatigue aerodynamics structures and turbulence.

[Ohiero, 2015] Ohiero, P. (2015). Development of fast multi-system simulation models for permanent magnet synchronous motor and generator drive systems.

[Ouezgan et al., 2017] Ouezgan, K., Bossoufi, B., and Bargach, M. (2017). Dtc control of dfig-generators for wind turbines: Fpga implementation based.

[Palejiya and Chen, 2016] Palejiya, D. and Chen, D. (2016). Performance improvements of switching control for wind turbines. *IEEE Transactions on Sustainable Energy*, 7(2):526–534.

[Pozo et al., 2021a] Pozo, N., Muñoz, E., and Ayala, E. (2021a). Direct speed control of a 9 mw dfig wind turbine.

[Pozo et al., 2021b] Pozo, N., Muñoz, E., and Ayala, E. (2021b). Fuzzy pi control strategy applied to a doubly fed induction wind turbine in order to maximize the power extraction in the presence of disturbances.

[Rashid, 2014] Rashid, M. (2014). *Power Electronics: circuits, devices and applications, ISBN 978-0-13-312590-0*. Pearson Education.

[Semrau et al., 2015] Semrau, G., Rimkus, S., and Das, T. (2015). Nonlinear systems analysis and control of variable speed wind turbines for multiregime operation. *Journal of Dynamic Systems, Measurement, and Control*, 137(4):1–10.

[Singh et al., 2014] Singh, M., Muljadi, E., Jonkman, J., Girsang, I., Dhupia, J., and Gevorgian, V. (2014). *Simulation for Wind Turbine Generators—With FAST and MATLAB-Simulink Modules*. National Renewable Energy Laboratory (NREL).

[Tahiri et al., 2018] Tahiri, F., Chikh, K., and Khafallah, M. (2018). Mppt strategy using fuzzy-pi controller applied to a standalone wind energy conversion system.

[Thongam et al., 2009a] Thongam, J., Bouchard, P., Ezzaidi, H., and Ouhrouche, M. (2009a). Artificial neural network-based maximum power point tracking control for variable speed wind energy conversion systems. *Control Systems, IEEE*, pages 1668–1671.

[Thongam et al., 2009b] Thongam, J., Bouchard, P., Ezzaidi, H., and Ourouche, M. (2009b). Wind speed sensorless maximum power point tracking control of variable speed wind energy conversion systems. *IEEE International Electric Machines and Drives Conference*.

[Thongam and Ouhrouche, 2011] Thongam, J. and Ouhrouche, M. (2011). Mppt control methods in wind energy. pages 339–360.

[Uluyol et al., 2011] Uluyol, O., Parthasarathy, G., Foslien, W., and Kim, K. (2011). Power curve analytic for wind turbine performance monitoring and prognostics.

[Wang and Chang, 2004] Wang, Q. and Chang, L. (2004). An intelligent maximum power extraction algorithm for inverter-based variable speed wind turbine systems. *Transactions on Power Electronics, IEEE*, 19(5):1242–1249.

[WWEA, 2010] WWEA (2010). World wind energy report 2010. Technical report.